

COLORADO SCHOOL OF MINES

A SCALE-UP STUDY OF STAGGERED LINE
WATERFLOOD PERFORMANCE USING LARGE
SCALED FLOW MODELS

A DISSERTATION
SUBMITTED TO THE GRADUATE FACULTY
in partial fulfillment of the requirement for the
degree of
DOCTOR OF PHILOSOPHY

BY
FABIAN O. IWERE
GOLDEN, COLORADO
1979

ProQuest Number: 11016688

All rights reserved

INFORMATION TO ALL USERS

The quality of this reproduction is dependent upon the quality of the copy submitted.

In the unlikely event that the author did not send a complete manuscript and there are missing pages, these will be noted. Also, if material had to be removed, a note will indicate the deletion.



ProQuest 11016688

Published by ProQuest LLC (2019). Copyright of the Dissertation is held by the Author.

All rights reserved.

This work is protected against unauthorized copying under Title 17, United States Code
Microform Edition © ProQuest LLC.

ProQuest LLC.
789 East Eisenhower Parkway
P.O. Box 1346
Ann Arbor, MI 48106 – 1346

A Thesis submitted to the Faculty and the Board of Trustees of the Colorado School of Mines in partial fulfillment of the requirements for the degree of Doctor of Philosophy (Petroleum Engineering).

Signed: *Fenigshofer*
F. O. ~~Were~~

Golden, Colorado

Date: *May 14*, 19*79*

Approved: *Ching H. Wu*
Dr. C. H. Wu
Thesis Advisor

Dan M. Bass
Dr. D. M. Bass
Head, Department of
Petroleum Engineering

Golden, Colorado

Date: *May 14*, 19*79*

ABSTRACT

A series of scaled flow model experiments has been undertaken to investigate the validity of conventional scaling theories. Three geometrically similar models are used and the arrangement of the wells in the scaled models depicts staggered line pattern. Injection rates are determined from the criterion that the dimensionless group $(\phi L/v_t t)$ be equal in the models. The construction and operation of the flow models are described. Dyed fluid is used exclusively as the displacing phase so that the front movement and sweep patterns could be observed.

Results of the investigation indicate that the performances of the three models tested are nearly identical, with respect to oil recovery, water-oil ratio and sweep efficiency as functions of pore volume throughput. It is also found that for rectangular homogeneous models the dimensionless group (L'/h) and small variations in initial fluid saturation can be neglected in the design of scaled models. This indicates possible relaxation of scaling restrictions in the application of scaled models.

Based on the results of this investigation, it is found that ultimate oil recovery is independent of density difference.

TABLE OF CONTENTS

	page
ABSTRACT	iii
LIST OF FIGURES	vi
LIST OF TABLES	xi
ACKNOWLEDGEMENTS	xii
CHAPTER I INTRODUCTION	1
CHAPTER II LITERATURE SURVEY	3
Dimensional Analysis	3
Inspectional Analysis	5
Dimensional-Inspectional Analysis	16
Comparison of Scaling Theories	17
CHAPTER III THEORETICAL ANALYSIS	21
Dimensional Analysis	21
Inspectional Analysis	24
CHAPTER IV EXPERIMENTAL WORK	32
Apparatus	32
Materials	34
Procedure	35
1. Physical Properties of Fluids and Sand	35
2. Calibration Runs	37
3. Displacement Runs	39
CHAPTER V EXPERIMENTAL RESULTS AND DISCUSSIONS	43
Reproducibility of Results	44
Effect of Model Dimensions	44
Effect of Viscous Forces	47
Effect of Gravity Forces	50
Validity of Scaled Models	52
Areal Coverage	54
CHAPTER VI CONCLUSIONS AND RECOMMENDATIONS	57

TABLE OF CONTENTS (cont'd)

	page
NOMENCLATURE	59
LITERATURE CITED	63
APPENDIX - EXPERIMENTAL RESULTS (25 Tables)	123

LIST OF FIGURES

<u>Figure</u>	<u>page</u>
1. Calibration of Conductivity Meter.	68
2. Experimental Appartus.	69
3. Reproducibility.	70
4. Oil Recovery at Water Breakthrough at High Rate Versus Length-Thickness Ratio (L/h) . . .	71
5. Oil Recovery at Water Breakthrough at Low Rate Versus Length-Thickness Ratio (L/h) . . .	72
6. Oil Recovery at One Pore Volume Throughput at High Rate Versus Length-Thickness Ratio (L/h).	73
7. Oil Recovery at One Pore Volume Throughput at Low Rate Versus Length-Thickness Ratio (L/h).	74
8. Effect of Rate on Oil Recovery (Model I, Hexane).	75
9. Effect of Rate on Water-Oil Ratio (Model I, Hexane).	76
10. Effect of Rate on Oil Recovery (Model II, Hexane).	77
11. Effect of Rate on Water-Oil Ratio (Model II, Hexane).	78
12. Effect of Rate on Oil Recovery (Model III, Hexane).	79
13. Effect of Rate on Water-Oil Ratio (Model III, Hexane).	80
14. Effect of Rate on Oil Recovery (Model I, Kerosene).	81

Figure	page
15. Effect of Rate on Water-Oil Ratio (Model I, Kerosene)	82
16. Effect of Rate on Oil Recovery (Model II, Kerosene)	83
17. Effect of Rate on Water-Oil Ratio (Model II, Kerosene)	84
18. Effect of Rate on Oil Recovery (Model III, Kerosene)	85
19. Effect of Rate on Water-Oil Ratio (Model III, Kerosene)	86
20. Effect of Rate on Oil Recovery (Model I, Soltrol)	87
21. Effect of Rate on Water-Oil Ratio (Model I, Soltrol)	88
22. Effect of Rate on Oil Recovery (Model II, Soltrol)	89
23. Effect of Rate on Water-Oil Ratio (Model II, Soltrol)	90
24. Effect of Rate on Oil Recovery (Model III, Soltrol)	91
25. Effect of Rate on Water-Oil Ratio (Model III, Soltrol)	92
26. Oil Recovery at Water Breakthrough at High Rate Versus Viscosity Ratio (μ_o/μ_w)	93
27. Oil Recovery at Water Breakthrough at Low Rate Versus Viscosity Ratio (μ_o/μ_w)	94
28. Oil Recovery at One Pore Volume Throughput at High Rate Versus Viscosity Ratio (μ_o/μ_w)	95

Figure	page
29. Oil Recovery at One Pore Volume Throughput at Low Rate Versus Viscosity Ratio (μ_o/μ_w)	96
30. Comparison of the Positions of the Fronts at High Rate (Hexane, Viscosity Ratio = 0.34) . . .	97
31. Comparison of the Positions of the Fronts at Low Rate (Hexane, Viscosity Ratio = 0.34). . .	98
32. Comparison of Cumulative Oil Recoveries at High Rate (Hexane, Viscosity Ratio = 0.34) . . .	99
33. Comparison of Water-Oil Ratio Curves at High Rate (Hexane, Viscosity Ratio = 0.34) . . .	100
34. Comparison of Cumulative Oil Recoveries at Low Rate (Hexane, Viscosity Ratio = 0.34). . .	101
35. Comparison of Water-Oil Ratio Curves at Low Rate (Hexane, Viscosity Ratio = 0.34). . .	102
36. Comparison of Cumulative Oil Recoveries at High Rate (Kerosene, Viscosity Ratio = 1.76).	103
37. Comparison of Water-Oil Ratio Curves at High Rate (Kerosene, Viscosity Ratio = 1.76).	104
38. Comparison of Cumulative Oil Recoveries at Low Rate (Kerosene, Viscosity Ratio = 1.76).	105
39. Comparison of Water-Oil Ratio Curves at Low Rate (Kerosene, Viscosity Ratio = 1.76).	106
40. Comparison of Cumulative Oil Recoveries at High Rate (Soltrol, Viscosity Ratio = 4.43).	107
41. Comparison of Water-Oil Ratio Curves at High Rate (Soltrol, Viscosity Ratio = 4.43).	108

Figure	page
42. Comparison of Cumulative Oil Recoveries at Low Rate (Soltrol, Viscosity Ratio = 4.43)	109
43. Comparison of Water-Oil Ratio Curves at Low Rate (Soltrol, Viscosity Ratio = 4.43)	110
44. Comparison of Cumulative Glycerine Recoveries at Low Rate (Glycerine-Water, Viscosity Ratio = 7.93)	111
45. Comparison of Water-Glycerine Ratio Curves at Low Rate (Glycerine-Water, Viscosity Ratio = 7.93)	112
46. Comparison of Cumulative Fresh Water Recoveries at High Rate (Fresh Water, Viscosity Ratio = 1.0)	113
47. Comparison of Water-Fresh Water Ratio Curves at High Rate (Fresh Water, Viscosity Ratio = 1.0)	114
48. Comparison of Areal Sweep Efficiency at High Rate (Hexane, Viscosity Ratio = 0.34)	115
49. Comparison of Areal Sweep Efficiency at Low Rate (Hexane, Viscosity Ratio = 0.34)	116
50. Comparison of Areal Sweep Efficiency at High Rate (Kerosene, Viscosity Ratio = 1.76)	117
51. Comparison of Areal Sweep Efficiency at Low Rate (Kerosene, Viscosity Ratio = 1.76)	118
52. Comparison of Areal Sweep Efficiency at High Rate (Soltrol, Viscosity Ratio = 4.43)	119
53. Comparison of Areal Sweep Efficiency at Low Rate (Soltrol, Viscosity Ratio = 4.43)	120

Figure	page
54. Comparison of Areal Sweep Efficiency at Low Rate (Glycerine-Water, Viscosity Ratio = 7.93)	121
55. Comparison of Areal Sweep Efficiency at High Rate (Fresh Water, Viscosity Ratio = 1.0)	122

LIST OF TABLES

<u>Table</u>		<u>page</u>
1	Scaling Groups from Dimensional Analysis	18
2	Scaling Groups from Inspectional Analysis	19
3	Internal Dimensions of the Models.	32
4	Fluids and Sand Properties	36
5	Water Injection Rates.	38
6	Initial Water Saturations.	40
7	Summary of Runs.	43
8	Oil Recovery, %OIP, from the Respective Models and Liquids	45
9	Test 2. Oil Recovery, %OIP.	46
Appendix	Experimental Results	123

ACKNOWLEDGEMENTS

The author is most appreciative of Dr. C. H. Wu, thesis advisor, for his guidance throughout this study. Sincere gratitude is also extended to Dr. D. M. Bass, Dr. D. W. Hilchie, Dr. R. E. D. Woolsey and D. I. Dickinson, for their services as thesis committee members.

For their financial assistance, the author is indebted to the Government of the Bendel State of Nigeria, and Colorado School of Mines for a research assistantship which was granted when it was most needed.

Finally, I express my most sincere appreciation to my fiancée, Renee McConduit, for her love, devotion and patience with me during the course of this study.

Chapter I

INTRODUCTION

Laboratory displacement experiments have been extensively used in the study of two-phase flow in porous media influenced by capillary, viscous and gravitational forces. Results of such experiments, if carried out in properly scaled models, are considered reasonable simulation of fluid flow in petroleum reservoirs.

The design of dimensionally-scaled models demands a complete understanding of the reservoir flow process and geometry, and an ability to select variables pertinent to the process which must be scaled. Two conventional methods, dimensional analysis and inspectional analysis, are usually employed to determine dimensionless scaling groups.

The validity of the scaling laws have been experimentally demonstrated for the five-spot and direct line drive patterns, using relatively small models. The internal dimensions of the largest model reported in the literature were 32x16x2 in. (1). The well arrangement allowed the surface area of the model to be varied while the thickness was constant.

The objective of this thesis is to investigate experimentally the validity of the scaling laws for staggered

line drive pattern using large scaled three-dimensional flow models. For this purpose, three geometrically similar physical models are fabricated and used in the experiments. Immiscible displacement runs are conducted using injection rates ranging from 21.5 cc/min in the smallest model to 360 cc/min in the largest. Dyed salt water is used as the displacing fluid in all runs. Displaced phases used include n-hexane, kerosene, soltrol and a 50-50 percent mixture of glycerine and water. All experimental measurements are made at room temperature.

Chapter II

LITERATURE REVIEW

In the literature the theories of dimensional analysis, inspectional analysis and their combination have been applied in the design of dimensionally-scaled models. For convenience, the literature review is discussed under these theories. The author has taken the liberty of changing the various notations in the original studies to the form used in this thesis.

DIMENSIONAL ANALYSIS

The application of dimensional analysis in the design of scaled model experiments to study petroleum reservoir problems is first proposed by Leverett, Lewis and True (2). The relationship between length and time is fixed in the analysis since acceleration due to gravity is necessarily the same in the model and prototype. Furthermore, because the density difference for practical modeling fluids is about the same as the density difference for fluids occurring in petroleum reservoirs the mass ratio is fixed for all practical purposes. The important conclusion is that the ratios between all corresponding parameters in the model and prototype are completely determined by the choice

of either a time or length scale ratio.

Leverett et al have studied waterflooding in linear and radial systems. The scaling criteria proposed are:

- 1) The initial and boundary conditions must be the same for geometrically similar model and prototype.
- 2) The relative permeability to the wetting phase must be the same function of saturation in both model and prototype.
- 3) The relative permeability to the nonwetting phase must be the same function of saturation in both model and prototype.

- 4) The capillary pressure function, dimensionless,

$$J(S) = \frac{P_c}{\sigma} \sqrt{K/\phi} \quad \dots (1)$$

must be the same in model and prototype.

- 5) The porosity, ϕ must be the same in model and prototype.
- 6) The viscosity ratio, μ_o/μ_w must be the same in model and prototype.

Engelberts and Klinkenberg (3) have studied viscous fingering using linear scaled models. Six independent dimensionless groups,

$$\mu_o/\mu_w, L/h, \alpha, L/K^{\frac{1}{2}}, \frac{\Delta\rho g K}{v\mu_w} \text{ and } \frac{\Delta\rho g L K^{\frac{1}{2}}}{\sigma \cos \theta}$$

have evolved from the dimensional analysis of the problem.

The results of their experiments show that ultimate recovery

is invariably between 80 and 90%, independent of the variations in the dimensionless groups. The breakthrough recoveries on the other hand are dependent on most of the dimensionless groups except $\frac{\Delta\rho g L K^{\frac{1}{2}}}{\sigma \cos \theta}$. In addition, their results show that the viscosity ratio, μ_o/μ_w is a very important variable when waterflooding at high injection rates.

The scaled model displacement experiments carried out by Croes and Schwarz (4) have utilized the dimensionless groups proposed by Engelberts and Klinkenberg. Their investigation has extended the range of the viscosity ratio and their results have confirmed those obtained by the previous authors.

Greenkorn (5) reviewed the theory of models and demonstrated the derivation of scaling laws for the flow of two miscible fluids flowing in a porous medium. He has also derived a complete set of dimensionless groups of all the important variables for flow in porous media.

INSPECTIONAL ANALYSIS

The scaling criteria obtained from dimensional analysis of oil displacement from porous media are impossible to achieve in practice. Rapoport and Leas (6), recognizing the limitations of dimensional analysis, have used the inspectional analysis approach. They have evaluated the capillary

pressure effects in horizontal linear systems and derived differential equations permitting explicit evaluation of the effects. On the basis of theory and experiments, the product, $Lv\mu_w$, is proposed as a "scaling coefficient." Furthermore, by including the oil-water interfacial tension, σ and the contact angle, θ , Rapoport and Leas have proposed a "generalized scaling coefficient," $\sigma \cos \theta / Lv\mu_w$.

A more detailed development of scaling laws for use in design and operation of water-oil flow models has been reported by Rapoport (7). He has derived a differential equation which accounts explicitly for the viscous, gravitational and capillary forces in the simultaneous flow of two immiscible and incompressible fluids through a three-dimensional, homogeneous porous medium. Rapoport has proposed the following requirements for proper modelling of water-oil flow processes:

- 1) The prototype geometry (boundaries, well distribution, well penetration) must be reproduced in the model.
- 2) The initial fluid distribution, the succession and distribution of operations (water injections and oil withdrawals) must be the same for model and prototype.
- 3) The relative permeability functions and the

viscosity ratio, μ_o/μ_w must be the same for model and prototype.

- 4) The capillary pressure as a function of saturation must be proportional or linearly related in the model and prototype.
- 5) If there is direct proportionality between model and prototype capillary pressure functions, the pore size distributions are similar and the contact angle are the same for model and prototype. The design and operation of the model must satisfy the following "basic" scaling laws:

$$\left[\frac{q\mu_w}{L^2 K \Delta \rho} \right] \text{ model} = \left[\frac{q\mu_w}{L^2 K \Delta \rho} \right] \text{ prototype} \quad . \quad (2)$$

$$\left[\frac{q\mu_w}{L^2 K P_c} \right] \text{ model} = \left[\frac{q\mu_w}{L^2 K P_c} \right] \text{ prototype} \quad . \quad (3)$$

$$\left[\frac{K P_c^2}{\phi \sigma^2} \right] \text{ model} = \left[\frac{K P_c^2}{\phi \sigma^2} \right] \text{ prototype} \quad . \quad (4)$$

- 6) If the pore size distributions are not similar, the design and operation of the model must be conducted in accordance with the following expressions:

$$\left[\frac{q\mu_w}{L^2 K \Delta \rho} \right] \text{ model} = \left[\frac{q\mu_w}{L^2 K \Delta \rho} \right] \text{ prototype} \quad . \quad (5)$$

$$\left[q\mu_w / L K \frac{dP_c}{dS} \right] \text{ model} = \left[q\mu_w / L K \frac{dP_c}{dS} \right] \text{ prototype} \quad . \quad (6)$$

$$\left[K / \phi (\sigma \cos \theta)^2 \int_0^1 \frac{dS}{P_c^2} \right] \text{ model} = \left[K / \phi (\sigma \cos \theta)^2 \int_0^1 \frac{dS}{P_c^2} \right] \text{ prototype} \quad . \quad (7)$$

Equations (5) through (7) constitute Rapoport's "generalized" scaling laws. It should be noted that the generalized scaling laws have not found popular application.

Nielson and Tek (8) have evaluated the basic scaling laws of Rapoport with the use of computers. They have assumed a hypothetical reservoir and assigned typical properties to it. They also assumed a hypothetical model made of glass beads to which relative permeability and capillary pressure functions are assigned. Simplified equations describing two-dimensional systems were programmed for computation. The scaling laws are evaluated by comparing the results of the computations for the field situation with that of the model. One computation is made by assuming that the relative permeability and capillary pressure functions are identical in the model and prototype. The model predicts the saturation distribution in the hypothetical reservoir quite well. However, poor results are obtained when different relative permeability and capillary pressure functions are used.

Rapoport, Carpenter and Leas have applied the theory derived by Rapoport to study the performance of five-spot waterfloods. By neglecting gravity segregation, they have determined that the displacement of oil by water in a two-dimensional flow system is governed by the dimensionless

group, $\frac{q\mu_w}{\sigma\sqrt{K\phi}}$, designated as the capillary pressure coefficient. This statement implies that for a given value of the capillary pressure coefficient, all porous flow systems of a given geometry, operated under similar boundary conditions, and characterized by the same oil-to-water viscosity ratio and the same dimensionless flux, saturation and J-functions, will yield the same flooding behavior.

Rapoport et al have used models packed with 120-micron graded glass beads models, rendered preferentially oil-wet by dri-film treatment. All the flooding experiments are performed in the absence of connate water. The same relation between oil production and cumulative water injection was obtained for the model and prototype. In addition, they have reported that for a given porous medium there exists a critical value of the capillary pressure coefficient, above which waterfloods achieve stabilized displacement. The critical value of the scaling factor required to reach stabilized displacement behavior appears to decrease with increasing oil-water viscosity ratios.

Carpenter, Bail and Bobek (9) have verified Rapoport's basic scaling laws in heterogeneous communicating flow models. Two four-layer models, representing quadrants of five-spots are used in their studies. The models are geometrically similar and have the same glass-bead packing.

The investigators have concluded that the model can simulate the prototype performance very well. The highest oil recovery per unit of water injected was obtained at the lowest water injection rate where capillary forces are most important relative to gravitational and viscous forces.

The theory of inspectional analysis have been applied in the study of various reservoir engineering problems. Perkins (10) has investigated the role of capillary forces in laboratory waterfloods. Tests are carried out in lucite columns packed with unconsolidated sand. The value of the ratio of viscous to capillary forces, $q_{\mu_o} L / \sqrt{K\phi} f(\theta) J(S)$, is the same for model and prototype. It is found that the influence of capillary pressure gradients on the macroscopic flow of oil and water is minimized by using longer columns and/or higher injection rates. Also, the results of the experiments show that the residual oil saturation is independent of rate or column length. It can be inferred from this that the microscopic fluid distribution is controlled by capillary forces and is not rate sensitive.

Richardson and Perkins (11) have studied the effect of rate on oil recovery by waterflooding. The authors have used linear models packed with uniform sand. The models are designed and operated based on the following dimensionless parameters:

$$\frac{q_{\mu_o} L}{\sqrt{K\phi} f(\theta) J(S)}, \frac{K\Delta\rho g}{q_{\mu_o}}, \frac{\mu_w}{\mu_o}$$

Richardson and Perkins have concluded that "decreasing the rate at which water is injected into a thick homogeneous reservoir sand increases the tendency of the water to underrun the oil." It is also found that oil recovery is independent of rate of water advance with or without gas present and independent of the pressure level of the water-flood.

Craig, Geffen and Morse (12) have experimentally investigated oil recovery performance of models, using gas or water as displacing phase. The flow is essentially horizontal in the models made of consolidated sandstones and gravity was neglected. Because the primary interest in the study was the determination of flooding patterns, a time scaling factor is unnecessary. The models are operated so that

$$\left[\frac{q_i \mu_o L}{\sigma \cos \theta} \right]_{\text{model}} = \left[\frac{q_i \mu_o L}{\sigma \cos \theta} \right]_{\text{prototype}} \dots (8)$$

where q_i is the unit injection rate and L is the distance between producing and injection wells.

The scaling laws discussed thus far indicate that the relative permeability and capillary pressure relations must be the same functions of saturation in the model and prototype. Perkins and Collins (13) have attempted to remove this restriction by using a normalized saturation,

$$S' = \frac{S_w - S_{cw}}{1 - S_{ro} - S_{cw}} \quad . \quad (9)$$

where S_w is the water saturation, S_{cw} is the connate water saturation, and S_{ro} is the residual oil saturation, and

$$K'_w = \frac{K_w}{K_{wro}} \quad ; \quad K'_o = \frac{K_o}{K_{ocw}} \quad . \quad (10)$$

where K'_w and K'_o are the normalized relative permeabilities to water and oil respectively. K_w and K_o are the effective permeabilities to water and oil respectively, and K_{wro} is the permeability to water at residual oil saturation, and K_{ocw} is the permeability to oil at the connate water saturation.

The scaling criteria derived from this theory follow:

- 1) Dimensionless initial and boundary conditions must be the same in model and prototype.
- 2) K'_o , K'_w , and $J(S')$ must be the same functions of dimensionless saturation S' in the model and prototype. $J(S')$ is the dimensionless capillary pressure.
- 3) The following scaling groups must have the same values in model and prototype:

$$\mu_o/\mu_w, \quad \frac{\sigma K_{wro}}{q\mu_w h} (\phi/K)^{\frac{1}{2}} \quad \text{and} \quad \frac{K_{wro} \Delta \rho g L}{q\mu_w h}.$$

The application of this theory in the design and operation of scaled models is not found in the literature.

Inspectional analysis has been used also in the design and operation of models to study displacement of oil from porous media by miscible liquids. Offeringa and Van der Poel (14) have deduced scaling rules and checked their correctness by carrying out experiments in tubes of various sizes. These authors have studied the effect of oil-solvent viscosity ratio on the efficiency of the displacement process. The viscosity ratio studied ranged from 1.5 to 5,000. The results obtained suggest that model experiments on the displacement of oil by miscible liquid may not be carried out on too small a scale. Results with tubes of 1.60 and 3.00cm length are in good agreement, whereas those with a 1.03cm tube show appreciable deviation. The oil recovery decreases with increase in viscosity ratio. Furthermore, breakthrough recoveries obtained when flooding oils of different viscosities with kerosene as a solvent in unconsolidated sands are equal to those obtained in waterflooding.

Several factors influencing the efficiency of miscible displacement have been experimentally investigated by Blackwell, Rayne, and Terry (15). These factors include rate, mobility ratio, dimensions and gravity segregation effects on recovery.

It is found that the mixing between solvent and oil results principally from molecular diffusion which is the

dominant dispersion mechanism for reservoir conditions of rate, length and pore sizes. In horizontal reservoirs, recovery at breakthrough decreased as mobility ratio increased and the volume of solvent required for complete recovery of the oil increases as the mobility ratio increases. In addition, the study shows that the formation of channels is due to viscous fingering, gravity segregation and variations in permeability. Channeling and bypassing of oil will occur in horizontal reservoirs, even in homogeneous sands.

Blackwell (16) has studied microscopic dispersion phenomena in miscible displacement. Mixing both in the direction of and perpendicular to the direction of mean flow was measured in sand-packed columns. Both longitudinal and lateral mixing are governed by molecular diffusion at low rates and by convection at high rates. The transverse mixing should be scaled in the direction of the thickness of the reservoir.

Pozzi and Blackwell (17) have evaluated the relative importance of various mechanisms affecting miscible displacement. The authors have attempted to ascertain whether the essential features of the displacement process can be simulated even though some scaling groups are not satisfied. These studies are performed with completely miscible systems in linear, horizontal models packed with unconsolidated

media. However, for a two-dimensional system, where longitudinal mixing is unimportant, the relaxed criteria are as follows:

- 1) The ratio L/h , need not be scaled so long as

$$\frac{v_{\mu_o} L}{K_x \Delta \rho g h} < C_u \quad . . . (11)$$

- 2) The viscous-gravity ratio must be identical in model and prototype when

$$\frac{v_{\mu_o} L}{K_x \Delta \rho g h} < C_L \quad . . . (12)$$

the viscous-gravity ratio need not be scaled when

$$C_L < \frac{v_{\mu_o} L}{K_x \Delta \rho g h} < C_u$$

where C_L and C_u are lower and upper limits of viscous-gravity ratio. They must be determined experimentally.

- 3) Boundary and initial conditions must be the same in model and prototype.
- 4) Dimensionless fluid properties must be congruent functions of concentration in model and prototype.
- 5) The transverse mixing group ($K_t L / v_a h^2$) must be identical in model and prototype. K_t - effective transverse dispersion coefficient and

$$v_a = v / (1 - S_{wc}) \phi. \quad . . . (13)$$

Good agreement of dimensionless solvent penetration and effluent composition shows that equivalent model performance

is obtained even though $v\mu_o L/K_x \Delta\rho gh$ is unscaled. The results are for viscosity ratio of 1.85, 7.4 and 16.3.

DIMENSIONAL-INSPECTIONAL ANALYSIS

Geertsma, Croes and Schwarz (18) have proposed a method which combines the theories of both dimensional and inspectional analyses. The derivation of the dimensionless groups by this method is carried out by means of the basic equations (inspectional analysis). The resulting set of groups are subsequently completed by means of dimensional analysis. Geertsma et al have derived dimensionless groups for three types of displacements, viz, cold water drive, hot water drive and solvent injection.

The scaling criteria proposed by the authors for waterfloods are listed below:

- 1) The model and prototype are geometrically similar and have similar initial and boundary conditions.
- 2) The model and prototype have the same relative permeability and capillary pressure saturation functions.
- 3) The values of the following groups must be the same in model and prototype.

$$\frac{\mu_o}{\mu_w}, \frac{\Delta\rho gK}{\mu_w v}, \frac{\sigma \cos \theta \sqrt{K\phi}}{\mu_w vL} \text{ and } \frac{\rho_w vK^{\frac{1}{2}}}{\mu_w}$$

This set of scaling criteria developed by Geertsma et

al is termed inspectional-dimensional analysis in this thesis. The dimensionless groups consist of the same variables as those derived from the application of dimensional or inspectional analysis. Although the validity of this theory has not been experimentally tested, it could be inferred that a model designed and operated according to these scaling criteria will simulate the prototype performance with about the same accuracy as those criteria developed by means of dimensional or inspectional analysis.

COMPARISON OF SCALING THEORIES

A great many scaling theories have been presented. It is the purpose of this section to reduce the theories presented in this chapter to a common presentation so that they can be compared.

Table 1 presents a summary of dimensionless groups proposed by various investigators based on dimensional analysis. The groups derived by Leverett et al and Engelbert and Klinkenberg for immiscible systems are essentially the same except for the combination of the variables which constitute these groups. The diffusion coefficient in miscible displacement replaces capillary pressure in immiscible displacement process. The theory of dimensional analysis requires that dimensionless parameters common to model and prototype

must be the same. Thus the porosities of the model and prototype material must be identical.

TABLE 1 Scaling Groups from Dimensional Analysis

<u>Investigators</u>	<u>Dimensionless Groups</u>
Leverett, Lewis and Truce (1942)	$\frac{\mu_o}{\mu_w}, \frac{*\Delta\rho}{\Delta\rho^r}, \frac{q_t}{q_t^r}, \frac{P_c}{P_c^r}, \frac{L}{L^r}$
Engelbert and Klinkenberg (1951)	$\frac{\mu_o}{\mu_w}, \frac{L}{h}, \frac{L_s}{K^{\frac{1}{2}}}, \frac{\Delta\rho g K}{v\mu_w}, \frac{\Delta\rho g L K^{\frac{1}{2}}}{\sigma \cos \theta}$
Greenkorn (1964)	$\frac{\mu_o}{\mu_w}, \frac{L}{d}, \frac{\rho_o}{\rho_s}, \frac{D_o}{D_s}, \frac{\rho g K}{\mu v}, \frac{D_o}{dv}, \frac{tv}{d}, \frac{KP}{\mu dv}$

*The variables characterizing the model is primed.

The dimensionless groups developed by several authors using inspectional analysis are summarized in Table 2. Most of the groups are stated in terms of the ratios of the significant forces in the model and prototype. These ratios are essentially the same despite the approaches used in their derivation. Differences are obtained if the initial and boundary conditions of the particular problem under study are incorporated into the general differential equation.

The scaling criteria for similitude can be stated with reference to the variables in Table 2:

- 1) The geometry of model and prototype must be the same.

TABLE 2 Scaling Groups from Inspectional Analysis

<u>Investigators</u>	<u>Dimensionless Groups</u>
Rapoport and Leas (1953)	$L/h, \mu_o/\mu_w, Lv\mu_w, \frac{\sigma \cos \theta}{Lv\mu_w}$
Rapoport (1955)	$L/h, \mu_o/\mu_w, \frac{q\mu_w}{L^2K\Delta\rho}, \frac{q\mu_w}{L^2KP_c}, \frac{KP_c^2}{\phi\sigma^2}$
Rapoport, Carpenter, and Leas (1958)	$L/h, \mu_o/\mu_w, \frac{q\mu_w}{\sigma(K\phi)^{1/2}}$
Perkins (1957)	$L/h, \frac{\mu_o}{\mu_w}, \frac{q\mu_o L}{\sqrt{K\phi}f(\theta)J(S)}$
Richardson and Perkins (1957)	$L/h, \frac{\mu_o}{\mu_w}, \frac{q\mu_o L}{\sqrt{K\phi}f(\theta)J(S)}$
Craig, Geffen and Morse (1955)	$\frac{\mu_o}{\mu_w}, \frac{q_i\mu_o L}{\sigma \cos \theta}$
Perkin and Collins	$L/h, \frac{\mu_o}{\mu_w}, \frac{\sigma K_{wro}}{q\mu_w h} \left(\frac{\phi}{K}\right)^{1/2}, \frac{K_{wro} \Delta\rho g L}{q\mu_w h}$
*Geertsma, Croes, and Schwarz (1956)	$L/h, \frac{\mu_o}{\mu_w}, \frac{\Delta\rho g K}{\mu_w v}, \frac{\sigma \cos \theta \sqrt{K\phi}}{\mu_w v L}, \frac{\rho_w v K^{1/2}}{\mu_w}$
Offeringa and Van der Poel (1954)	$\frac{L}{d}, \frac{\mu_o}{\mu_s}, \frac{\rho_o}{\rho_s}, \frac{\rho_o g K d^2}{q\mu_o}, \frac{q}{D_o d}, \frac{D_o}{D_s}$
Blackwell, Rayne, and Terry (1959)	$\frac{L}{h}, \frac{\mu_o}{\mu_s}, \frac{KA\Delta\rho \sin\alpha}{q\mu}, \frac{L^2}{Kt}$
	K - effective dispersion coefficient

*Inspectional-Dimensional Analysis

- 2) Initial and boundary conditions must be similar in model and prototype.
- 3) The viscosity ratio, μ_o/μ_w , must be the same in model and prototype.
- 4) The permeability-saturation functions must be identical in model and prototype. Different authors have defined scaled permeability and saturation differently. Capillary pressure-saturation functions also must be the same.
- 5) The ratio of the pertinent forces must be the same in model and prototype.

The comparison of the scaling theories has shown that very little difference exist among the theories derived, whether applying dimensional and/or inspectional analysis. The number of dimensionless groups and their combinations depend on the particular conditions studied by the various authors. The selection of the dimensionless groups is important from the standpoint of being able to satisfy the similitude requirements in practical applications.

Chapter III

THEORETICAL ANALYSIS

DIMENSIONAL ANALYSIS

A detail discussion of the theory of dimensional analysis has been presented by Langhaar (19). The first step in the dimensional analysis of a problem is to ascertain which variables are relevant to the problem. The variables are then combined into several dimensionless groups or π -terms by the application of Buckingham's pi-theorem. The pi-theorem states that the minimum number of dimensionless groups in a complete set is equal to the total number of variables minus the number of fundamental dimensions, e.g. mass, length and time.

From an inspection of Darcy's law and the continuity equation it is assumed that the displacement of oil by water from porous media is controlled by the following variables:

- 1) Geometrical dimensions
 - a) distance between injection and production wells, L [L]
 - b) sand thickness, h [L]
 - c) angle of dip of the formation, α [dimensionless]
- 2) Rock properties
 - a) specific permeability, K [L^2]

- b) porosity, ϕ [dimensionless]
- 3) Dynamic flow characteristic
 - a) velocity of fluid movement, v [L/T]
- 4) Fluid properties
 - a) viscosities of oil and water, μ_o, μ_w [M/LT]
 - b) density difference between the oil and water phase, $\Delta\rho g$ [M/L²T²]
 - c) interfacial characteristics, $\sigma \cos \theta$ [M/T²]

The functional relationship between these variables is expressed by

$$F(L, h, \alpha, K, \phi, v, \mu_w, \mu_o, (\Delta\rho)g, \sigma \cos \theta) = 0 \dots (14)$$

Applying the principle of dimensional homogeneity and using the mass, length, time system of fundamental dimensions:

$$M^0 L^0 T^0 \underline{d} L^{a_1} h^{a_2} K^{a_3} v^{a_4} \mu_w^{a_5} \mu_o^{a_6} (\Delta\rho g)^{a_7} (\sigma \cos \theta)^{a_8} \phi^0 \alpha^0 \dots (15)$$

where a_1, a_2, \dots, a_8 are constants.

Substituting the fundamental dimensions into equation (15)

$$M^0 L^0 T^0 \underline{d} (L)^{a_1} (L)^{a_2} (L^2)^{a_3} (LT^{-1})^{a_4} (ML^{-1}T^{-1})^{a_5} \\ * (ML^{-1}T^{-1})^{a_6} (ML^{-2}T^{-2})^{a_7} (MT^{-2})^{a_8} \dots (16)$$

$$M^0 L^0 T^0 \underline{d} M^{a_5+a_6+a_7+a_8} L^{a_1+a_2+2a_3+a_4-a_5-a_6-2a_7} \\ * T^{-a_4-a_5-a_6-2a_7-2a_8} \dots (17)$$

Equate the exponents of M, L and T

$$\begin{aligned} \text{M: } a_5 + a_6 + a_7 + a_8 &= 0 \\ \text{L: } a_1 + a_2 + 2a_3 + a_4 - a_5 - a_6 - 2a_7 &= 0 \\ \text{T: } -a_4 - a_5 - a_6 - 2a_7 - 2a_8 &= 0 \end{aligned} \quad . \quad (18)$$

Solving equation (18) simultaneously gives

$$\begin{aligned} a_1 &= -a_2 - 2a_3 + 2a_7 \\ a_5 &= -a_6 - a_7 - a_8 \\ a_4 &= -a_7 - a_8 \end{aligned} \quad . \quad (19)$$

Substitution of equation (19) into equation (15) yields

$$M^0 L^0 T^0 \underline{d} L^{(-a_2 - 2a_3 + 2a_7)} h^{a_2} K^{a_3} v^{(-a_7 - a_8)} *_{\mu_w}^{(-a_6 - a_7 - a_8)} \mu_o^{a_6} (\Delta \rho g)^{a_7} (\sigma \cos \theta)^{a_8} \phi^0 \alpha^0 . . . (20)$$

$$M^0 L^0 T^0 \underline{d} (hL^{-1})^{a_2} (KL^{-2})^{a_3} (\mu_o \mu_w^{-1})^{a_6} (L^2 v^{-1} \mu_w^{-1} \Delta \rho g)^{a_7} (v^{-1} \mu_w^{-1} \sigma \cos \theta)^{a_8} \phi^0 \alpha^0 . . . (21)$$

The dimensionless scaling groups from equation (21) are:

$$\pi_1 = h/L \quad . . . (22)$$

$$\pi_2 = K/L^2 \quad . . . (23)$$

$$\pi_3 = \mu_o / \mu_w \quad . . . (24)$$

$$\pi_4 = \frac{L^2 \Delta \rho g}{v \mu_w} \quad . . . (25)$$

$$\pi_5 = \frac{\sigma \cos \theta}{v \mu_w} = \frac{\sigma}{v \mu_w} \quad (\text{waterwet systems } \theta = 0) \quad . . . (26)$$

INSPECTIONAL ANALYSIS

Ruark (20) has introduced inspectional analysis to supplement dimensional analysis. In inspectional analysis, all equations describing the process of interest are combined to form a single differential equation. The coefficients of this equation or their combinations constitute the dimensionless scaling groups. In this section, the differential equation for incompressible flow of two immiscible fluids in porous media is derived and the following assumptions are made:

- 1) Darcy's law is valid.
- 2) The displaced and the displacing fluids are immiscible and incompressible.
- 3) The physical properties of the fluids and medium are constant with time and space.
- 4) The medium is homogeneous and isotropic.

The generalized form of Darcy's equation for multiphase flow can be expressed as:

$$v_i = -K \frac{K_{ri}}{\mu_i} \Delta\phi_i \quad \dots (27)$$

where

i = subscript denoting wetting or nonwetting phase

v_i = velocity vector, cm/sec

K_{ri} = relative permeability

K = absolute permeability, darcies

- μ_i = viscosity, cp
 Φ_i = $P_i + \rho_i gz$ = potential
 ρ_i = density, gm/cc
 P_i = pressure, atm
 g = gravitational constant, cm/sec²
 z = height above datum, cm.

Writing equation (27) for the nonwetting and wetting phases

$$v_o = - \frac{KK_{ro}}{\mu_o} \nabla(P_o + \rho_o gz) \quad \dots (28)$$

$$v_w = - \frac{KK_{rw}}{\mu_w} \nabla(P_w + \rho_w gz) \quad \dots (29)$$

It is convenient to eliminate the pressure gradients for each phase in favor of the capillary pressure gradient. Also it is expedite to eliminate the velocity of each phase and replace them by their combined total velocity.

$$\nabla P_o = - \frac{v_o \mu_o}{KK_{ro}} - \nabla(\rho_o gz) \quad \dots (30)$$

$$\nabla P_w = - \frac{v_w \mu_w}{KK_{rw}} - \nabla(\rho_w gz) \quad \dots (31)$$

The capillary pressure gradient is expressed by

$$\nabla P_c = \nabla P_o - \nabla P_w \quad \dots (32)$$

and the substitution of equation (30) and (31) into equation (32) yields

$$\nabla P_c = \frac{\mu_w}{KK_{rw}} (v_w - v_o \frac{K_{rw} \mu_o}{K_{ro} \mu_w}) + \nabla[(\rho_w - \rho_o)gz] \quad \dots (33)$$

From the assumption of incompressible fluids

$$\mathbf{v} = \mathbf{v}_o + \mathbf{v}_w \quad \dots (34)$$

Letting $\Delta\rho = \rho_w - \rho_o$ and substituting equation (34), equation (33) may be rearranged so that

$$\mathbf{v}_o = \mathbf{v} \left[1 + \frac{K_{rw}\mu_o}{K_{ro}\mu_w} \right]^{-1} + \frac{KK_{rw}}{\mu_w} \left[\nabla(\Delta\rho g z) - \nabla P_c \right] \left[1 + \frac{K_{rw}\mu_o}{K_{ro}\mu_w} \right]^{-1} \quad \dots (35)$$

For convenience, let

$$\psi = \left[1 + \frac{K_{rw}\mu_o}{K_{ro}\mu_w} \right]^{-1} \quad \dots (36)$$

$$\lambda = K_{rw}\psi \quad \dots (37)$$

ψ and λ are functions of the relative permeabilities of the wetting and nonwetting phase only when the viscosities are specified.

The substitution of equations (36) and (37) into (35) yields

$$\mathbf{v}_o = \mathbf{v}\psi + \frac{K\lambda}{\mu_w} [\nabla(\Delta\rho g z) - \nabla P_c] \quad \dots (38)$$

The models used in this study are considered three-dimensional and writing equation (38) for the three axes, x , y , and z gives the following:

$$v_{ox} = v_x \psi - \frac{K}{\mu_w} \lambda \nabla P_c \quad \dots (39)$$

$$v_{oy} = v_y \psi - \frac{K}{\mu_w} \lambda \nabla P_c \quad \dots (40)$$

$$v_{oz} = v_z \psi + \frac{K}{\mu_w} \lambda [\nabla(\Delta\rho g z) - \nabla P_c] \quad \dots (41)$$

The continuity equation for incompressible fluid is expressed by

$$\nabla \cdot \mathbf{v} = \frac{\partial v_{ox}}{\partial x} + \frac{\partial v_{oy}}{\partial y} + \frac{\partial v_{oz}}{\partial z} = - \phi \frac{\partial S_w}{\partial t} \quad \dots (42)$$

where t -time.

The expansion of the terms of equation (39) gives

$$\begin{aligned}\frac{\partial v_{ox}}{\partial x} &= v_x \frac{\partial \psi}{\partial x} - \frac{K}{\mu_w} \frac{\partial}{\partial x} \left(\lambda \frac{dP_c}{dS_w} \frac{\partial S_w}{\partial x} \right) \\ &= v_x \frac{\partial S_w}{\partial x} \frac{d\psi}{dS_w} - \frac{K}{\mu_w} \frac{\partial}{\partial x} \left(\lambda \frac{dP_c}{dS_w} \frac{\partial S_w}{\partial x} \right) \dots (43)\end{aligned}$$

Similarly,

$$\frac{\partial v_{oy}}{\partial y} = v_y \frac{\partial S_w}{\partial y} \frac{d\psi}{dS_w} - \frac{K}{\mu_w} \frac{\partial}{\partial y} \left(\lambda \frac{dP_c}{dS_w} \frac{\partial S_w}{\partial y} \right) \dots (44)$$

$$\begin{aligned}\frac{\partial v_{oz}}{\partial z} &= v_z \frac{\partial S_w}{\partial z} \frac{d\psi}{dS_w} - \frac{K}{\mu_w} \frac{\partial}{\partial z} \left(\lambda \frac{dP_c}{dS_w} \frac{\partial S_w}{\partial z} \right) + \frac{K\Delta\rho g}{\mu_w} \frac{\partial \lambda}{\partial z} \\ &\dots (45)\end{aligned}$$

$$\text{when } \frac{\partial v_x}{\partial x} = \frac{\partial v_y}{\partial y} = \frac{\partial v_z}{\partial z} = 0. \dots (46)$$

Upon substitution of equations (43) through (45) into (42) the differential equation describing the system can be written thus:

$$\begin{aligned}\phi \frac{\partial S_w}{\partial t} + \left(v_x \frac{\partial S_w}{\partial x} + v_y \frac{\partial S_w}{\partial y} + v_z \frac{\partial S_w}{\partial z} \right) \frac{d\psi}{dS_w} - \frac{K}{\mu_w} \frac{\partial}{\partial x} \left(\lambda \frac{dP_c}{dS_w} \frac{\partial S_w}{\partial x} \right) \\ - \frac{K}{\mu_w} \frac{\partial}{\partial y} \left(\lambda \frac{dP_c}{dS_w} \frac{\partial S_w}{\partial y} \right) - \frac{K}{\mu_w} \frac{\partial}{\partial z} \left(\lambda \frac{dP_c}{dS_w} \frac{\partial S_w}{\partial z} \right) + \frac{K\Delta\rho g}{\mu_w} \frac{\partial \lambda}{\partial z} = 0. \dots (47)\end{aligned}$$

Equation (47) expresses the relationship between the rate of accumulation of water in a volume element and the effects of viscous, capillary and gravitational forces on flow of two phases at the point and time interval of interest. This equation cannot be solved by known methods. However, it is useful in the development of scaling criteria by inspectional

analysis, because the coefficients of this equation can be combined to form the similarity groups.

The normalized total velocities along the three principal axes are obtained by dividing each by the total velocity, v_t :

$$\bar{v}_x = \frac{v_x}{v_t}, \quad \bar{v}_y = \frac{v_y}{v_t} \quad \text{and} \quad \bar{v}_z = \frac{v_z}{v_t}. \quad \dots (48)$$

Similarly the normalized distance variables are obtained by dividing each by its corresponding characteristic length:

$$\bar{x} = \frac{x}{\ell}, \quad \bar{y} = \frac{y}{w} \quad \text{and} \quad \bar{z} = \frac{z}{h} \quad \dots (49)$$

where ℓ , and w are length and width of the model respectively.

Leverett defined the capillary pressure function as:

$$P_c = \frac{\sigma \cos \theta}{(K/\phi)^{1/2}} J(S_w) \quad \dots (50)$$

For water-wet systems, $\cos \theta = 1$ and equation (50) becomes:

$$P_c = \sigma (\phi/K)^{1/2} J(S_w) \quad \dots (51)$$

$$\text{and} \quad \frac{dP_c}{dS_w} = \sigma (\phi/K)^{1/2} \frac{d}{dS_w} J(S_w) \quad \dots (52)$$

Multiplying equation (47) through by $\frac{L'}{v_t}$ and substituting equations (48), (49) and (52) results in:

$$\begin{aligned} & \frac{\phi L'}{v_t} \frac{\partial S_w}{\partial t} + L' \left(\frac{v_x}{\ell} \frac{\partial S_w}{\partial \bar{x}} + \frac{v_y}{w} \frac{\partial S_w}{\partial \bar{y}} + \frac{v_z}{h} \frac{\partial S_w}{\partial \bar{z}} \right) \frac{d\psi}{dS_w} \\ & - \frac{\sigma (K\phi)^{1/2}}{v_t \mu_w} \left\{ \frac{L'}{\ell} \frac{\partial}{\partial \bar{x}} \left(\lambda \frac{dJ(S_w)}{dS_w} \frac{\partial S_w}{\partial \bar{x}} \right) + \frac{L'}{w} \frac{\partial}{\partial \bar{y}} \left(\lambda \frac{dJ(S_w)}{dS_w} \frac{\partial S_w}{\partial \bar{y}} \right) + \frac{L'}{h} \frac{\partial}{\partial \bar{z}} \left(\lambda \frac{dJ(S_w)}{dS_w} \frac{\partial S_w}{\partial \bar{z}} \right) \right\} \\ & + \frac{K \Delta \rho g L'}{v_t \mu_w h} \frac{\partial \lambda}{\partial \bar{z}} = 0 \end{aligned}$$

From the theory of inspectional analysis, the parameters of the foregoing equation correspond to the π -terms developed in the section on dimensional analysis. Thus the similarity groups are:

$$\begin{aligned}
 \text{I.} & \quad \frac{L'\phi}{v_t t} \\
 \text{II.} & \quad \frac{L'}{L^*} ; \text{ i.e. } \frac{L'}{\ell} , \frac{L'}{w} , \frac{L'}{h} \\
 \text{III.} & \quad \frac{\sigma(K\phi)^{\frac{1}{2}}}{v_t \mu_w L^*} \\
 \text{IV.} & \quad \frac{K\Delta\rho g L'}{v_t \mu_w h} \\
 \text{V.} & \quad \frac{\mu_o}{\mu_w}
 \end{aligned}$$

where L^* - some characteristic length.

Other similarity groups can be obtained by either multiplying or dividing one group by the other. For example, the division of the third group by the fourth yields the ratio of capillary to gravity forces.

The scaling criteria for the system under study, therefore, may be summarized as follows:

- 1) The geometry of model and prototype must be the same: The length to width ratio, L'/w , and length to thickness ratio, L'/h , must have the same numerical value in model and prototype.
- 2) Initial and boundary conditions must be similar in model and prototype.

- 3) The ratio of capillary to viscous forces must be similar in model and prototype.
- 4) The ratio of gravity to viscous forces must be similar in model and prototype.
- 5) The ratio of gravity to capillary forces in model and prototype must be equal.
- 6) The viscosity ratio must be the same in model and prototype.
- 7) The relation between times for the same fraction of pores volumes to be injected or produced must be the same for model and prototype.

The models employed in this study were operated according to condition (7) above and for each liquid model I and III satisfy the foregoing scaling criteria.

A comparison of the dimensionless groups developed by means of dimensional and inspectional analysis shows that both analyses yield the same scaling criteria. For example, the multiplication of equation (23) by equation (25) gives $\frac{\Delta\rho gK}{v\mu_w}$ - corresponding to condition (4) above. It may be recognized that the other conditions listed under inspectional analysis could be obtained by some combinations of the various π -terms under dimensional analysis. However, the physical meaning of the dimensionless groups, as derived by inspectional analysis, is generally more apparent than

that of the groups derived by dimensional analysis.

Chapter IV

EXPERIMENTAL WORK

The experimental work performed in this thesis is described under the headings: Apparatus, Materials and Procedure.

APPARATUS

Three rectangular physical models were constructed with 1 inch thick plexiglass (lucite). The internal dimensions of the models are shown in Table 3.

TABLE 3 Internal Dimensions of the Models

	Length, Ft.	Width, Ft.	Thickness, Ft.
Model I	2.0	1.5	0.25
Model II	4.0	3.0	0.25
Model III	4.0	3.0	0.50

The sides of the models, except the top were screwed and glued together with catalyzed cement PS-30. The top was held down with 1/2 inch screws spaced 2 inches apart. A quarter of 3/8 inch bores at the corners of the boxes served

either as producing or injection wells. The models were braced with 1 inch by 2 inches rectangular tubing beams, spaced 6 inches apart, to prevent buckling of its sides when pressurized. A maximum pressure of 50psi was used in the selection of the size of the beams and their spacing. Generally, experiments were carried out with pressures less than 20psig.

An A-frame and a block and tackle arrangement was employed to maneuver the models into a vertical position during compaction and saturation of the sand pack with liquids lighter than water.

A Wallace and Tiernan double simplex pump, Series 150A, supplied the constant liquid flow through the sand packs. A Nupro 60-micron in-line filter screened out all solid particles from the liquids prior to entering the sand packs. A Celesco electrical differential pressure (DP) transducer Model KP15 with a carrier-demodulator Model CD10 measured the differential pressure between the injection and producing wells. The electrical output from the Celesco carrier-demodulator was recorded on a Honeywell Electronik 194 recorder. In addition to this electrical arrangement, four 4 inch 0-50psig Master-gauge pressure gauges were connected to each well as a check of the Celesco arrangement. All pressure gauges were calibrated with a mercury manometer

before any run was performed in each model.

The fractions of the displacing and displaced fluids produced during the miscible runs were determined by means of a two-electrode specific conductance measurement system. This system comprised of two electrodes of copper screen, soldered at two points across a short tube connected to the producing wells, a Triplet Electrical Company specific conductance meter and the Honeywell Elektronik 194 recorder. The conductance meter measured the conductivity of the liquid flowing through the tube and its output was recorded on the recorder. The linearity between conductivity and salinity was established. (figure 1)

The setup of the equipment is illustrated by Figure 2.

MATERIALS

The models were packed with 60-100 mesh sand. The sand was treated with 0.1 hydrogen equivalent chromic acid to ensure that it was water-wet before each run.

The displacing fluid used in all runs was salt water with a salinity of 10,000 ppm NaCl. The salt water was colored with Durkee red food dye manufactured by Smith Corona Machines. The red coloration facilitated the tracing of the displacement fronts until breakthrough.

In the miscible runs, fresh water and a 50-50 percent

mixture of glycerine and fresh water represented the oil. The oil was simulated by three liquids--kerosene, soltrol 220, and n-hexane, in the displacement runs.

PROCEDURE

The experimental procedure is divided into three groups. The groups are as follows:

- 1) Physical properties of the fluids and sand
- 2) Calibration runs
- 3) Displacement runs.

1. PHYSICAL PROPERTIES OF THE FLUIDS AND SAND

The physical properties of the fluids, such as density, dynamic viscosity and surface tension, were measured at room temperature of 78°F, using standard procedures. Table 4 shows the results of these measurements.

The porosity of each sand pack was measured by volumetric method. The models were maneuvered into a vertical position, tapped and rocked in order to obtain uniform compaction. An average porosity of 0.31 was obtained. The maximum variation in the value of the porosities in the models was less than 0.64%. The pore volume of Model I was one-fourth and one-eighth of the pore volume of Model II and Model III respectively.

TABLE 4 Fluids and Sand Properties

	Viscosity (cps)	Oil-Water Viscosity Ratio	Density (gm/cc)	Density Difference (gm/cc)	Surface Tension (dyne/cm ²)
Hexane	0.302	0.34	0.67	0.33	24.46
Kerosene	1.55	1.76	0.81	0.19	31.90
Soltrol	3.90	4.43	0.80	0.20	33.90
Glycerine- Water	6.98	7.93	1.15	-0.15	74.33
Water	0.88	1.0	1.0	-	82.10

Sieve Analysis:

	80 mesh	100 mesh	120 mesh	140 mesh	160 mesh
Percent larger than	82.75	8.59	4.6	2.47	1.59

Absolute permeability to water determined from linear cell = 11.375 darcies.

The absolute permeability of the sand to water was measured in a linear cylindrical tube packed to the same compaction as the models. The tube was 1 ft. long with a diameter of 2 in. An absolute permeability of 11.375 darcies

was obtained. This value of absolute permeability was adopted since the values obtained from direct measurements in the models and the application of Muskat's equation (21) were obviously wrong; absolute permeability calculated from Muskat's equation are 2.0, 2.15 and 0.936 darcies for Model I, Model II and Model III respectively.

2. CALIBRATION RUNS

Two injection rates were used in these runs. The rates were selected based on the scaling criterion:

$$\left[\frac{\phi L}{v_t t} \right]_{\text{model}} = \left[\frac{\phi L}{v_t t} \right]_{\text{prototype}} \quad \dots (54)$$

and the magnitude of injection rates encountered in oil fields waterflood operations. The criterion, expressed by equation (54) and derived earlier, stipulates that the time (t) equivalent to pore volume throughput be equal in model and prototype. Since the velocity of the front could not be determined until a particular run has been accomplished, the time required to inject one pore volume of water was considered fixed and the corresponding injection rate calculated. For example, injecting at 21.5 cc/min, the water fronts in the models should move with the same velocity if:

$$\left[\frac{PV}{21.5} \right]_{\text{Model I}} = \left[\frac{PV}{q_2} \right]_{\text{Model II}} = \left[\frac{PV}{q_3} \right]_{\text{Model III}} \quad \dots (55)$$

Using equation (55), the injection rates in Model II and

Model III were determined. The values thus obtained and their field equivalents are presented in Table 5.

TABLE 5 Water Injection Rates

	Low Rate		High Rate	
	Lab (cc/min)	Field Equiv. (B/D/ft./well)	Lab (cc/min)	Field Equiv. (B/D/ft./well)
Model I	21.5	3.117	45.0	6.523
Model II	86.0	12.467	180.0	26.093
Model III	172.0	24.933	360.0	52.186

Subsequent runs justified the above assumption that the water fronts moved with the same velocity.

Before each calibration run the sand packs were evacuated of air by several hours of continuous vacuuming. If any air was left after vacuuming, it was in solution with water during the run. The sand packs were 100 percent saturated with the oil phase and then flushed with colored (dyed) salt water at a preset injection rate. The position of the water front was traced at fixed time intervals. The conductance measurement of the effluent liquid enabled the

rates of production of the displacing and displaced fluids to be determined.

While water was used as the oil phase in the first calibration run, a 50-50 percent mixture of glycerine and water represented the oil phase in the second calibration run. The glycerine-water mixture could only be displaced at the low injection rates because at high rates the pressures in the model were very high and the model started leaking. The results obtained from the runs are presented in the Appendix.

These runs were carried out for calibration purposes and to provide some basis of comparison with the results from the displacement runs.

3. DISPLACEMENT RUNS

After the calibration runs were accomplished the sand-packs were cleansed of coloration and saturated with a liquid representing the oil phase.

Percent oil in place in each model was determined by means of volumetric balance. The tanks holding the liquids were calibrated by filling them with known volumes and measuring the height of the liquid. The tanks had large cross-sectional areas. For example, a height of 1 in. in the water tank corresponded to 4.29 litres. Thus variations

in the volume measurements were inevitable. The variations were larger still, since a 100 mL, represented 1.9%, 0.47% and 0.24% of the pore volume of Model I, Model II and Model III respectively. Table 6 shows the variations in initial water saturations.

TABLE 6 Initial Water Saturations

	Hexane	Kerosene	Soltrol
Model I:			
High Rate	0.24	0.17	0.20
Low Rate	0.30	0.25	0.22
Model II:			
High Rate	0.27	0.25	0.18
Low Rate	0.27	0.25	0.20
Model III:			
High Rate	0.26	0.20	0.20
Low Rate	0.20	0.20	0.20
Average S_{wi}	0.26	0.215	0.20
Standard Deviation	0.031	0.0283	0.0186

Since the scaling theories require that the same initial conditions exist in the model and prototype, an attempt was made to reduce the variations in initial saturations to their minima.

However, after three days of continuous saturation of Model I with hexane, water was still being produced. Because of the number of runs, the sizes of the models and time constraints, irreducible water saturation before each displacement run was not attained.

After saturating the sand pack, the oil phase was displaced with colored salt water at the high injection rate. The run was continued until two pore volumes of water had been injected or no oil was produced, whichever came first. The sand pack was cleansed of coloration and resaturated for another run with the low injection rate. The sand-pack was left to sit for 24 hours after each saturation with the oil phase. This was an attempt to allow the oil and water phases to attain equilibrium.

It was difficult to completely cleanse the sand-packs of the liquids representing the oil phase especially in the bigger models. To avert this difficulty the models were repacked with new sand for subsequent runs with other liquids.

In all the displacement runs the rates of production of the oil and water phase were recorded and the movement of

the fronts were traced. The data obtained are enclosed in the Appendix.

Chapter V

EXPERIMENTAL RESULTS AND DISCUSSIONS

A total of twenty-five runs were performed in three models. Nineteen of these runs were data runs while the remaining were calibration runs. Table 7 is a summary of these runs.

TABLE 7 Summary of Runs

Water Displacing	Model I		Model II		Model III	
	High Rate	Low Rate	High Rate	Low Rate	High Rate	Low Rate
Hexane	1	1	1	1	1	1
Kerosene	1	1	1	1	1	1
Soltrol	1	2	1	1	1	1
*Glycerine-Water	0	1	0	1	0	1
*Fresh Water	1	0	1	0	1	0

*Calibration runs.

The raw data obtained from the experiments are included in the Appendix. These data were analysed and plots of

oil recovery and water-oil ratio as functions of pore volume throughput are presented. Oil recoveries as percent of initial oil in place at water breakthrough, 1 PV, 1.5 PV and 2.0 PV throughput are presented in Table 8. Table 7 and 8 are included as quick references for determining the number of runs made in each model and the corresponding oil recoveries at the various volumes of water throughput.

REPRODUCIBILITY OF RESULTS

Two runs were made using soltrol and water in Model I to test reproducibility of the data. Figure 3 compares the results of these runs. The data points coincided until water breakthrough, thereafter, the difference in oil recovery (HCPV) gradually increased to a maximum of 5% at two pore volumes of water throughput. The initial oil saturations were 0.22 and 0.20 in the first and repeated runs respectively.

EFFECT OF MODEL DIMENSIONS

The theoretical analysis developed in Chapter III stipulates that the geometry of the model and prototype must be the same. That is, the diagonal length to length ratio, the diagonal length to width ratio and the diagonal length to thickness ratio must be the same in model and prototype.

The diagonal length to length ratios are the same in

TABLE 8

Oil Recovery, %OIP, from the Respective Models
and Liquids

	Model I		Model II		Model III	
	High Rate	Low Rate	High Rate	Low Rate	High Rate	Low Rate
<u>Hexane:</u>						
Breakthrough	66.50	66.68	66.33	65.33	67.49	67.50
1.0PV	68.67	75.60	69.0	75.0	69.0	75.0
<u>Kerosene:</u>						
Breakthrough	70.0	70.0	69.90	70.00	70.00	70.12
1.0PV	77.0	80.99	78.0	80.67	77.50	78.83
1.5PV	78.0	82.33	78.33	81.33	78.33	80.35
2.0PV	78.32	82.46	78.39	81.61	78.78	80.93
<u>Soltrol:</u>						
Breakthrough	60.0	*63.40	60.83	64.12	60.00	58.32
1.0PV	71.70	73.32	68.17	71.67	70.00	69.30
1.5PV	74.00	76.67	72.00	76.00	74.05	74.00
2.0PV	75.33	76.70	74.58	76.67	75.00	74.32
<u>Glycerine-Water:</u>						
Breakthrough	-	41.7	-	**21.00	-	43.34
1.0PV	-	63.0	-	45.00	-	63.00
1.5PV	-	64.33	-	45.67	-	63.33
<u>Fresh Water:</u>						
Breakthrough	72.99	-	73.34	-	73.35	-
1.0PV	83.00	-	84.17	-	85.50	-
1.5PV	91.67	-	93.70	-	95.33	-
2.0PV	93.33	-	97.67	-	95.40	-

*Soltrol Test 1, see Table 9 for Test 2.

**Bad run, probably had leakage between top of cell and sand pack because of observed overrun.

all three models and their values equal 1.67. The same is true for the ratios of the diagonal length to width whose values equal 1.25. However, the ratios of the diagonal length to thickness are different. Model I and Model III have the same value of 10.0 while for Model II the value of the ratio equals 20.0. Thus Model I may be considered a model of Model III.

TABLE 9

Test 2. Oil Recovery, %OIP

	Breakthrough	1.0PV	1.5PV	2.0PV
Model I (Soltrol)	60.0	69.38	71.56	72.63

Figures 4 and 5 show the relation between oil recovery at breakthrough and the dimensionless group, L/h . Figures 6 and 7 illustrate the same relation at one pore volume of water throughput. These figures show that the ratio of the diagonal length to the thickness of the models has no effect on recovery. This group appears first in the second term of

equation (53). This term is the derivative of the velocity component in the vertical direction. When this component is neglected the group, L'/h disappears. This group also appears in combination in the groups,

$$\frac{\sigma(K\phi)^{\frac{1}{2}}}{v_t \mu_w} \frac{L'}{h} \text{ and } \frac{K\Delta\rho g}{v_t \mu_w} \frac{L'}{h}.$$

If L'/h in these groups is neglected, a two-dimensional system where there is no gravity effects is obtained. Since this is different from the system under study, L'/h cannot be neglected. These groups were not investigated in this work.

It is implied therefore that flow in the models were essentially in the horizontal directions. If transverse flow can be neglected, the same model can be used to scale several prototypes with differing L'/h ratios. This result indicates a greater flexibility in the application of scaled models than had previously been assumed.

EFFECTS OF VISCOUS FORCES

It is difficult, if not impossible, to consider the effects of viscous forces individually because of the interrelationships between several forces exhibiting themselves during two-phase flow in porous media. Rapoport and Leas evaluated viscous forces by introducing the "scaling coefficient," $\sigma \cos \theta / Lv_t \mu_w$. Other investigators used the ratio of capillary forces to gravity forces and/or the ratio of

gravity forces to imposed forces as derived from theory.

In this work, the effects of viscous resistance are evaluated in each model by injecting the displacing fluid at two rates. At each rate of water injection, the gravity and capillary forces are assumed constant. The ratio of the high to the low injection rate is approximately 2.0 in each model.

Oil recoveries and water-oil ratios as functions of pore volume of water throughput at the two injection rates are illustrated by Figures 8 through 13 with hexane as the oil phase, by Figures 14 through 19 with kerosene as the oil phase, and by Figures 20 through 25 with soltrol as the oil phase. At water breakthrough slightly higher recoveries are obtained for the low rate of water injection. After breakthrough the recoveries at the low rate remain higher. The average maximum differences in recoveries after breakthrough for all liquids are 3.39% for Model I, 3.56% for Model II and 1.67% for Model III.

The water-oil ratio and pore volume throughput relationship show identical trends. The water-oil ratios are slightly higher at the same pore volume throughput for the high rate of water injection. This is a confirmation of the results already obtained from the plots of oil recovery versus pore volume throughput.

The rate effect is explained by considering the shape and location of the flood fronts and the interaction between imposed gravitational and capillary pressure gradients at these fronts. In the region near the injection well the shape of the fronts is controlled by high viscous pressure gradients for both the high and low rates and radial fronts are observed. As the fronts progress away from the injection well bores, the velocity of the front declines (that is, the viscous pressure gradient declines and gravitational forces begin to influence the shape of the flood fronts). Near the producing wells, the velocity of the fronts increase again, developing cusps towards the producing wells. At high rates these "cusps" are more pronounced (overlay of fronts obtained from low and high rate). Thus at high rate viscous pressure gradient dominated the flow behavior resulting in lower recovery due to early cusping of the fronts.

After water breakthrough, the resulting pressure distribution causes the water injected to move faster than the oil and the rate of oil production declines rapidly because there is very little additional growth in the swept area.

At this point the results of the comparison of a previous run with the repeated run should be recalled. In the comparison, the maximum deviation in recovery after breakthrough was found to be 5.0% which is higher than the maximum

deviation obtained in the experiments. One may conclude from these experiments that rate appeared to have an effect on ultimate recovery, but based on the one reproducibility test, it would require further work to prove. The choice of an optimum injection rate might be determined by economic factors and formation injectivity.

Viscous resistance is inversely proportional to effective permeability and proportional to viscosity. The relation between oil recoveries and viscosity ratio, μ_o/μ_w is presented graphically in Figures 26 through 29. The results show that oil recoveries increase as the viscosity ratio decreased toward a value of 1 and subsequently decreased as the viscosity ratio decreased below 1. In the range of viscosity ratios used in this study only one liquid has μ_o/μ_w less than unity. The flooding behavior when viscosity ratio is less than one should be studied further by using appropriate liquids.

These results indicate that viscosity ratio is a correlatable parameter with oil recovery at any value of pore volume of water throughput.

EFFECTS OF GRAVITY FORCES

In waterfloods where there exists a difference between the oil-phase density and the water-phase density, gravity

effects need to be considered. The dimensionless group, $K\Delta\rho g/v_t\mu_w$, which is the ratio of gravity to imposed forces is generally used for this purpose. However, it is unnecessary to determine the magnitude of this group in this study, since the difference in densities of each pair of liquids used and the absolute permeability of the sand pack to these liquids are the same in all models.

Figures 30 and 31 show the overlays of the frontal position at the top and bottom of Model I at the same pore volume of water throughput, at high and at low rate of water injection respectively. The sweep efficiencies for hexane-water at the bottom of the model are slightly greater than those at the top. The maximum deviation in these sweep efficiencies is less than 1%. Furthermore, only minimal amounts of oil were produced after water breakthrough as may be seen from the relationships between oil recoveries and pore volumes of injected water. Thus the waterfronts were primarily sharp and vertical. These results show that the injection rates used did not allow gravity effects to predominate and that oil recoveries are independent of difference in the density range investigated.

In the calibration runs with the 50-50 percent glycerine-water, the density of the mixture is greater than the density of water. The injected water overrode the glycerine-

water mixture and very little waterfront movement was observed at the bottom of the models. In one case, Model II, it could have been separation of the top of the model and the sand pack. In the case of Models I and III, further study is suggested.

VALIDITY OF SCALED MODELS

From the theory presented in Chapter III and the analysis thus far, the following conclusions could be made for each liquid used:

- 1) The geometry and boundary conditions of the model (Model I) and prototype (Model III) are the same.
- 2) The relative permeabilities to the oil and water phase and the viscosity ratio are the same in model and prototype.
- 3) The ratio of gravitational forces to imposed forces is identical in model and prototype.
- 4) The initial conditions are approximately the same in model and prototype.
- 5) For a particular injection rate, the ratio of capillary forces to imposed forces is the same in model and prototype.

Thus the experiments were dimensionally scaled and the performance of the model should be identical to that of the

prototype. To verify this statement, the performances of the three models are compared in Figures 32 through 47. The performance of the models before water breakthrough are identical, the data points coincide. After water breakthrough slight deviations are observed. The deviations are larger for low injection rate. The maximum deviation in all runs is about 5.6% with soltrol. For hexane, and kerosene the deviations are very small. The run in Model II with glycerine-water representing the oil phase cannot be compared with the results from Model I and Model III because of possible sand movement and channeling which resulted in low recovery. This was the first run with the mixture of glycerine and water and consequently the unreliability of the results was not suspected at that time. However, after the runs in Model I and Model II with glycerine-water as oil phase it became obvious that the run in Model II was not representative.

In addition, the plots of water-oil ratio as a function of pore volume injected show the same trend--identical performance of model and prototype. As expected the maximum deviation obtained was with soltrol as the oil phase.

A comparison of the results obtained injecting water at low and high rates, indicates that the model simulated the prototype better at high injection rate. This could imply that a critical point exists for each system above which the

model exactly predicts the behavior of the prototype. The critical point(s) would have critical value for each dimensionless group, whose magnitude must be determined experimentally for a particular system.

The degree of applicability of scaled models in the solution of field problems would depend on the ability to obtain equality of the dimensionless groups in model and prototype. While the viscosity ratio, the geometry, and viscous forces may be scaled without difficulty, the same is not true for the gravity, imposed and capillary forces.

The application of the scaling laws requires considerations of porous media possessing identical relative permeability functions and similarly shaped capillary pressure curves. In practice such a situation is not likely to occur and in most cases, it may be impossible to find a suitable material for the construction of a model permitting quantitative scaling of a flow process occurring in the reservoir. However, valid information of great practical utility can be obtained by means of model studies scaled and interpreted on the basis of a "synthetic" approach.

AREAL COVERAGE

An attempt was made to study sweep efficiency in staggered line pattern since very little information is avail-

able in the literature. Visual observation of the fronts was made possible by the food dye which gave a red shade to the area invaded by the injected fluid. The fronts were traced at fixed pore volumes throughput.

Figures 48 through 55 show the area swept at different throughputs. The numbers at each front are the values of sweep efficiency and pore volumes of water injected. The sweep efficiency are found by dividing the area enclosed by a particular front by the total area of the face of the model, where the fronts are observed, and multiplying by 100. The areas were determined by means of a planimeter. Tracing of the fronts was terminated at water-breakthrough.

The water invaded zone is found to be radial during the initial stages of flooding. This stage lasted until an average 0.18PV throughput. During the latter stages the invaded zone gradually develops a cusp toward the producing well and finally breaks through. The fronts are not symmetrical about the diagonal connecting the injection and production wells because the widths of the models are three-quarters of the lengths. The average ratio of the distance travelled by the fronts along the width of the models to the distance travelled along the lengths was 0.72.

The results show that with increasing oil-water viscosity ratio the cusps became more pronounced and began to form

at an earlier flooding stage, resulting in an overall decrease of areal sweep at water breakthrough. Figure 54 where glycerine-water was the oil phase clearly illustrates this point. In the runs with hexane, kerosene and soltrol as the oil phase, slightly elongated cusps were observed at the high rate of water injection. However, there was little or no difference between the areal sweeps obtained at breakthrough for the two rates employed.

Chapter VI

CONCLUSIONS AND RECOMMENDATIONS

- 1) In the laboratory, the results obtained from a model matched the performance of its prototype very closely.
- 2) The model predicted the performance of the prototype very well even though an average standard deviation of 2.6% or less in initial water saturation existed.
- 3) The ratio of the diagonal length of the model to its thickness has no effect on the performance of the prototype in the range of L'/h used in the experiments.
- 4) Points (2) and (3) above indicate a greater flexibility in the application of scaled model experiments than had previously been assumed.
- 5) A study should be undertaken to investigate how adequately the dimensionless group, L'/h is accounted for by the ratios of capillary to viscous forces, and gravity to viscous forces.
- 6) Each dimensionless group seems to have a critical value above which the model predicts the performance of its prototype. Further research in this area is recommended.
- 7) Injection rates have little or no effect on ultimate recovery for the conditions of this study and the water-fronts were primarily sharp and vertical.

- 8) Oil recoveries at water breakthrough are independent of the density difference.

NOMENCLATURE

a	constant
C_L	lower limit of viscous-gravity ratio
C_u	upper limit of viscous-gravity ratio
d	diameter of linear, cylindrical model
D_o	diffusion coefficient of oil into solvent
D_s	diffusion coefficient of solvent into oil
E_A	areal sweep efficiency
f	function
g	acceleration due to gravity
h	thickness of the model
J(S)	Leverett capillary pressure function
J(S')	normalized Leverett capillary pressure function
K	specific permeability
K_o	effective permeability to oil
K_{ocw}	relative permeability to oil at connate water saturation
K_{ro}	relative permeability to oil
K_{rw}	relative permeability to water
K_w	effective permeability to water
K_{wro}	relative permeability to water at residual oil saturation
K_x	horizontal effective permeability
K'_o	normalized relative permeability to oil

K'_w	normalized relative permeability to water
K_t	effective transverse dispersion coefficient
ℓ	length of model
L	principal dimension, size of pattern
L'	diagonal length of model
L^*	characteristic length of model
M	fundamental unit of mass
P	pressure
P_c	capillary pressure
P'_c	capillary pressure in model
PV	pore volume
PV_{inj}	pore volume injected
q	flow rate
q_t	total flow rate
q'_t	total flow rate in model
S	saturation
S'	normalized saturation
S_w	water saturation
S_{cw}	connate water saturation
S_{ro}	residual oil saturation
t	time
T	fundamental unit of time
v	total velocity in one direction
v_a	average total velocity in one direction

v_t	average total velocity in x, y, and z axes
v_x	total velocity along the x-axis
v_y	total velocity along the y-axis
v_z	total velocity along the z-axis
\bar{v}_x	dimensionless total velocity along the x-axis
\bar{v}_y	dimensionless total velocity along the y-axis
\bar{v}_z	dimensionless total velocity along the z-axis
w	width of model
x	x-coordinate
\bar{x}	dimensionless x-coordinate
y	y-coordinate
\bar{y}	dimensionless y-coordinate
z	z-coordinate
\bar{z}	dimensionless z-coordinate
∇	divergence operator

Greek letters

α	angle of formation dip
Δ	difference operator
θ	contact angle
λ	$K_{rw}\psi$
μ_o	viscosity of oil
μ'_o	viscosity of oil in model
μ_s	viscosity of solvent
μ_w	viscosity of water

μ'_w	viscosity of water in model
π	dimensionless group
ρ_o	density of oil
ρ'_o	density of oil in model
ρ_w	density of water
ρ'_w	density of water in model
σ	interfacial tension
ϕ	porosity
Φ	potential

Subscript

a	average
c	capillary
cw	connate water
i	subscript
L	lower
o	oil
r	relative
s	solvent
t	total or transverse
u	upper
w	water
x	x - direction
y	y - direction
z	z - direction

LITERATURE CITED

- 1 Rapoport, L. A., Carpenter, C. W., Jr., and Leas, W. J.: "Laboratory Studies of Five-Spot Waterflood Performance," Trans., AIME (1958) v. 213, 113-120.
- 2 Leverett, M. C., Lewis, W. B., and True, M. E.: "Dimensional Model Studies of Oilfield Behavior," Trans., AIME (1942) Pt. 2, v. 225, 177-184.
- 3 Engelberts, W. E., and Klinkenberg, L. J.: "Laboratory Experiments on the Displacement of Oil by Water from Packs of Granular Materials," Proc., Third World Petroleum Cong., Sec. 2, 544.
- 4 Croes, G. A., and Schwarz, N.: "Dimensionally Scaled Experiments and the Theories on the Water-Drive Process," Trans., AIME (1955) v. 204, 35-42.
- 5 Greenkorn, R. A.: "Flow Models and Scaling Laws for Flow through Porous Media," Ind. Eng. Chem. (Mar. 1964) v. 56, No. 3, 32-37.
- 6 Rapoport, L. A., and Leas, W. J.: "Properties of Linear Waterfloods," Trans., AIME (1953) v. 198, 139-148.

- 7 Rapoport, L. A.: "Scaling Laws for Use in Design and Operation of Water-Oil Flow Model," Trans., AIME (1955) v. 204, 143-150.
- 8 Nielsen, R. L., and Tek, M. R.: "Evaluation of Scale-Up Laws for Two-Phase Flow through Porous Media," Soc. Pet. Eng. J. (June 1963) 164-176.
- 9 Carpenter, C. W., Jr., Bail, P. T., and Bobek, J. E.: "Verification of Waterflood Scaling in Heterogeneous Communicating Flow Models," Soc. Pet. Eng. J. (March 1962), 9-12.
- 10 Perkins, F. M., Jr.: "An Investigation of the Role of Capillary Forces in Laboratory Waterfloods," Trans., AIME (1957) v. 210, 409-411.
- 11 Richardson, J. G., and Perkins, F. M., Jr.: "A Laboratory Investigation of the Effect of Rate on Recovery of Oil by Water Flooding," Trans., AIME (1957) v. 210, 114-121.
- 12 Craig, F. F., Jr., Geffen, T. M., and Morse, R. A.: "Oil Recovery Performance of Pattern Gas or Water Injection Operations from Model Tests," Trans. AIME (1955) v. 204, 7-15.

- 13 Perkins, F. M., Jr., and Collins, R. E.: "Scaling Laws for Laboratory Flow Models of Oil Reservoirs," Trans., AIME (1960) v. 219, 383-385.
- 14 Offeringa, J., and Van der Poel, C.: "Displacement of Oil from Porous Media by Miscible Liquids," Trans., AIME (1954) v. 201, 310-315.
- 15 Blackwell, R. J., Rayne, J. R., and Terry, W. M.: "Factors Influencing the Efficiency of Miscible Displacements," Trans., AIME (1959) v. 216, 1-8.
- 16 Blackwell, R. J.: "Laboratory Studies of Microscopic Dispersion Phenomena," Trans., AIME (1962) v. 225, Pt. 2, 1-8.
- 17 Pozzi, A. L., and Blackwell, R. J.: "Design of Laboratory Models for Study of Miscible Displacement," Soc. Pet. Eng. J. (March 1963), 28-40.
- 18 Geertsma, J., Croes, G. A., and Schwarz, N.: "Theory of Dimensionally-Scaled Models of Petroleum Reservoirs," Trans., AIME (1956) v. 207, 118-127.
- 19 Longhaar, H. L.: "Dimensional Analysis and Theory of Models," John Wiley and Sons, Inc., New York (1951), 166.

- 20 Ruark, A. E.: "Inspectional Analysis: A Method which Supplements Dimensional Analysis," J. Mitchell Soc. (August 1935) v. 51, 127-132.
- 21 Muskat, M.: "Physical Principles of Oil Production," McGraw-Hill Book Co., Inc., New York (1949), 657.
- 22 Ryder, H. M.: "Effects of Higher Flooding Pressure," Prod. Monthly, (December 1937) v. II, No. 2, 21-22.
- 23 Calhoun, J. G., McCormick, R. L., and Yuster, S. T.: "The Effects of Pressure Gradients and Saturations on Recovery in Waterflooding," Prod. Monthly, (November 1944) v. IX, No. 1, 12-17.
- 24 Breston, J. N., and Hughes, R. V.: "Relation between Pressure and Recovery in Long Core Water Floods," Trans., AIME (1949) v. 186, 100-110.
- 25 Morse, R. A., and Yuster, S. T.: "Water Flood Tests on Long Cores," Prod. Monthly, (December 1946) v. IX, No. 2, 19-24.
- 26 Earlougher, R. C.: "Relationship between Velocity, Oil Saturation and Flooding Efficiency," Trans., AIME (1943) v. 151, 125-135.

- 27 Gaucher, D. H., and Lindley, D. C.: "Waterflood Performance in a Stratified, Five-Spot Reservoir -- A Scaled-Model Study," Trans., AIME (1960) v. 219, 208-215.

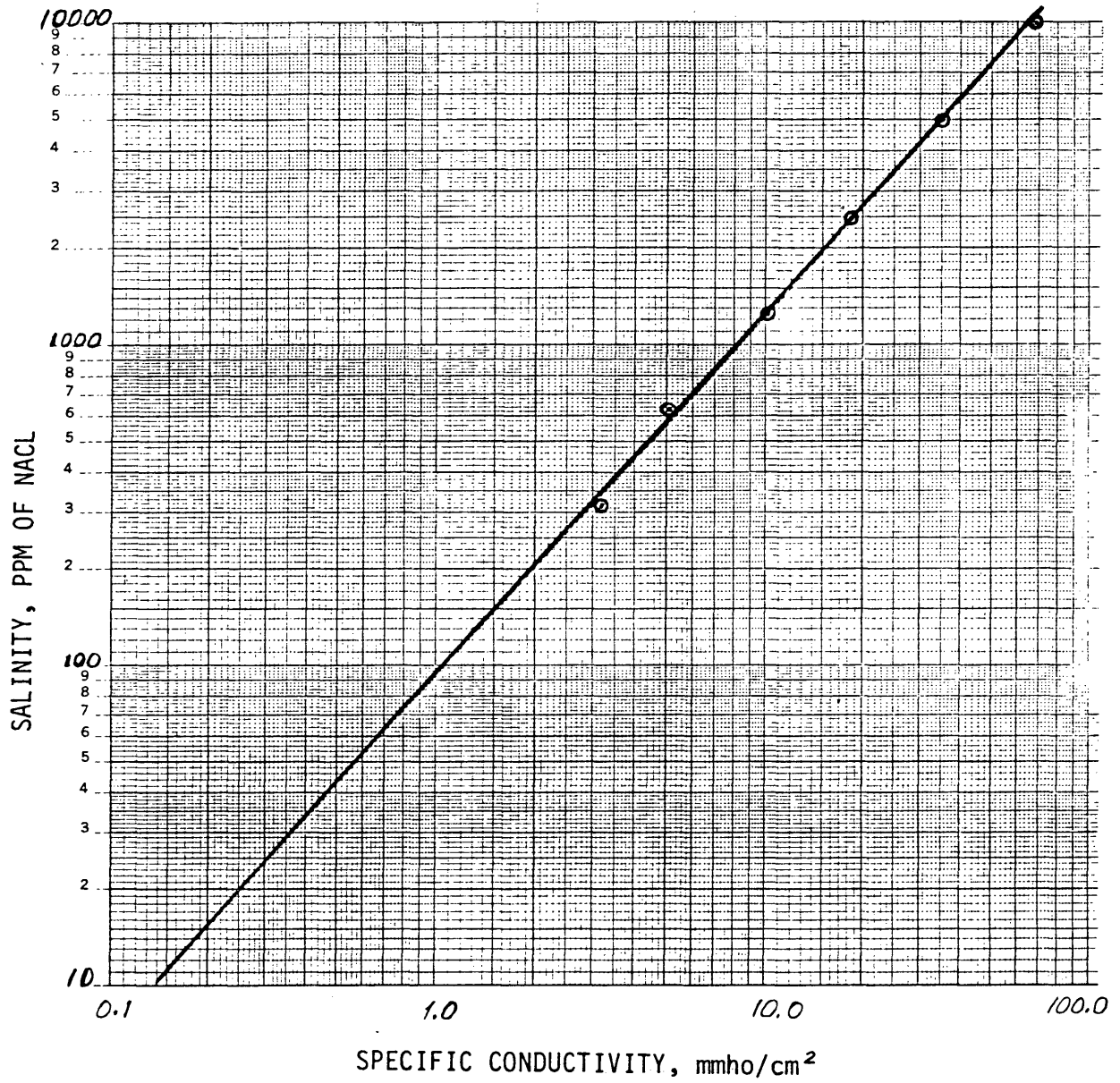


FIGURE 1 CALIBRATION OF CONDUCTIVITY METER

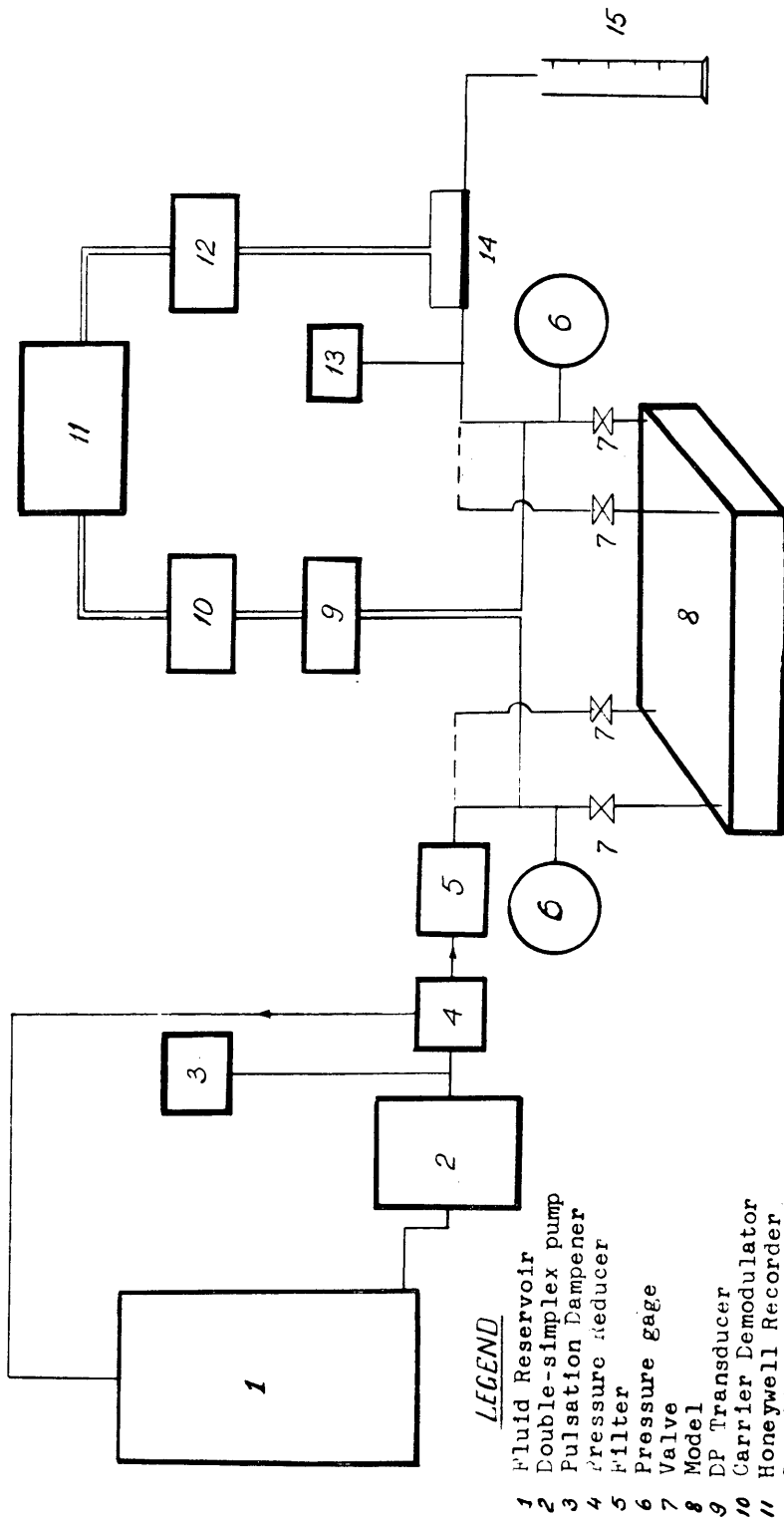


Figure 2. Experimental Apparatus

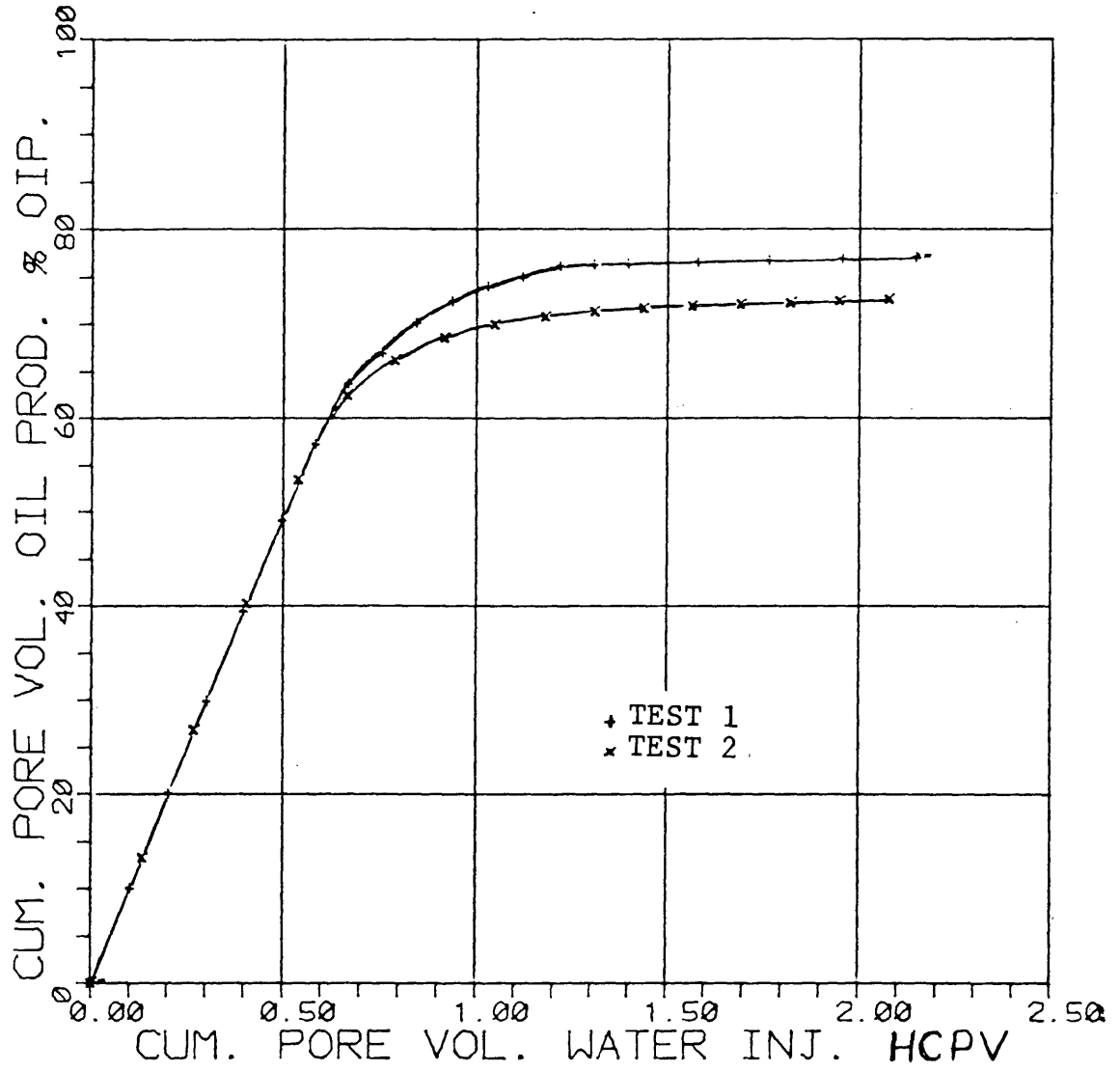


FIGURE 3 REPRODUCIBILITY

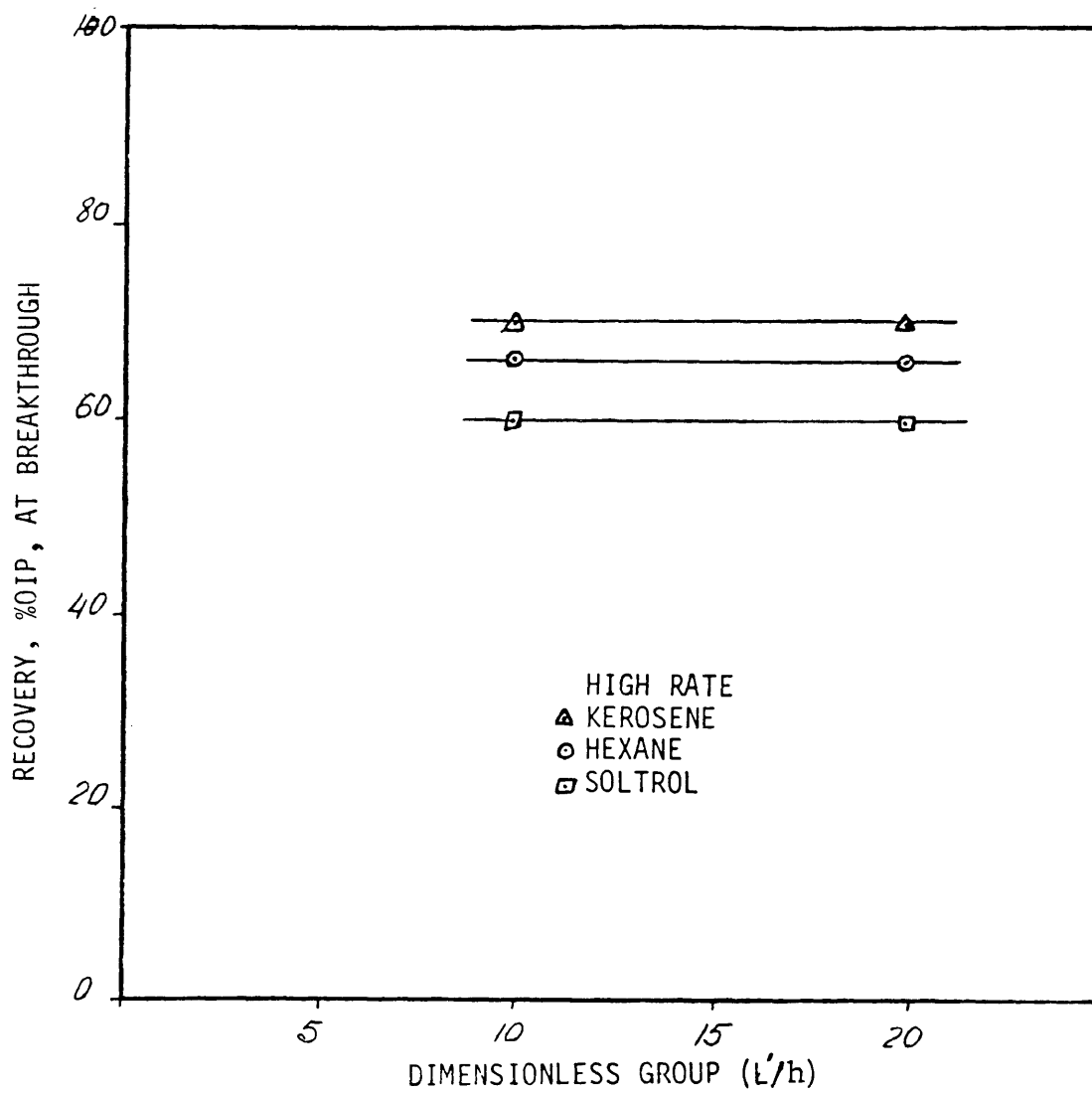


FIGURE 4 OIL RECOVERY AT WATER BREAKTHROUGH AT HIGH
RATE VERSUS LENGTH-THICKNESS RATIO (L'/h)

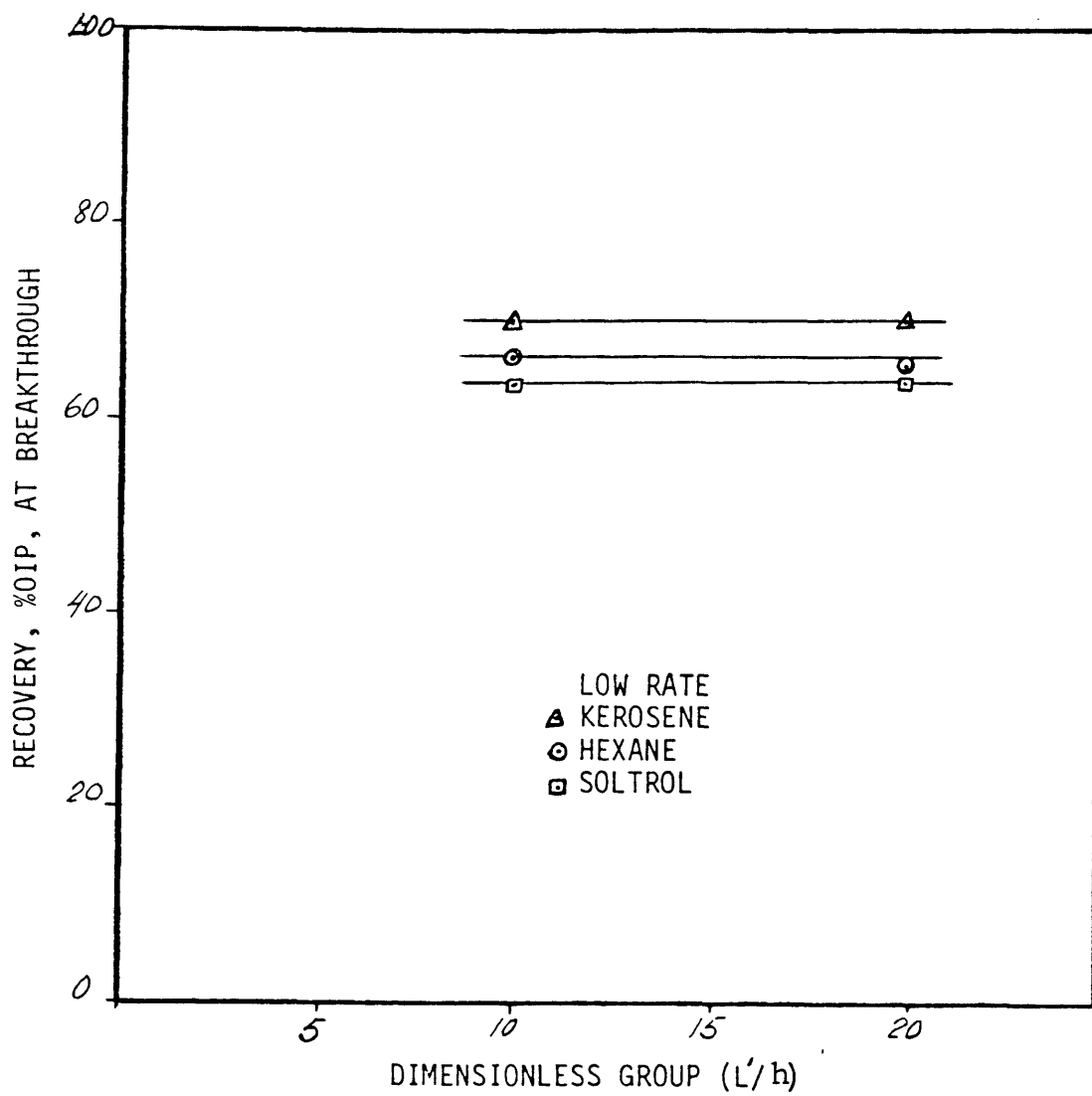


FIGURE 5 OIL RECOVERY AT WATER BREAKTHROUGH AT LOW
RATE VERSUS LENGTH-THICKNESS RATIO (L'/h)

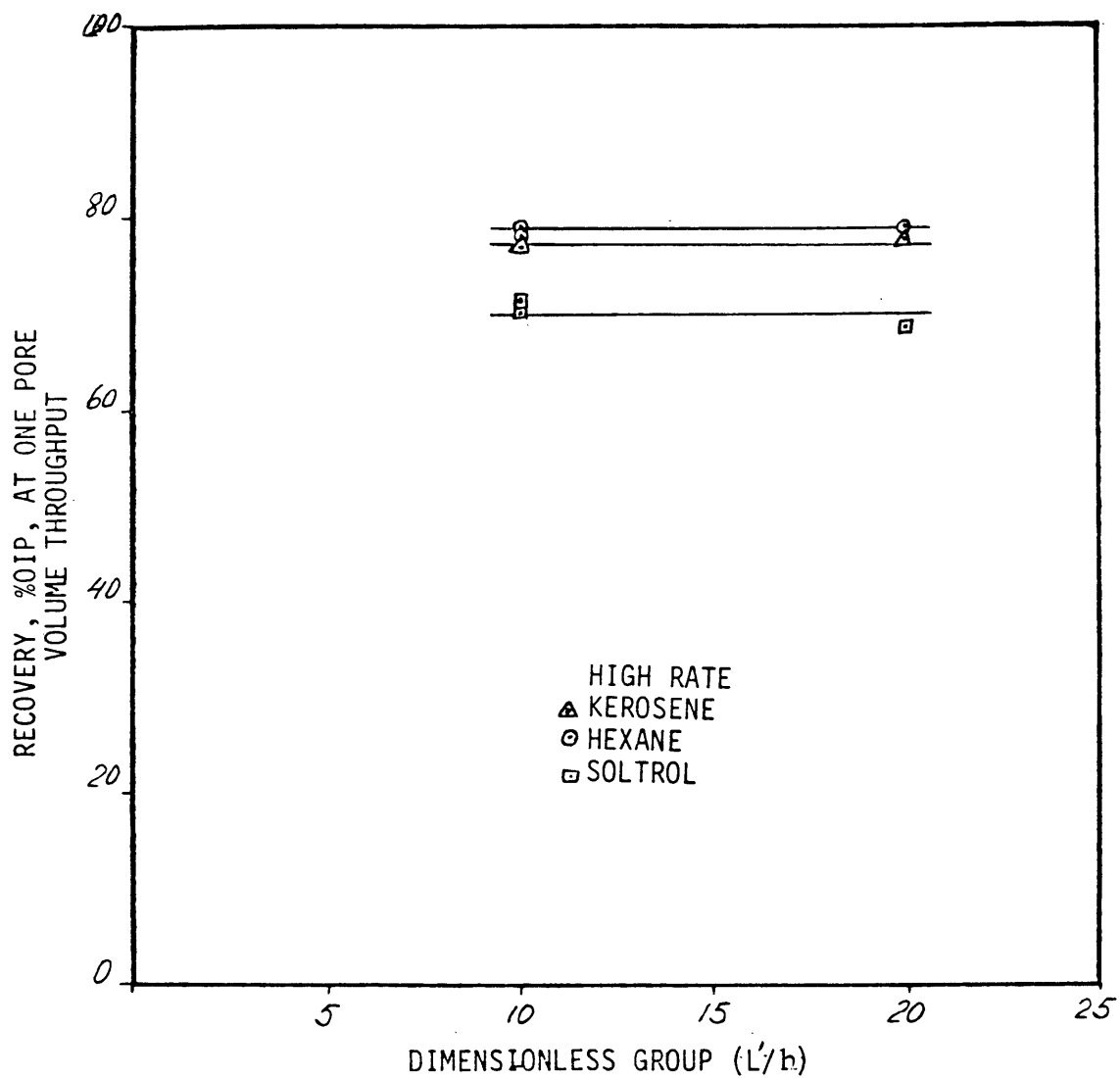


FIGURE 6 OIL RECOVERY AT ONE PORE VOLUME THROUGHPUT
AT HIGH RATE VERSUS LENGTH-THICKNESS
RATIO (L'/h)

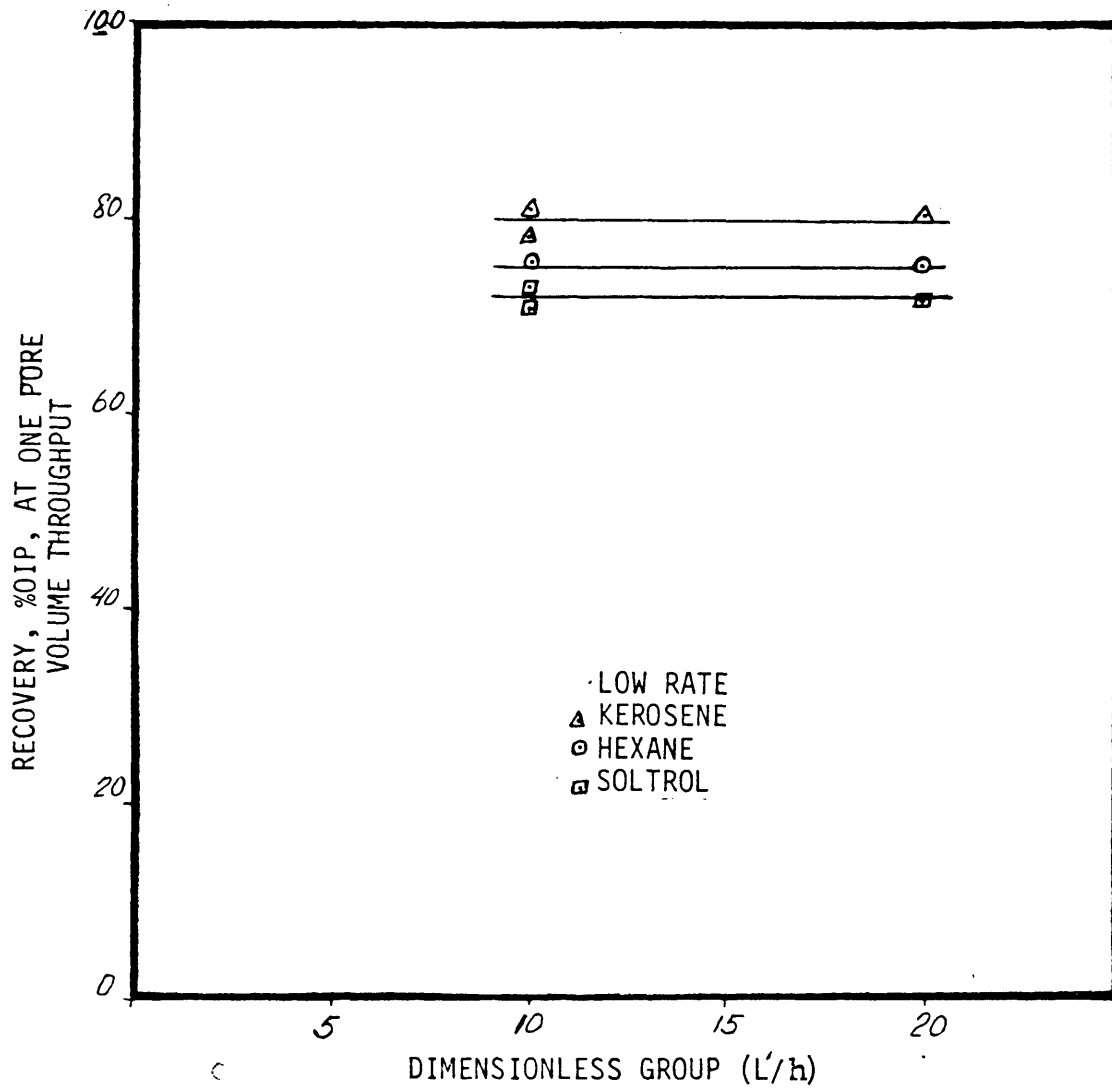


FIGURE 7 OIL RECOVERY AT ONE PORE VOLUME THROUGHPUT
AT LOW RATE VERSUS LENGTH-THICKNESS
RATIO (L'/h)

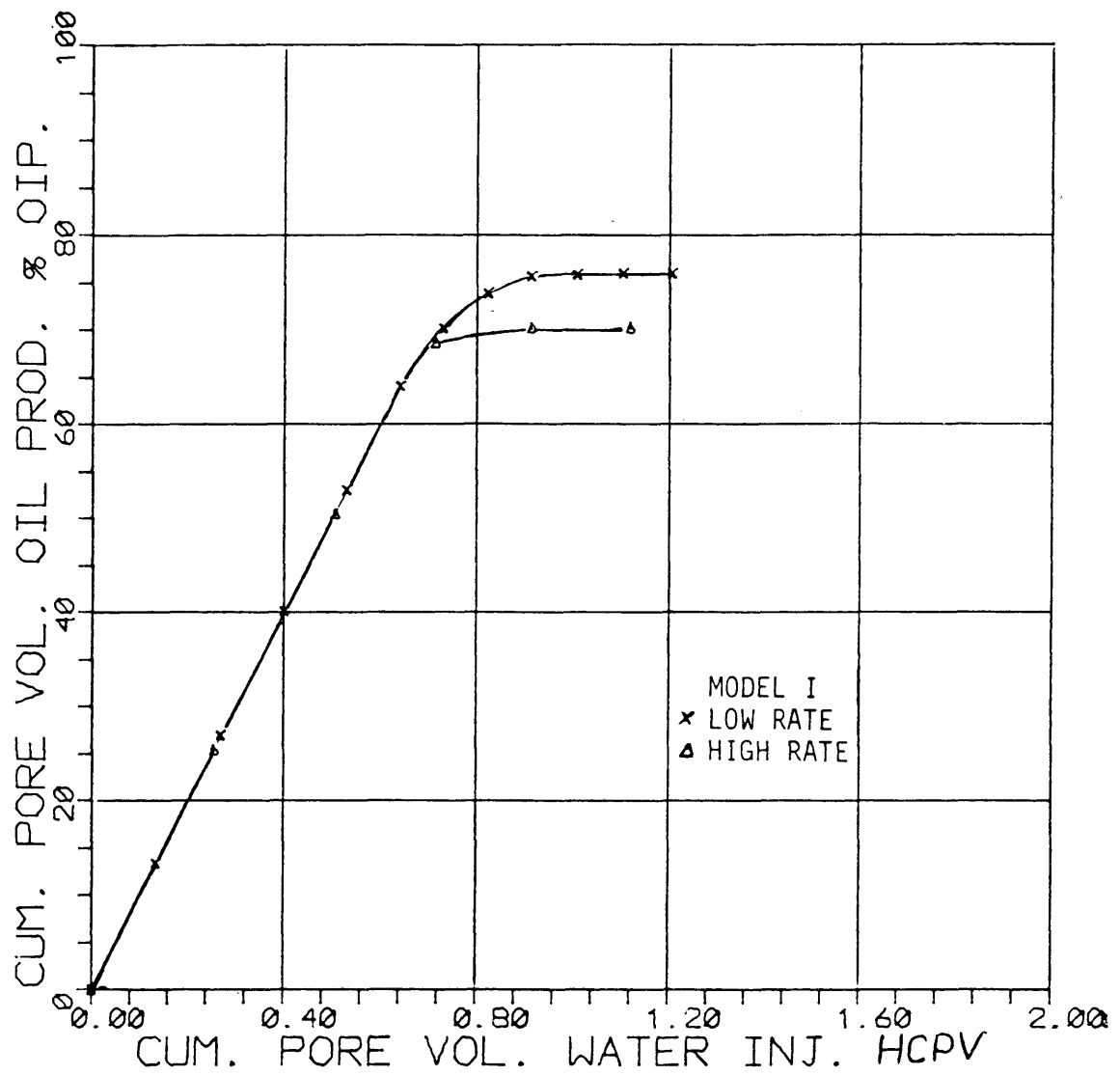


FIGURE 8 EFFECT OF RATE ON OIL RECOVERY
(MODEL I, HEXANE)

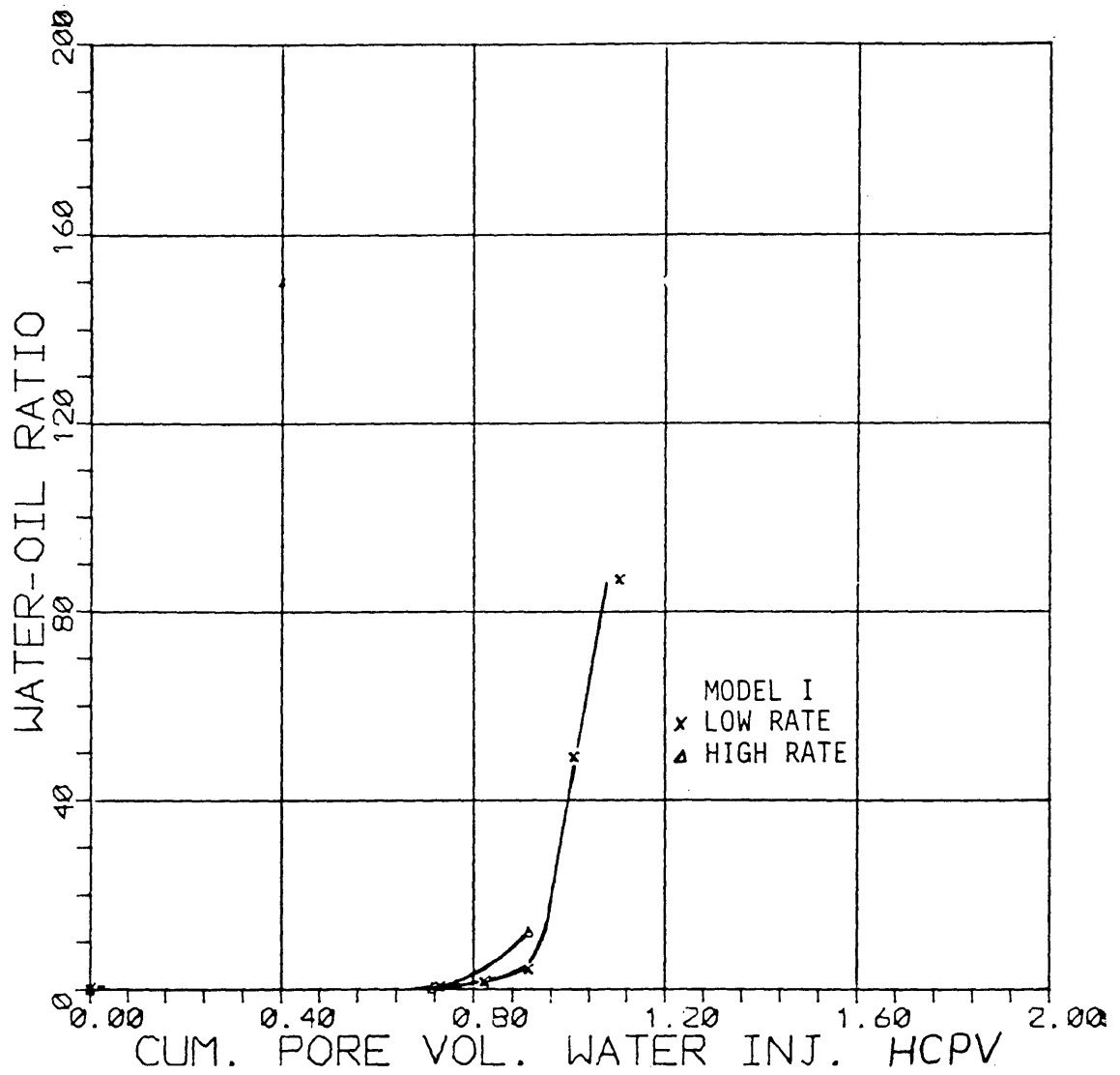


FIGURE 9 EFFECT OF RATE ON WATER-OIL RATIO
(MODEL I, HEXANE)

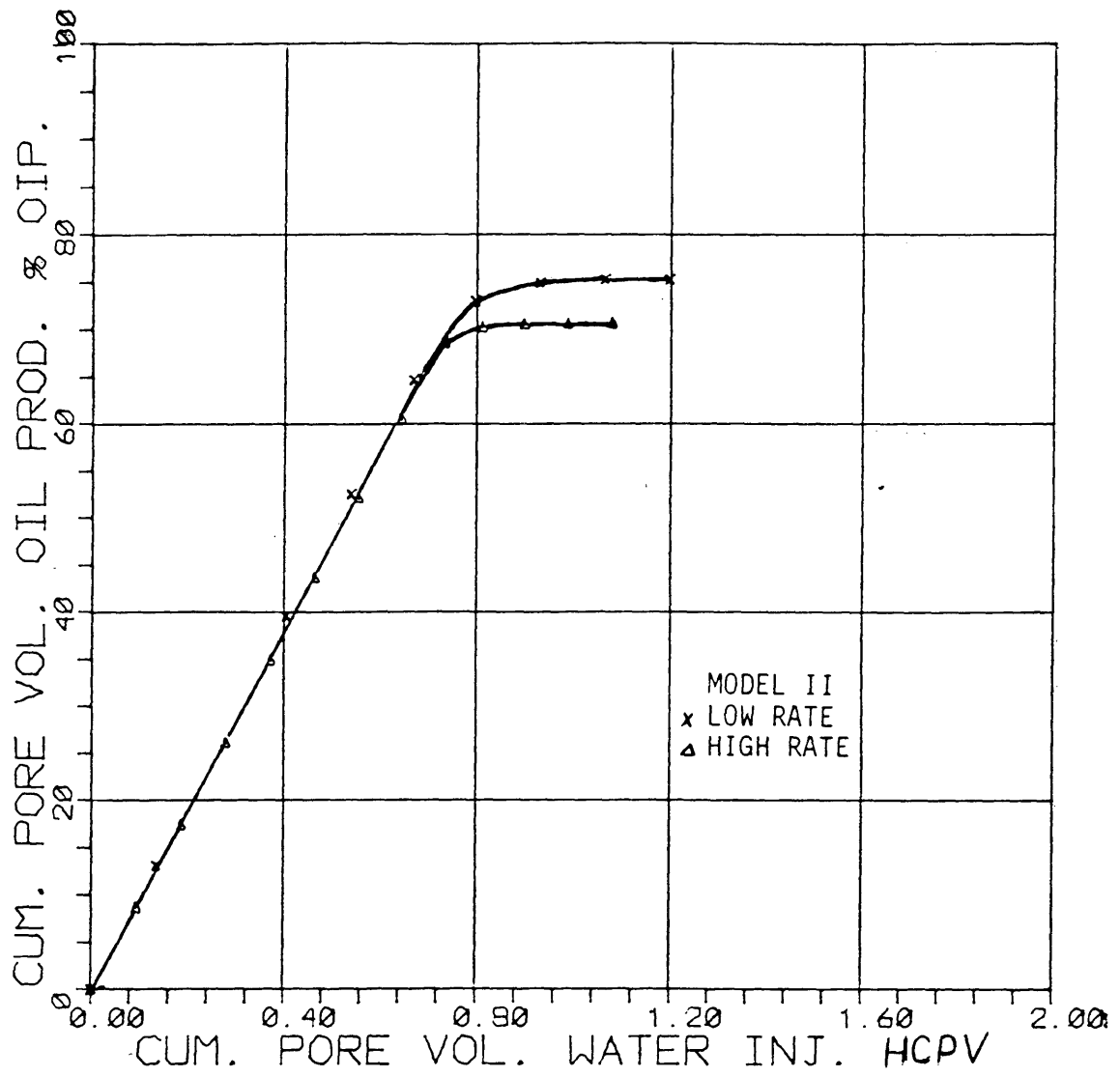


FIGURE 10 EFFECT OF RATE ON OIL RECOVERY
(MODEL II, HEXANE)

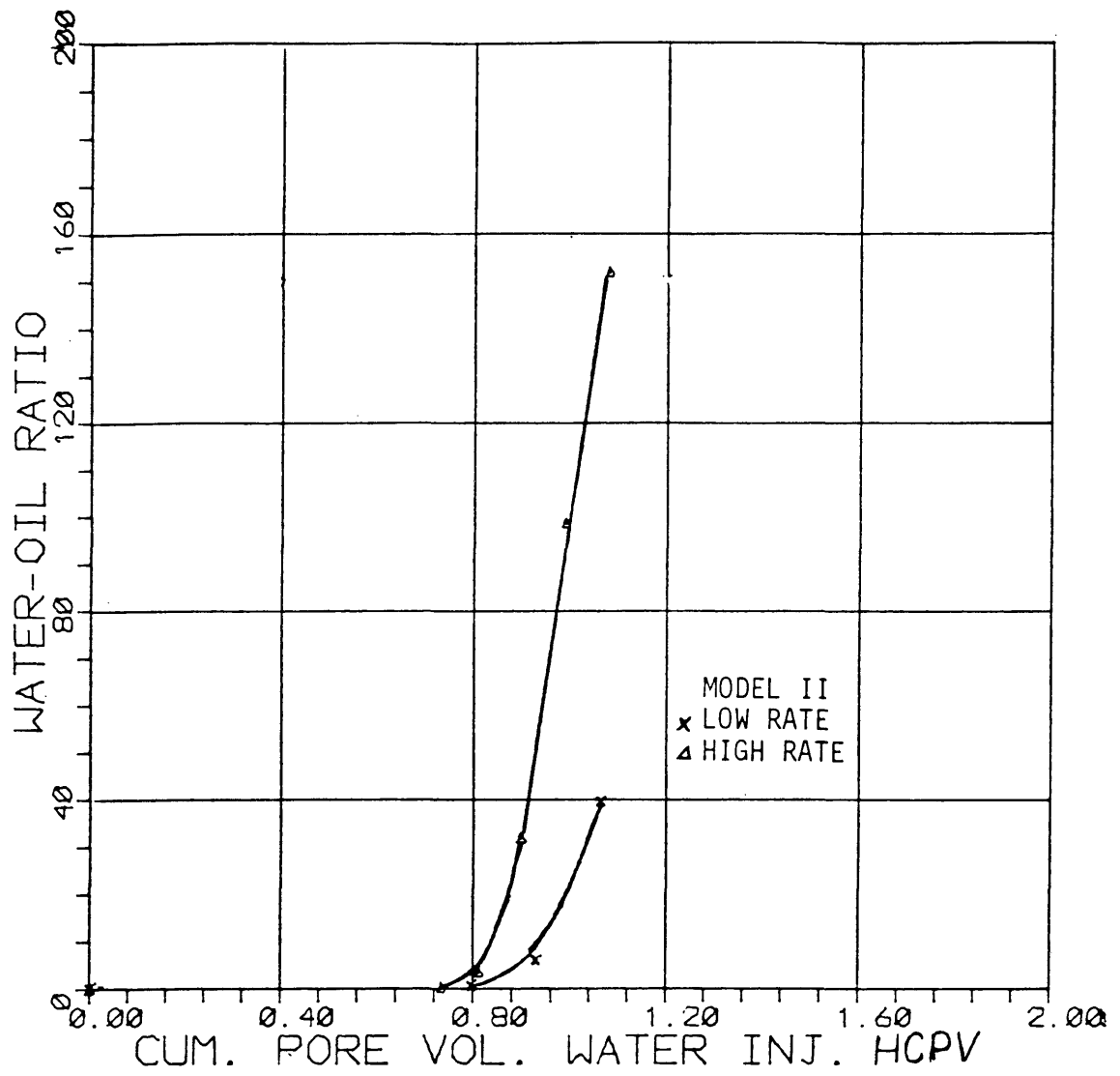


FIGURE 11 EFFECT OF RATE ON WATER-OIL RATIO
(MODEL II, HEXANE)

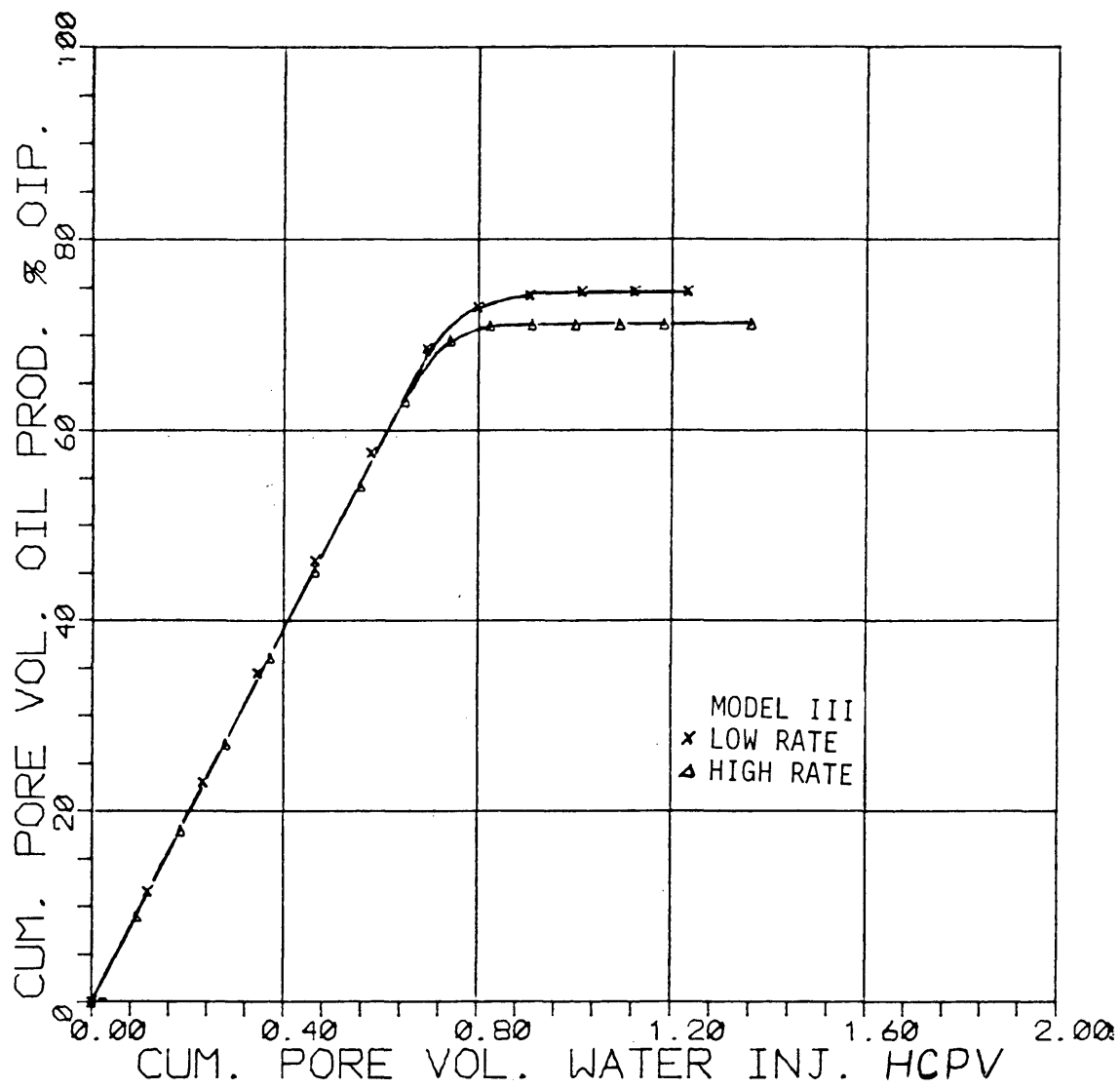


FIGURE 12: EFFECT OF RATE ON OIL RECOVERY
(MODEL III, HEXANE)

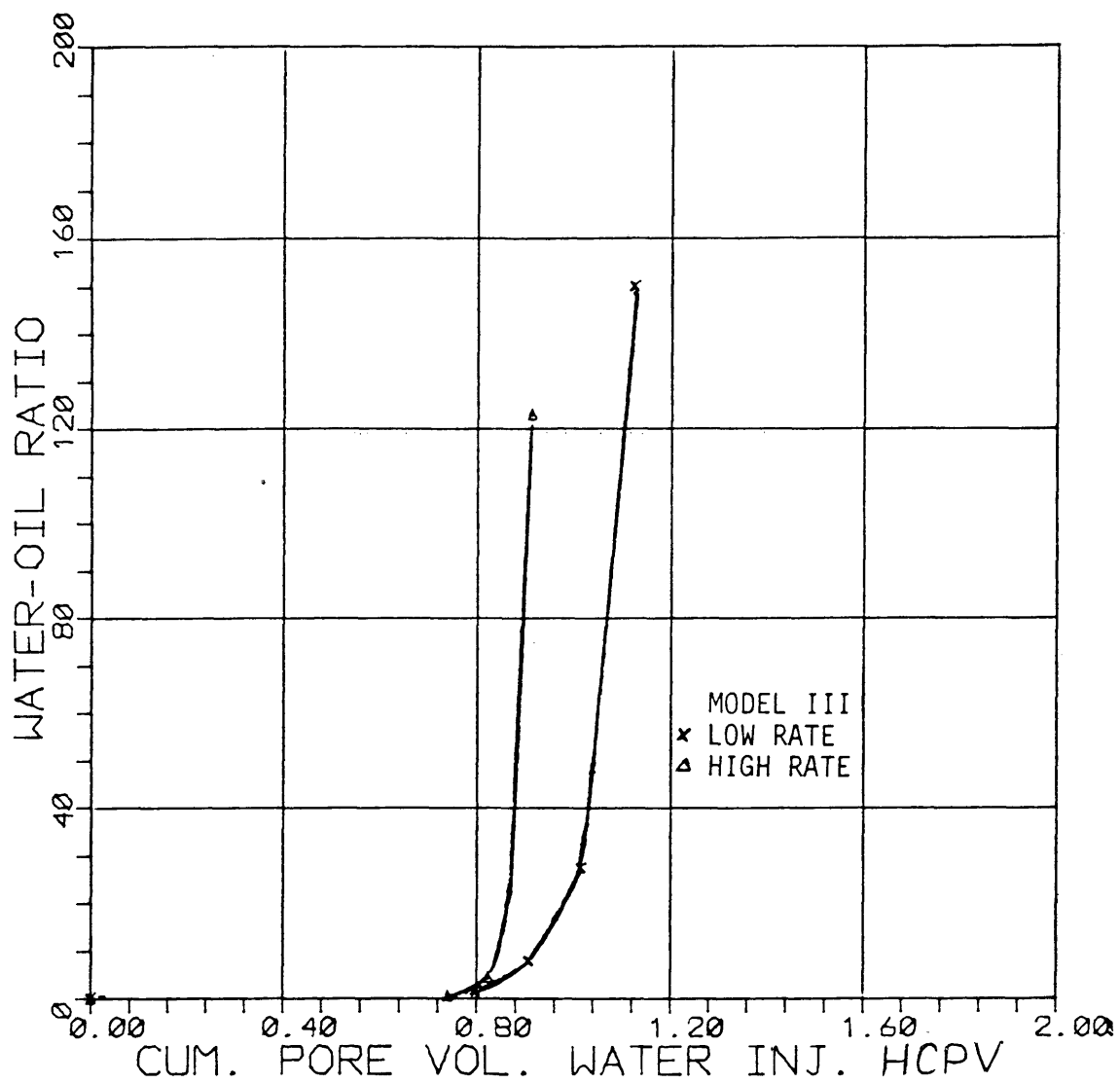


FIGURE 13 EFFECT OF RATE ON WATER-OIL RATIO
(MODEL III, HEXANE)

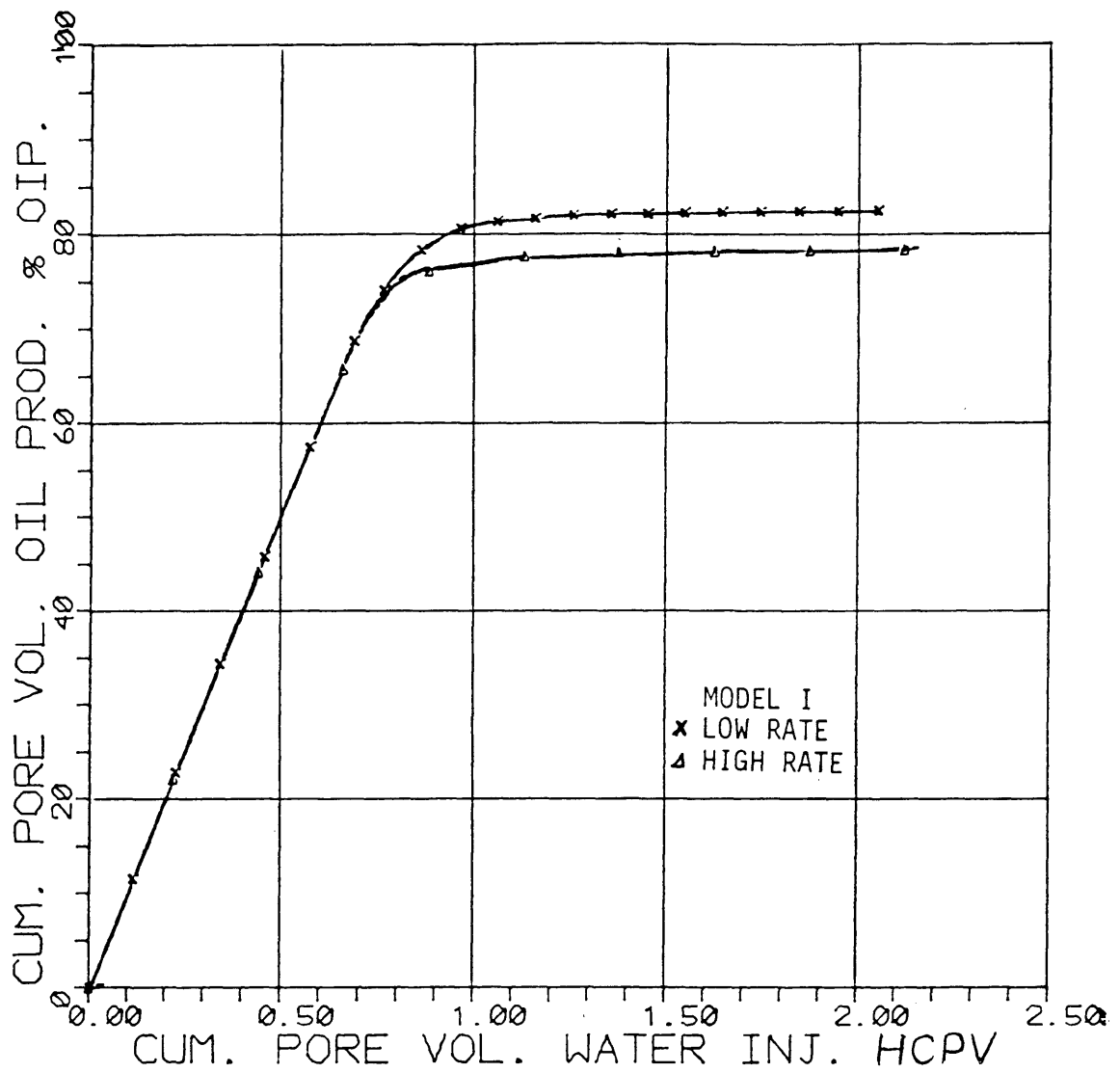


FIGURE 14 EFFECT OF RATE ON OIL RECOVERY
(MODEL I, KEROSENE)

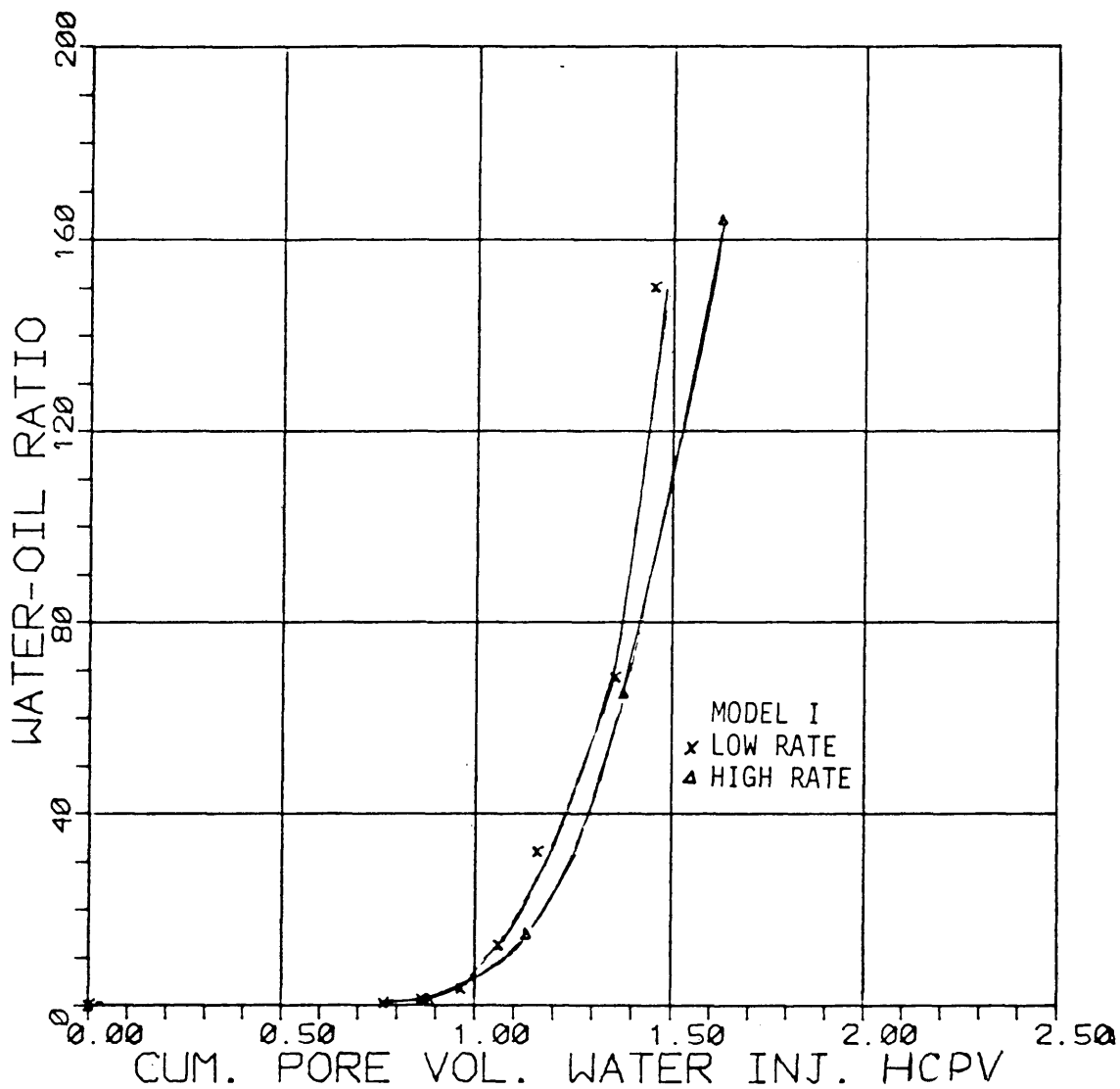


FIGURE 15 EFFECT OF RATE ON WATER-OIL RATIO
(MODEL I, KEROSENE)

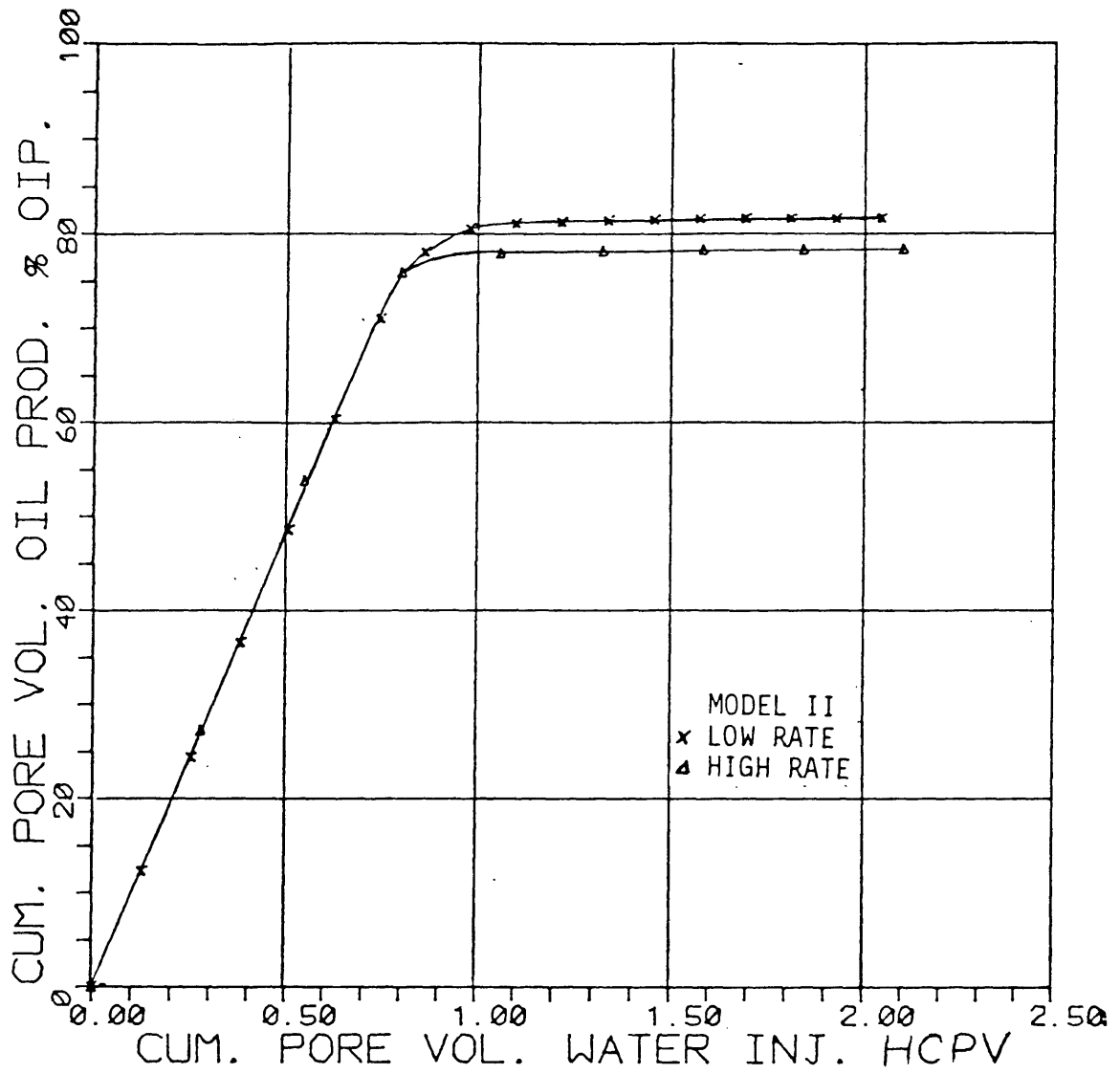


FIGURE 16 EFFECT OF RATE ON OIL RECOVERY
(MODEL II, KEROSENE)

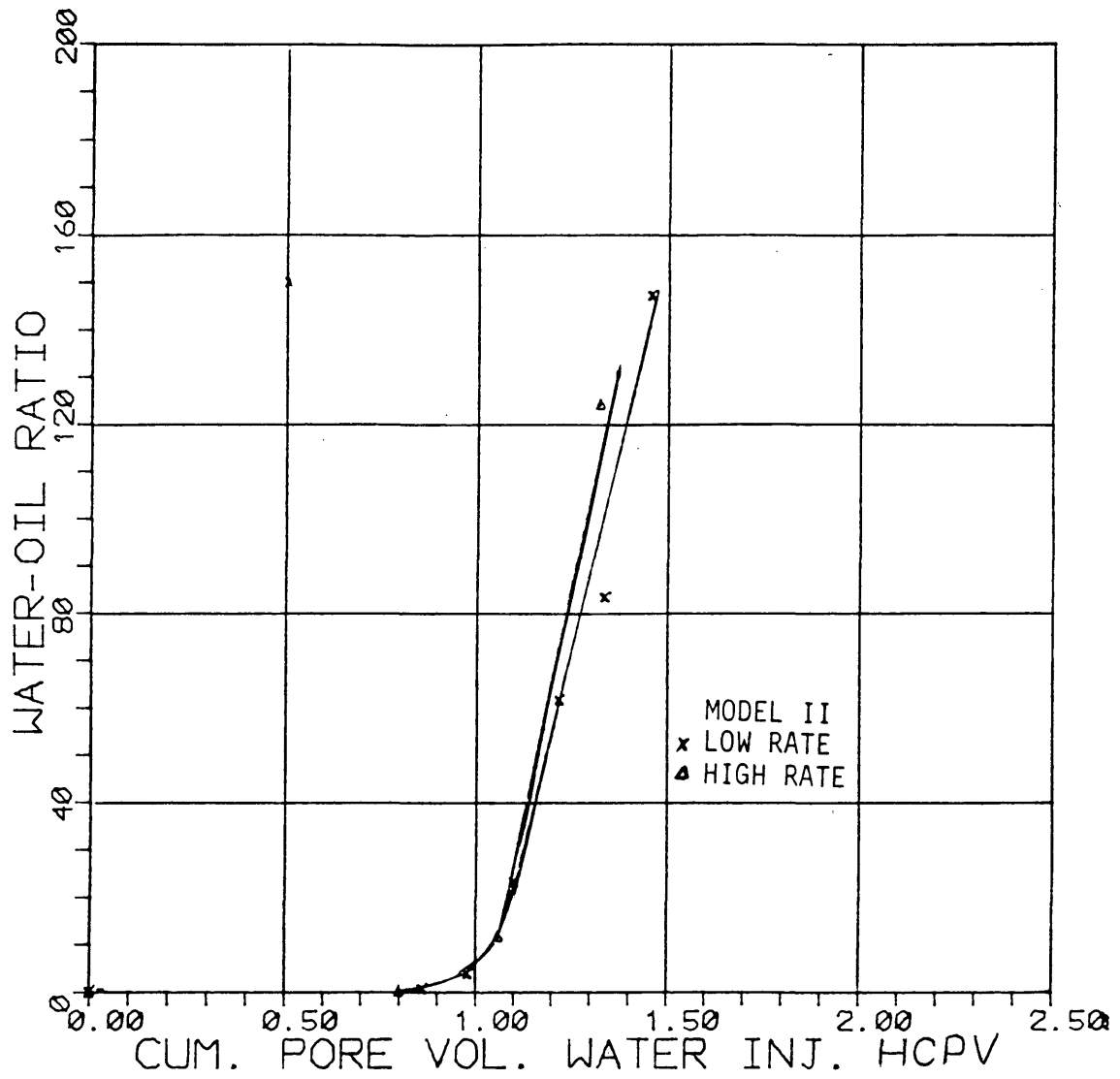


FIGURE 17 EFFECT OF RATE ON WATER-OIL RATIO
(MODEL II, KEROSENE)

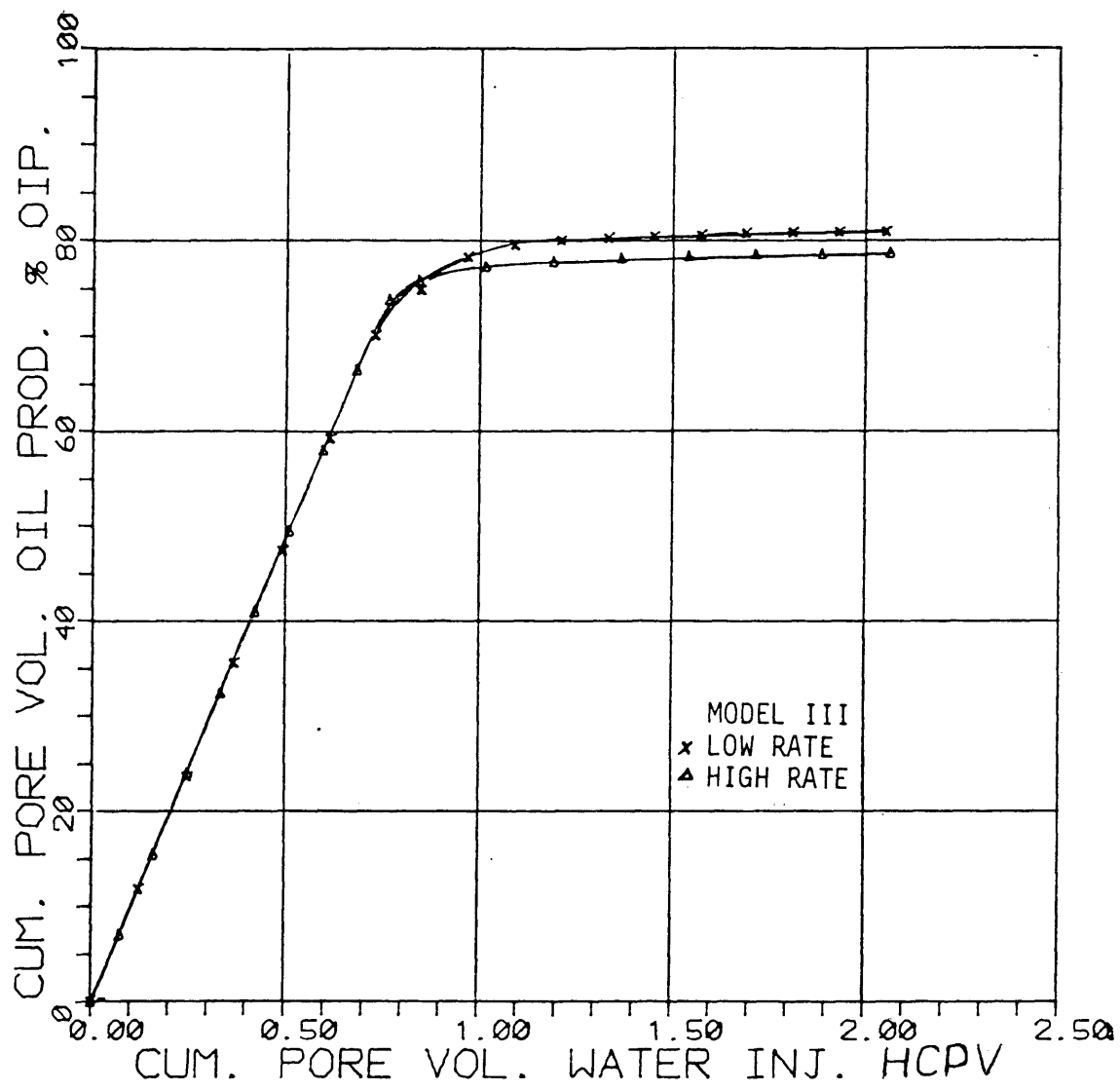


FIGURE 18 EFFECT OF RATE ON OIL RECOVERY
(MODEL III, KEROSENE)

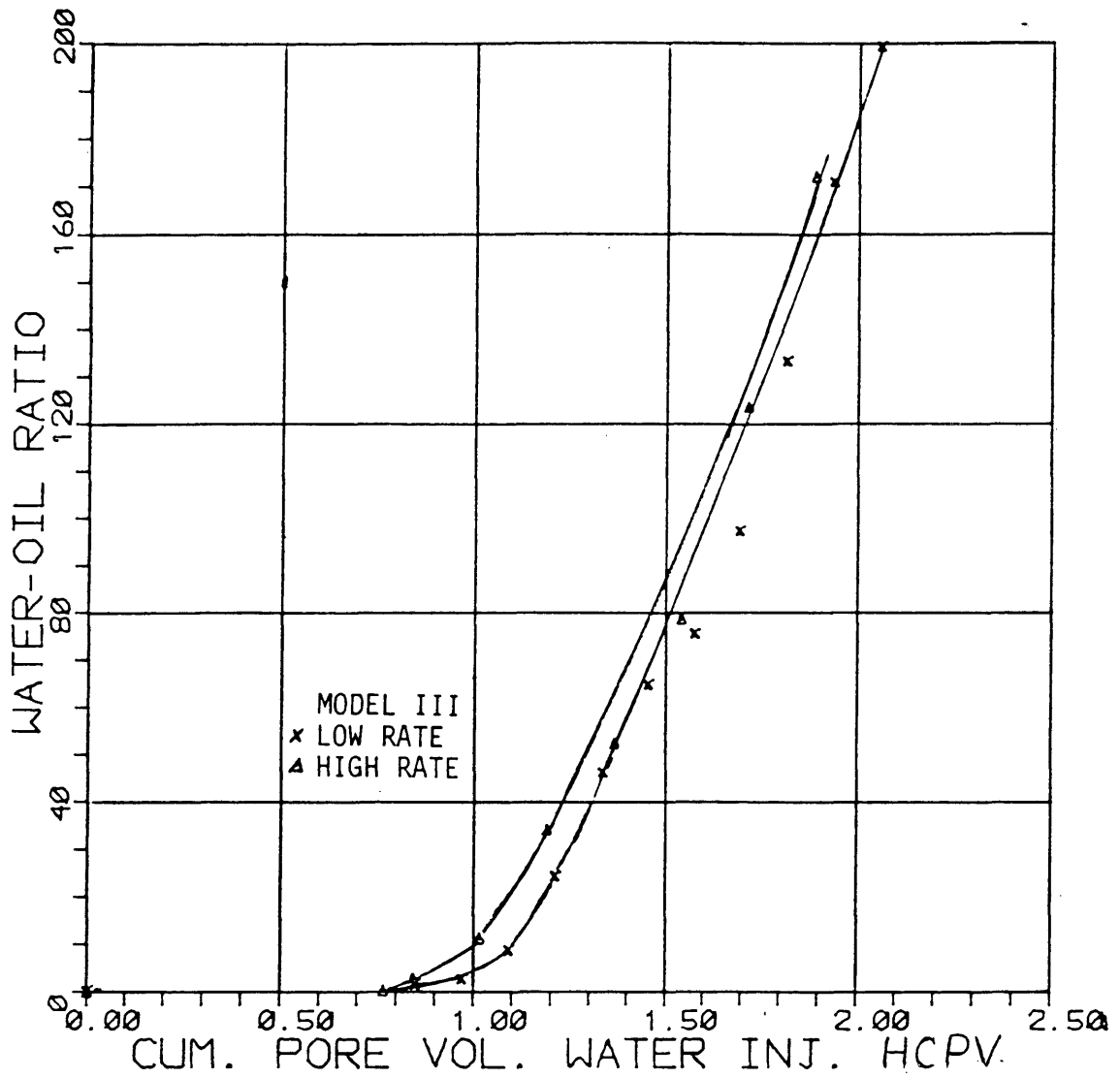


FIGURE 19 EFFECT OF RATE ON WATER-OIL RATIO
(MODEL III, KEROSENE)

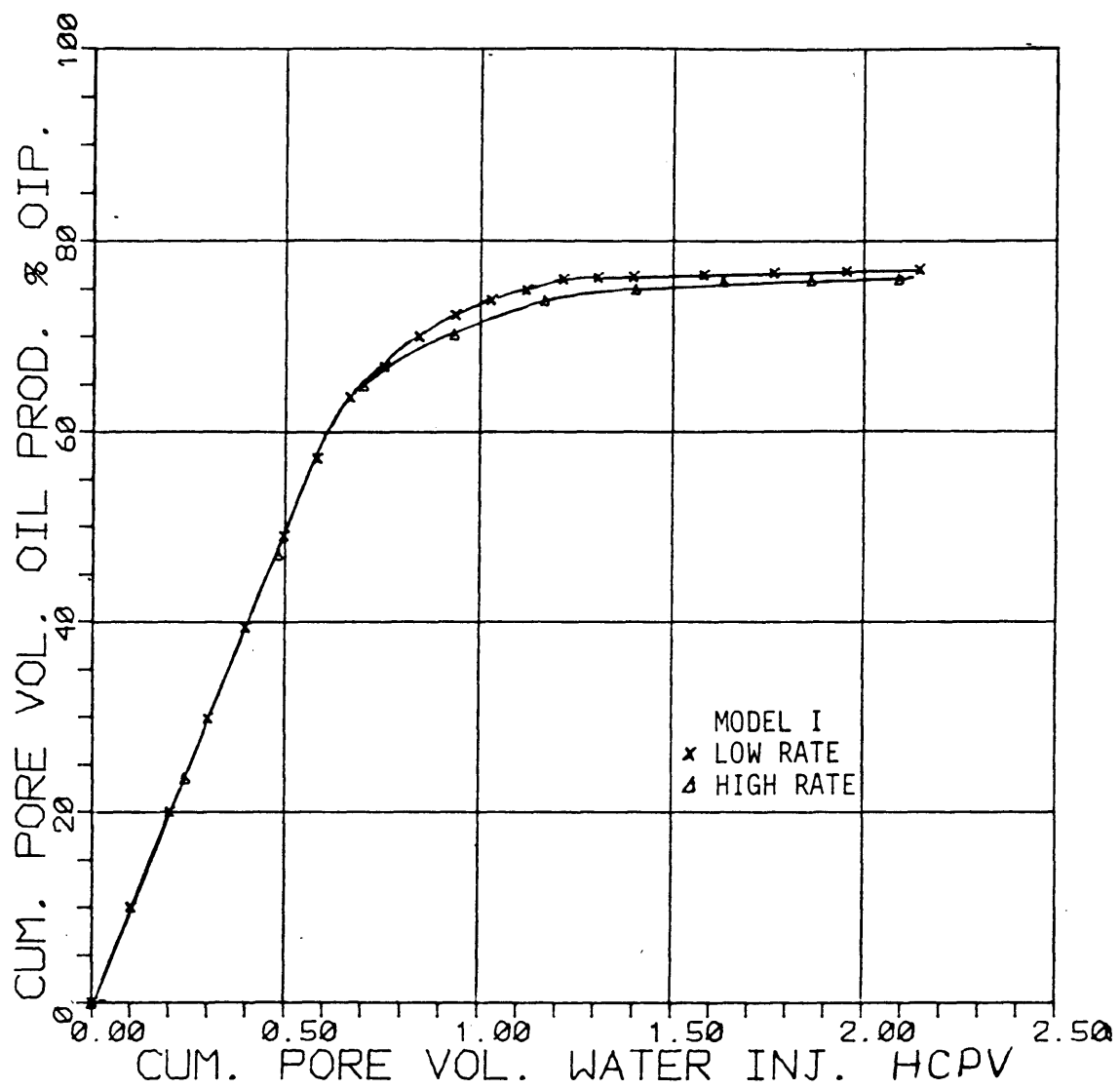


FIGURE 20 EFFECT OF RATE ON OIL RECOVERY
(MODEL I, SOLTROL)

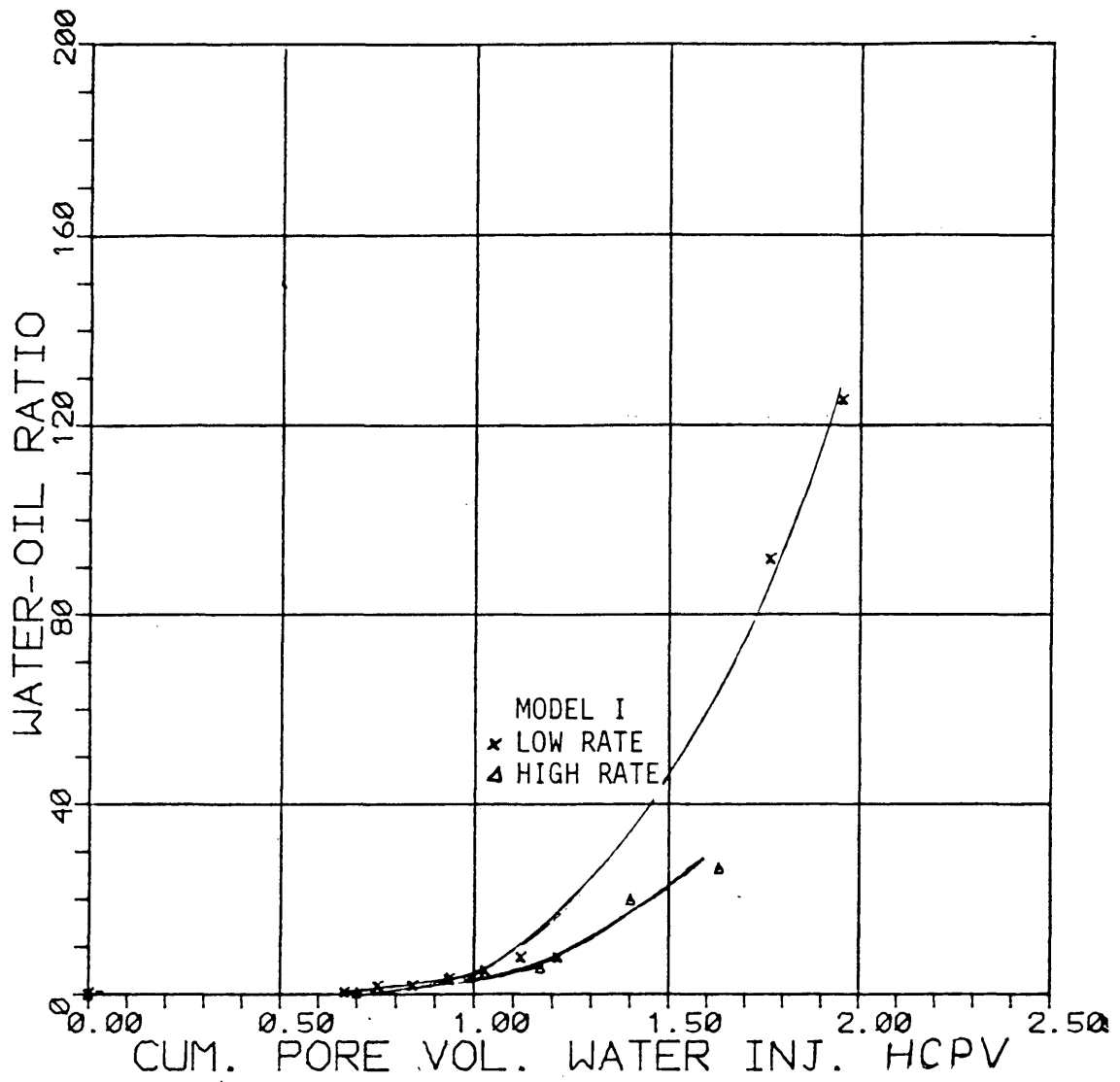


FIGURE 21 EFFECT OF RATE ON WATER-OIL RATIO
(MODEL I, SOLTROL)

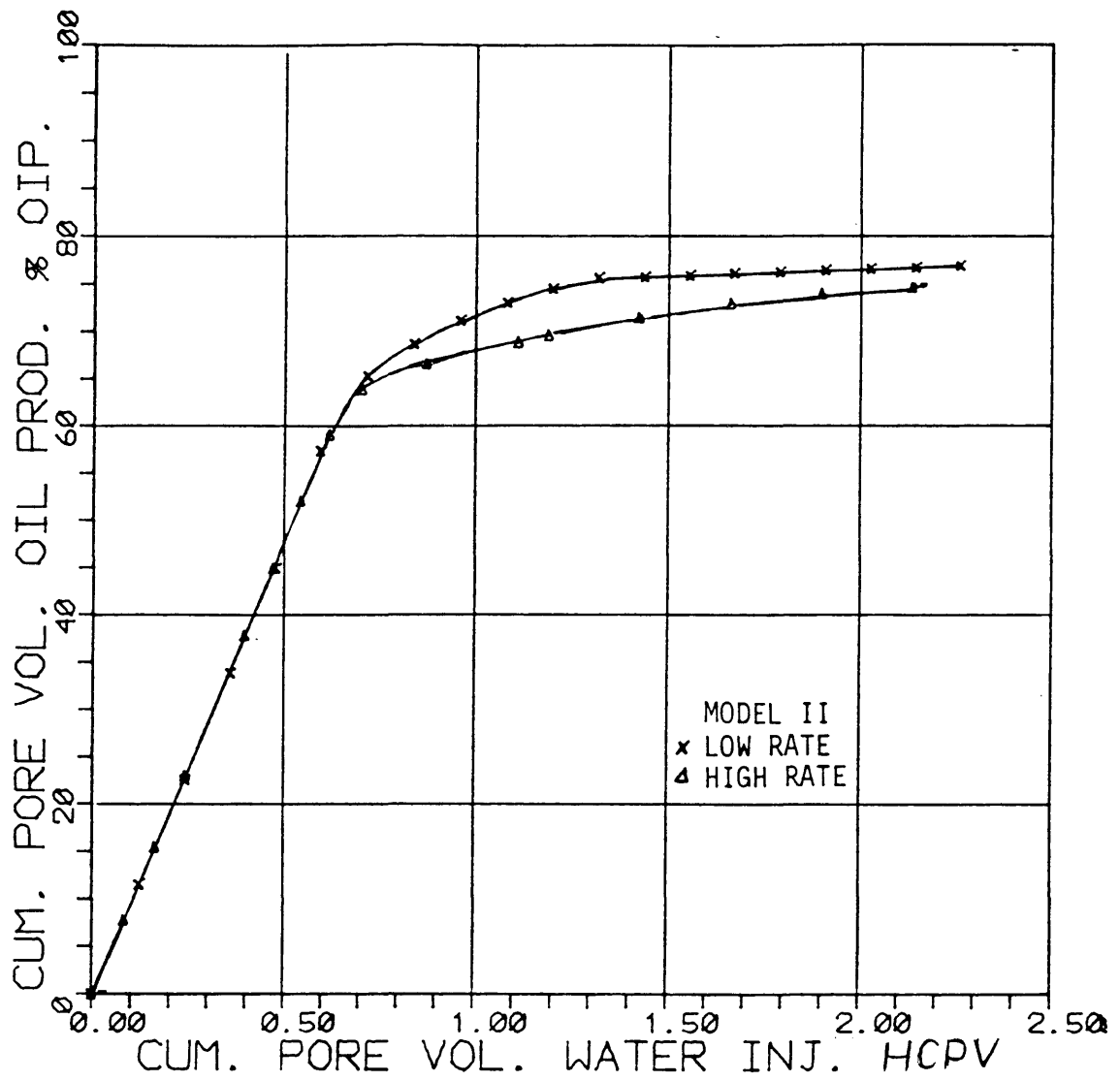


FIGURE 22 EFFECT OF RATE ON OIL RECOVERY
(MODEL II, SOLTROL)

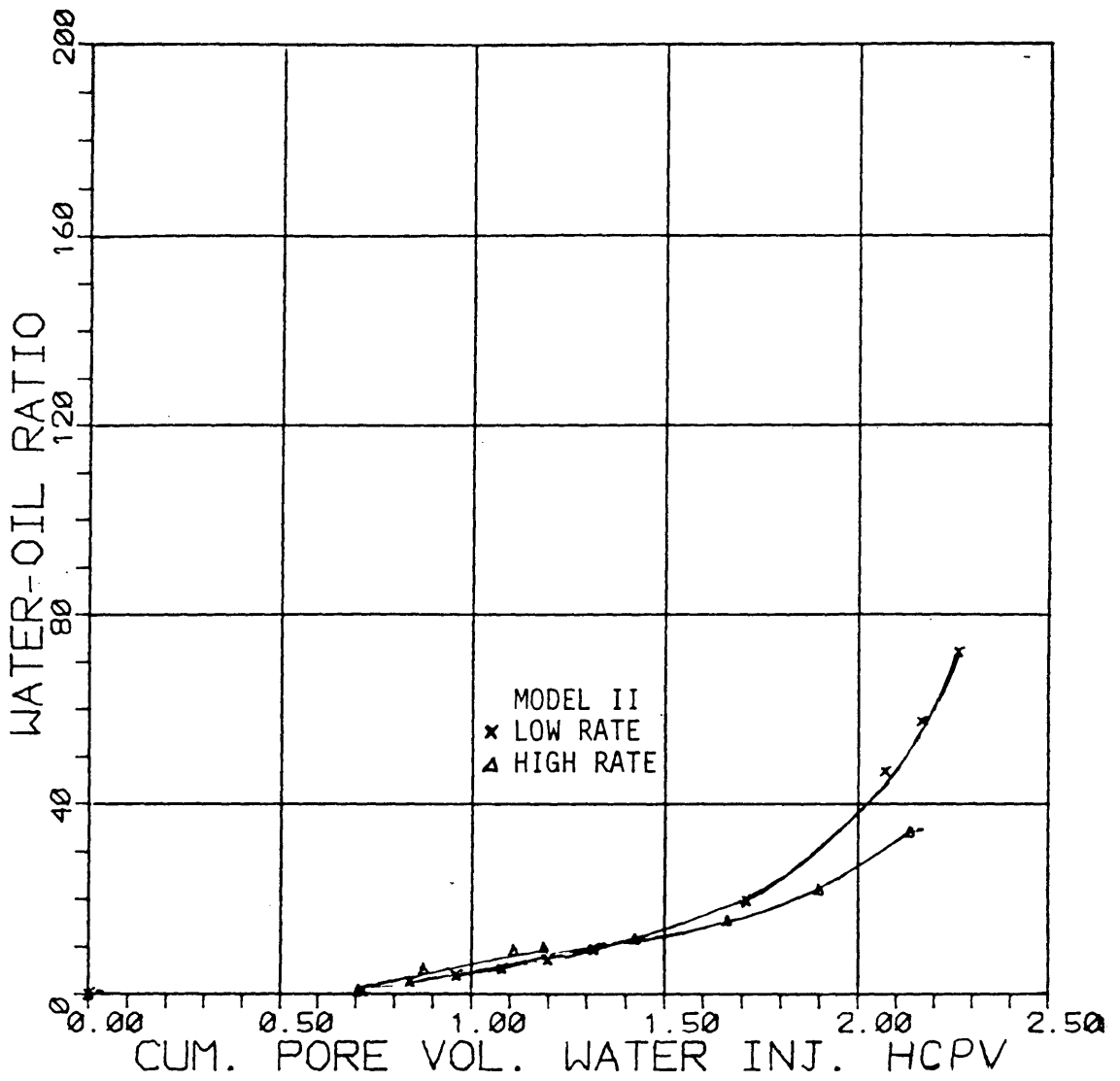


FIGURE 23 EFFECT OF RATE ON WATER-OIL RATIO
(MODEL II, SOLTROL)

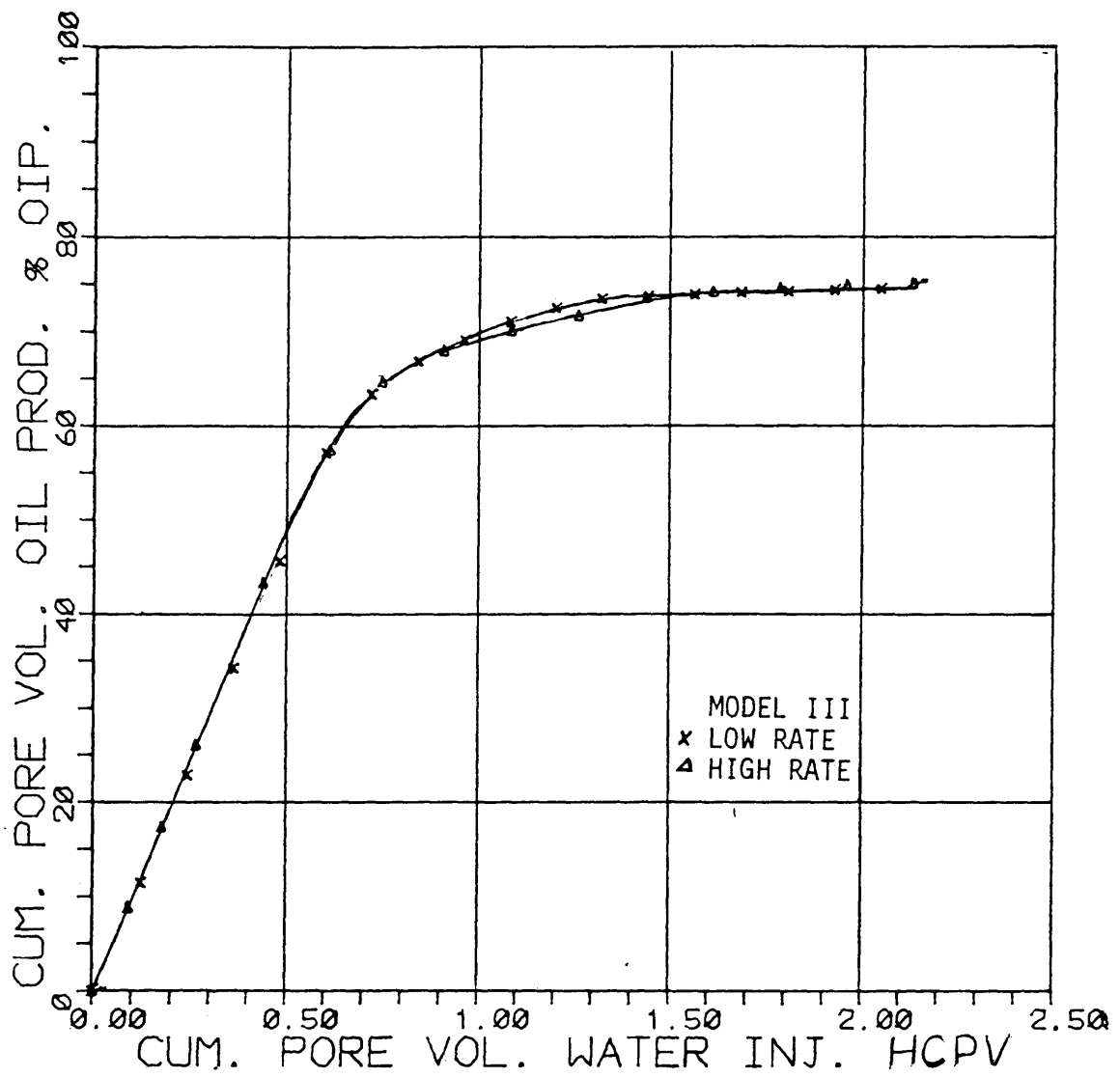


FIGURE 24 EFFECT OF RATE ON OIL RECOVERY
(MODEL III, SOLTROL)

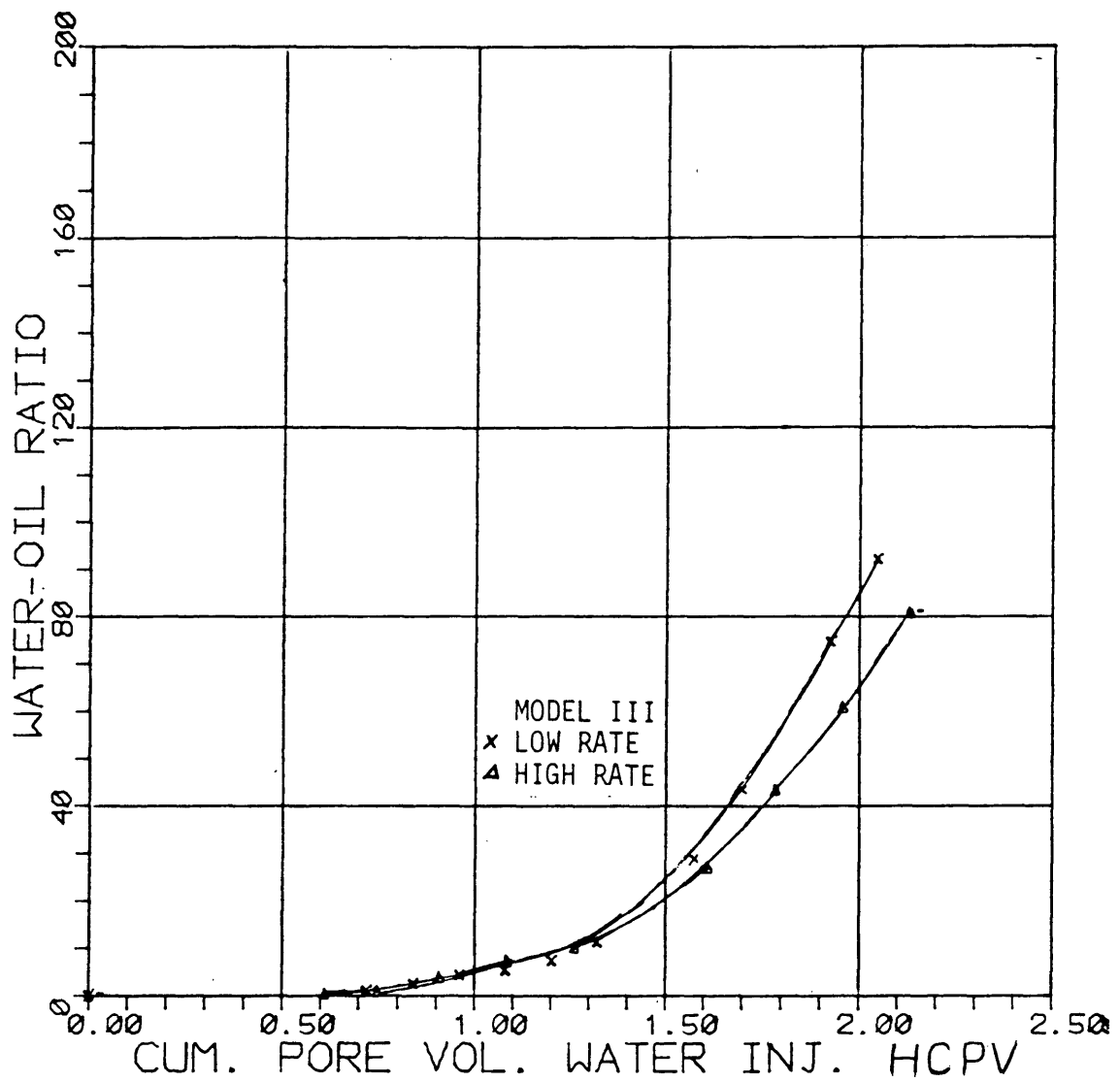


FIGURE 25. EFFECT OF RATE ON WATER-OIL RATIO
(MODEL III, SOLTROL)

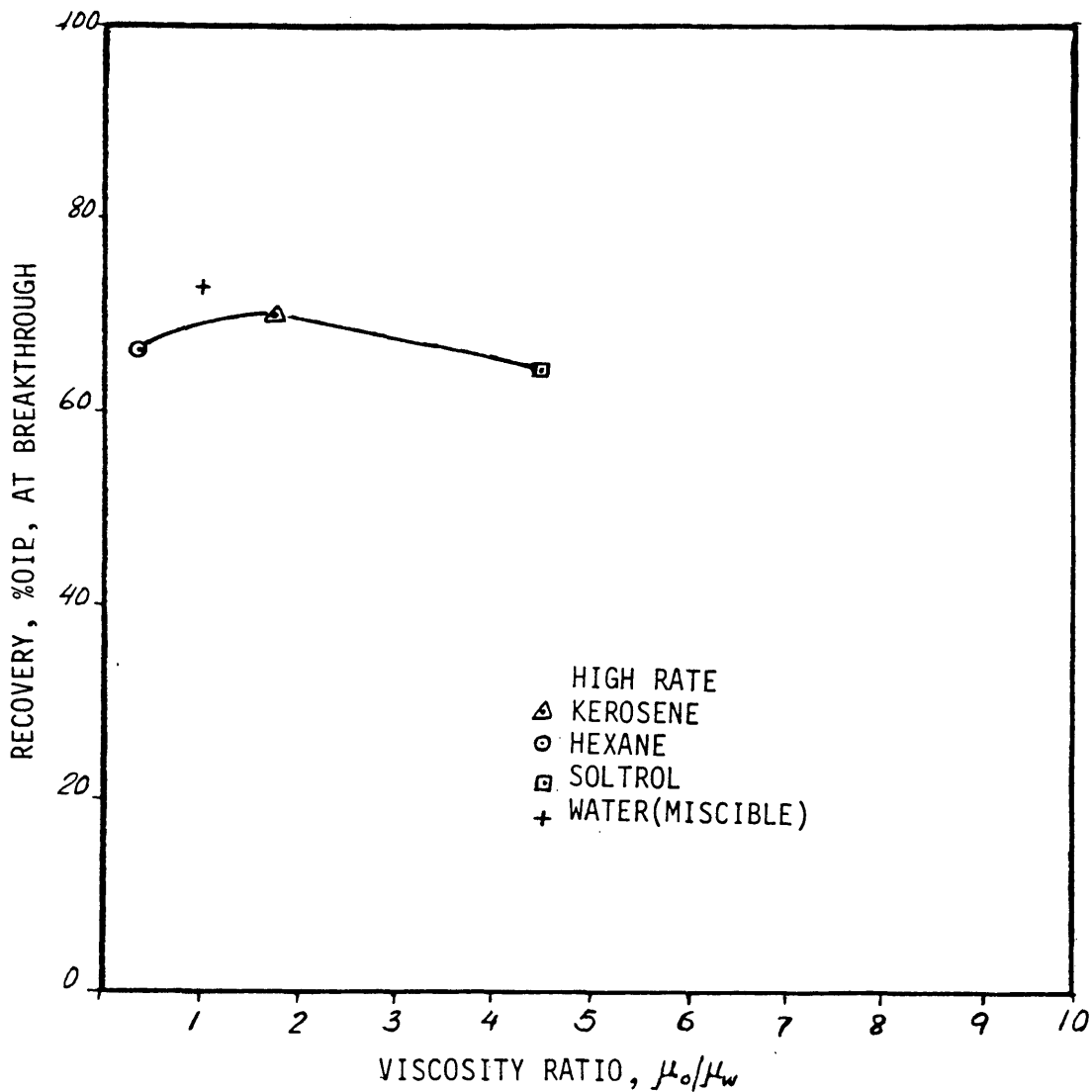


FIGURE 26 OIL RECOVERY AT WATER BREAKTHROUGH AT HIGH RATE VERSUS VISCOSITY RATIO (μ_o/μ_w)

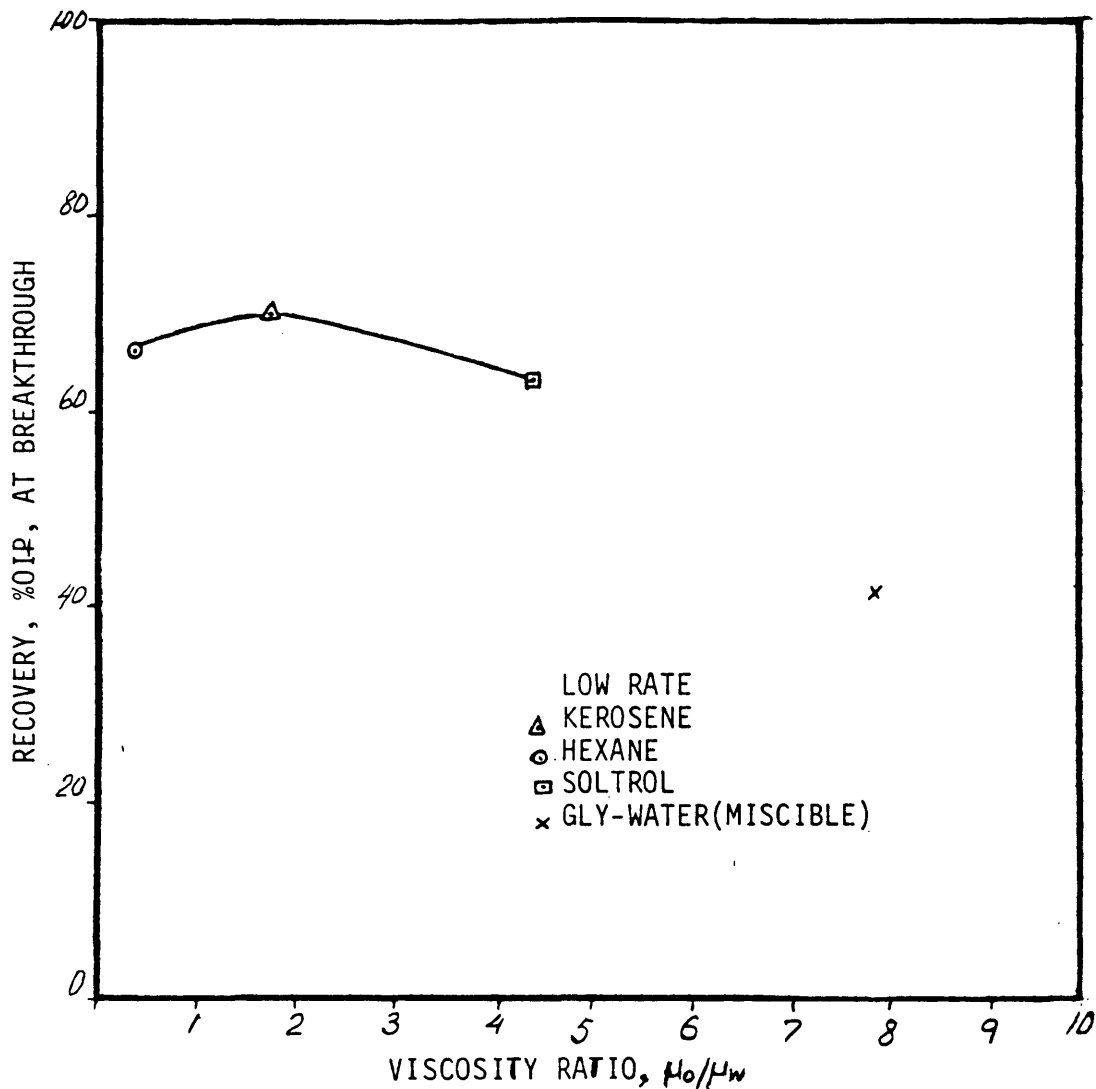


FIGURE 27 OIL RECOVERY AT WATER BREAKTHROUGH AT LOW RATE VERSUS VISCOSITY RATIO (μ_o/μ_w)

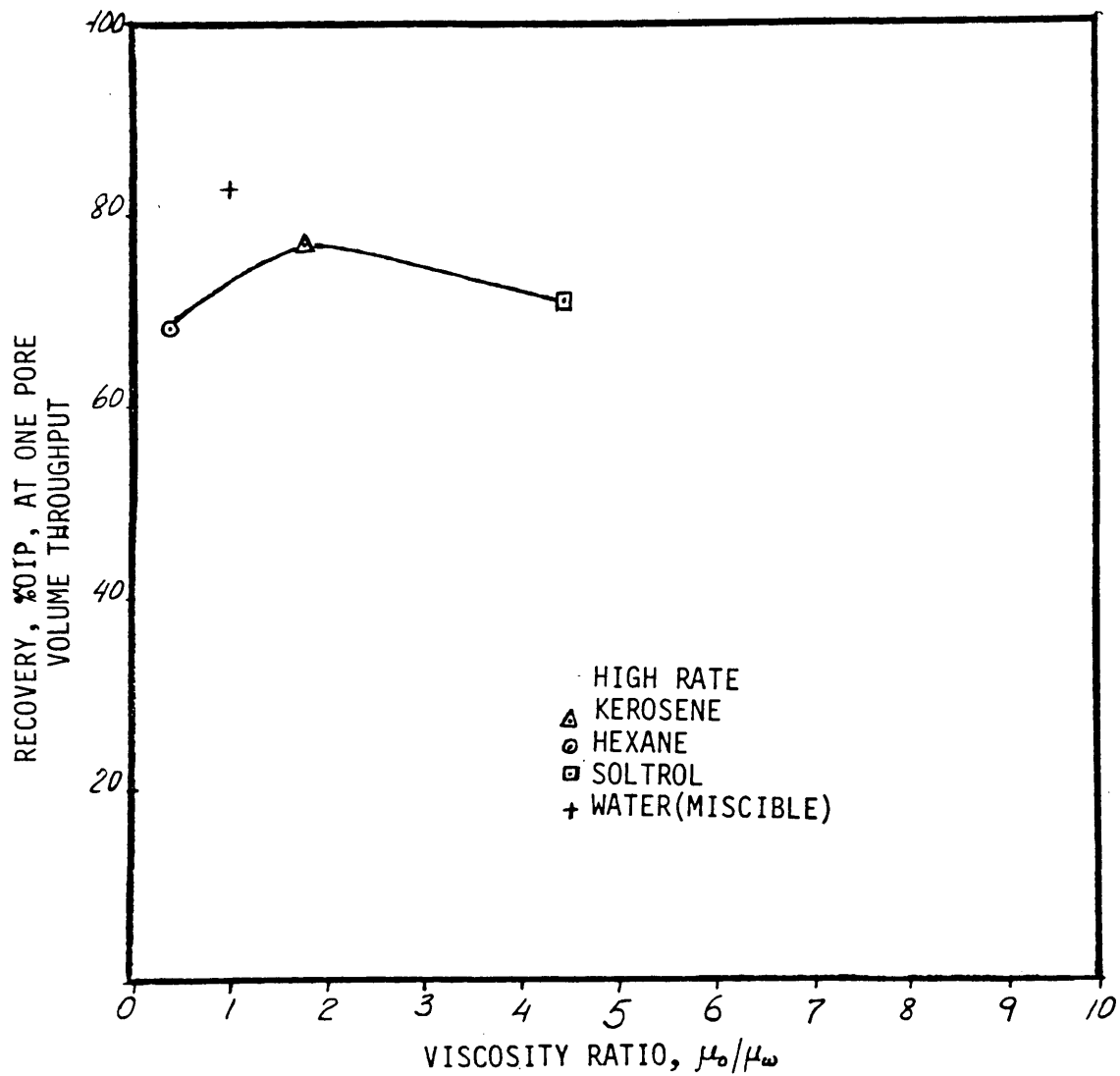


FIGURE 28 OIL RECOVERY AT ONE PORE VOLUME THROUGHPUT
AT HIGH RATE VERSUS VISCOSITY RATIO (μ_o/μ_w)

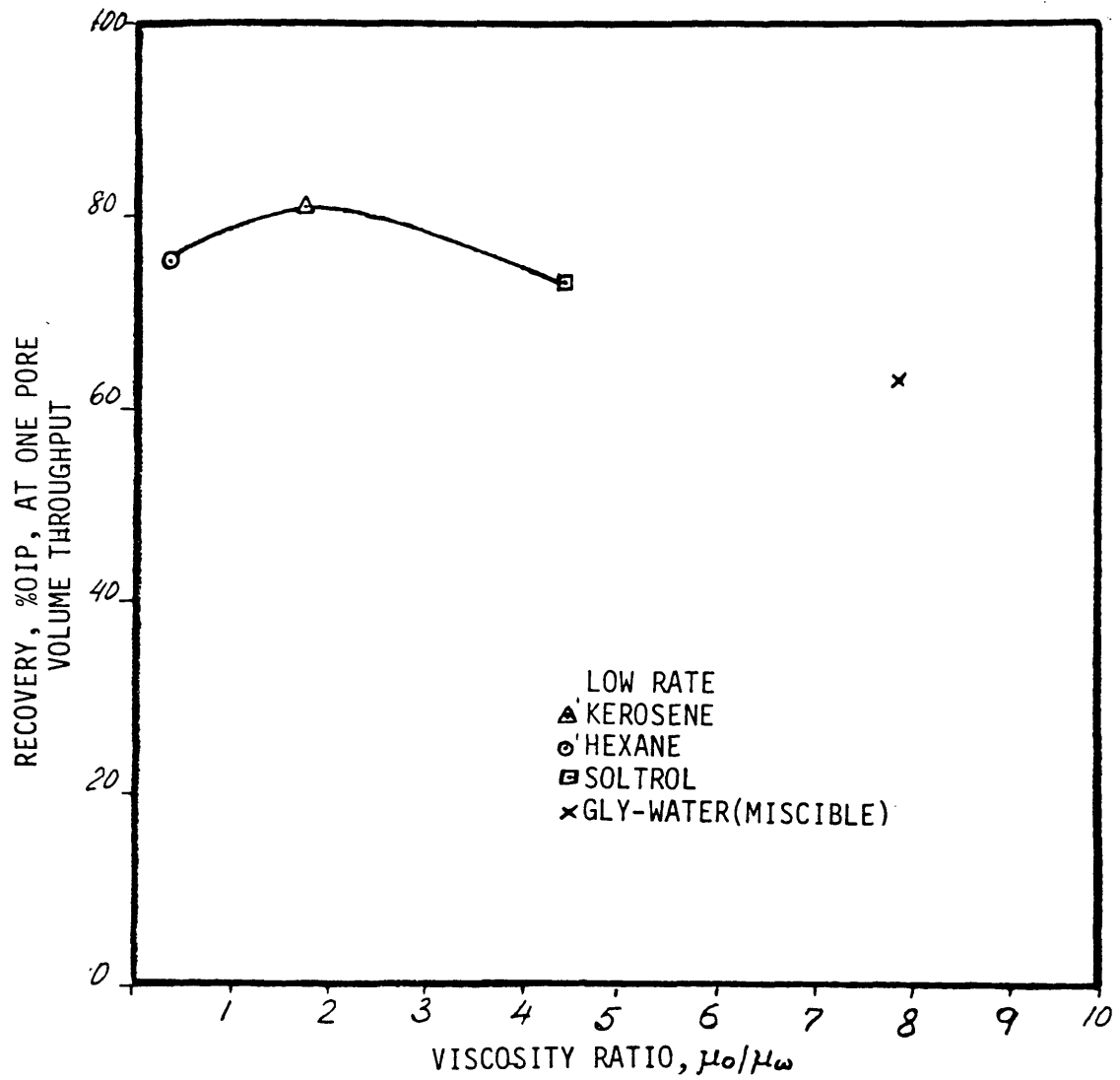


FIGURE 29 OIL RECOVERY AT ONE PORE VOLUME THROUGHPUT
AT LOW RATE VERSUS VISCOSITY RATIO (μ_o/μ_w)

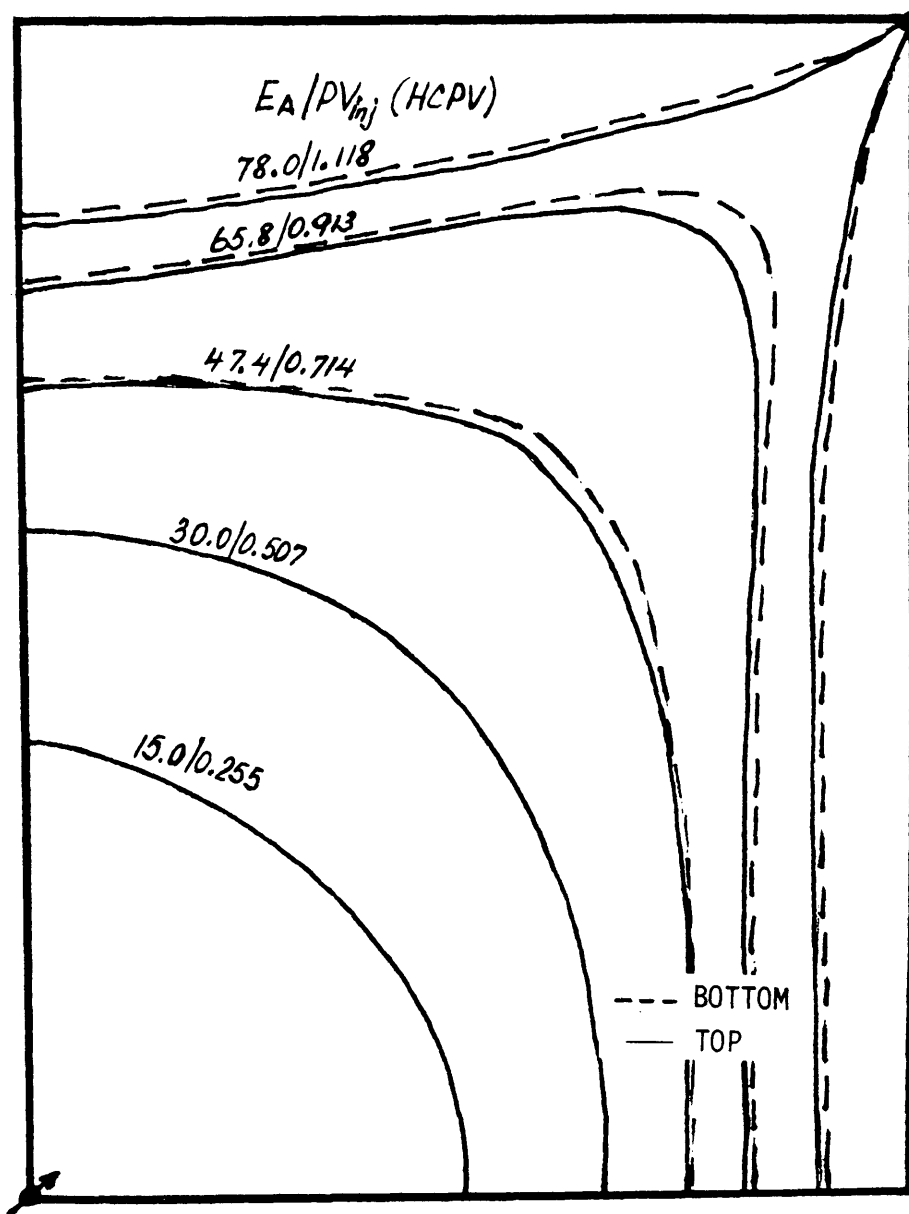


FIGURE 30 COMPARISON OF THE POSITIONS OF THE FRONTS
AT HIGH RATE (HEXANE, VISCOSITY RATIO = 0.34)

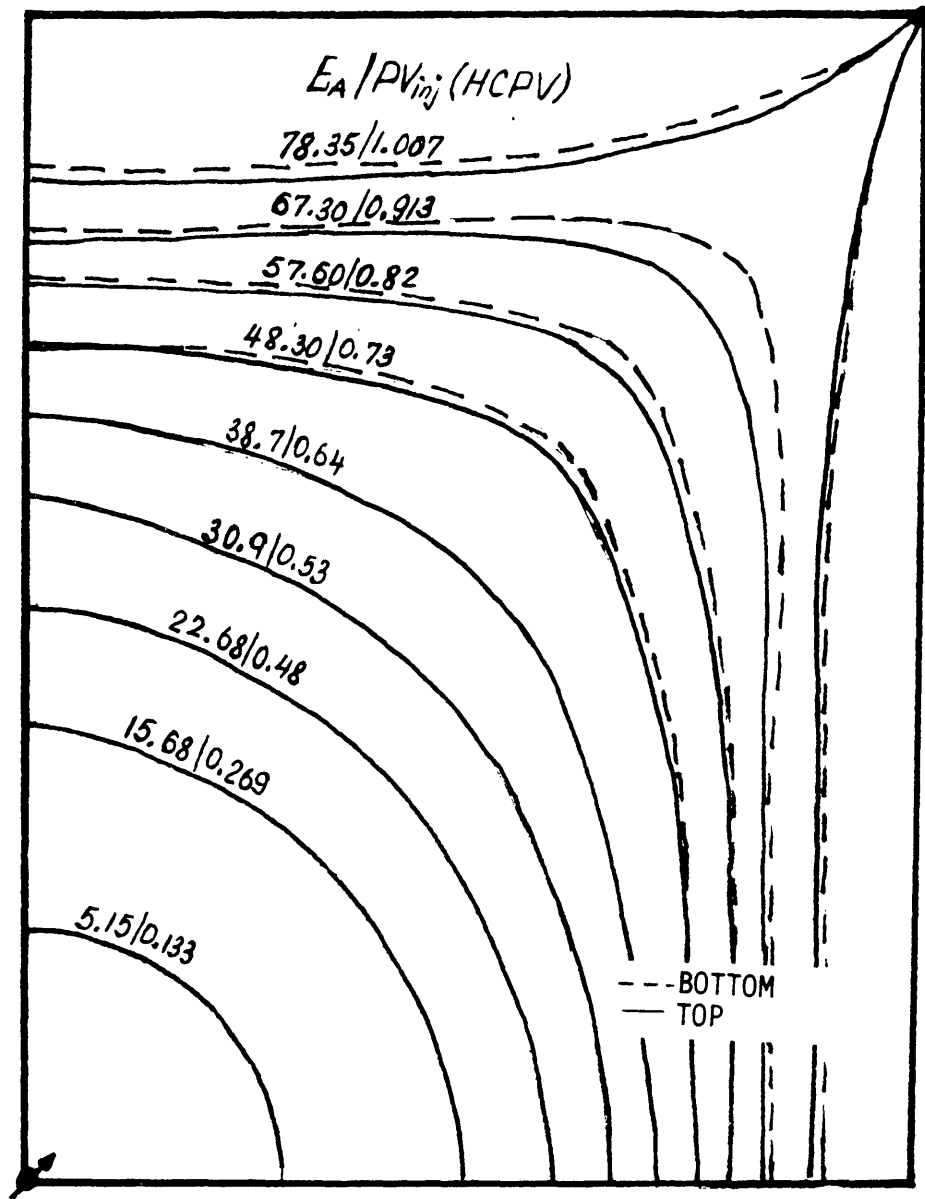


FIGURE 31 COMPARISON OF THE POSITIONS OF THE FRONTS
AT LOW RATE (HEXANE, VISCOSITY RATIO = 0.34)

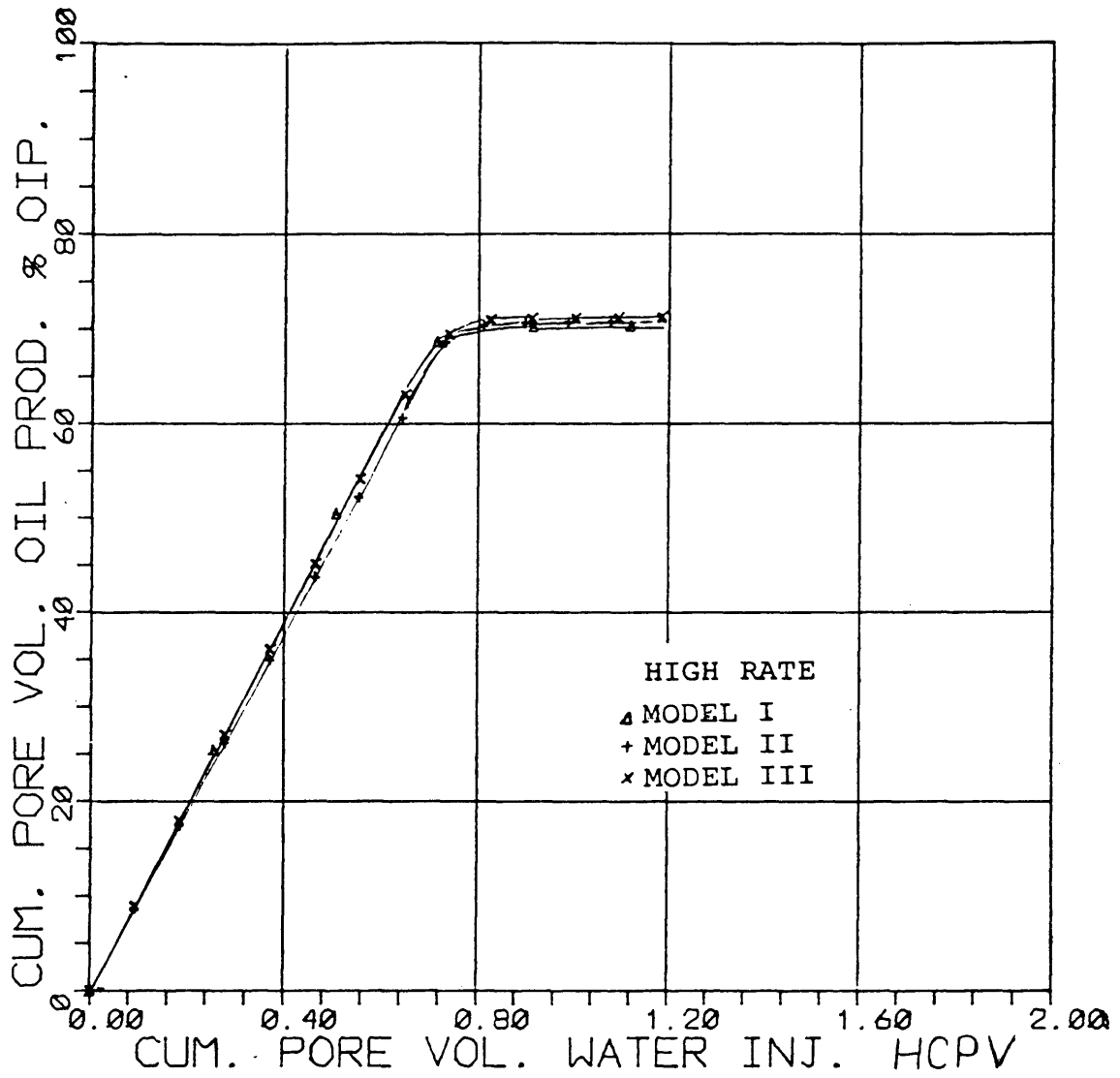


FIGURE 32 COMPARISON OF CUMULATIVE OIL RECOVERIES AT
HIGH RATE (HEXANE, VISCOSITY RATIO = 0.34)

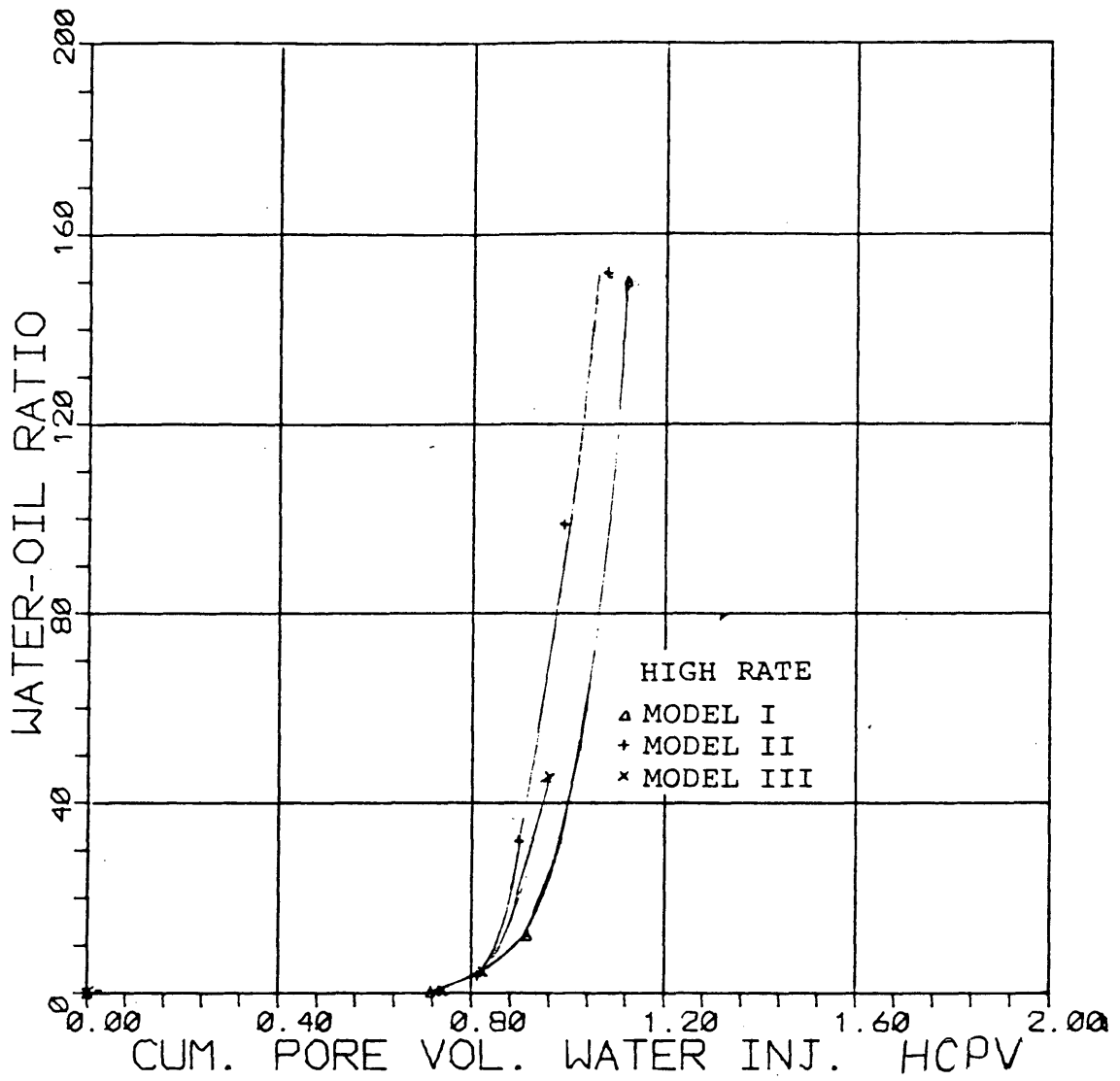


FIGURE 33 COMPARISON OF WATER-OIL RATIO CURVES AT
HIGH RATE (HEXANE, VISCOSITY RATIO = 0.34)

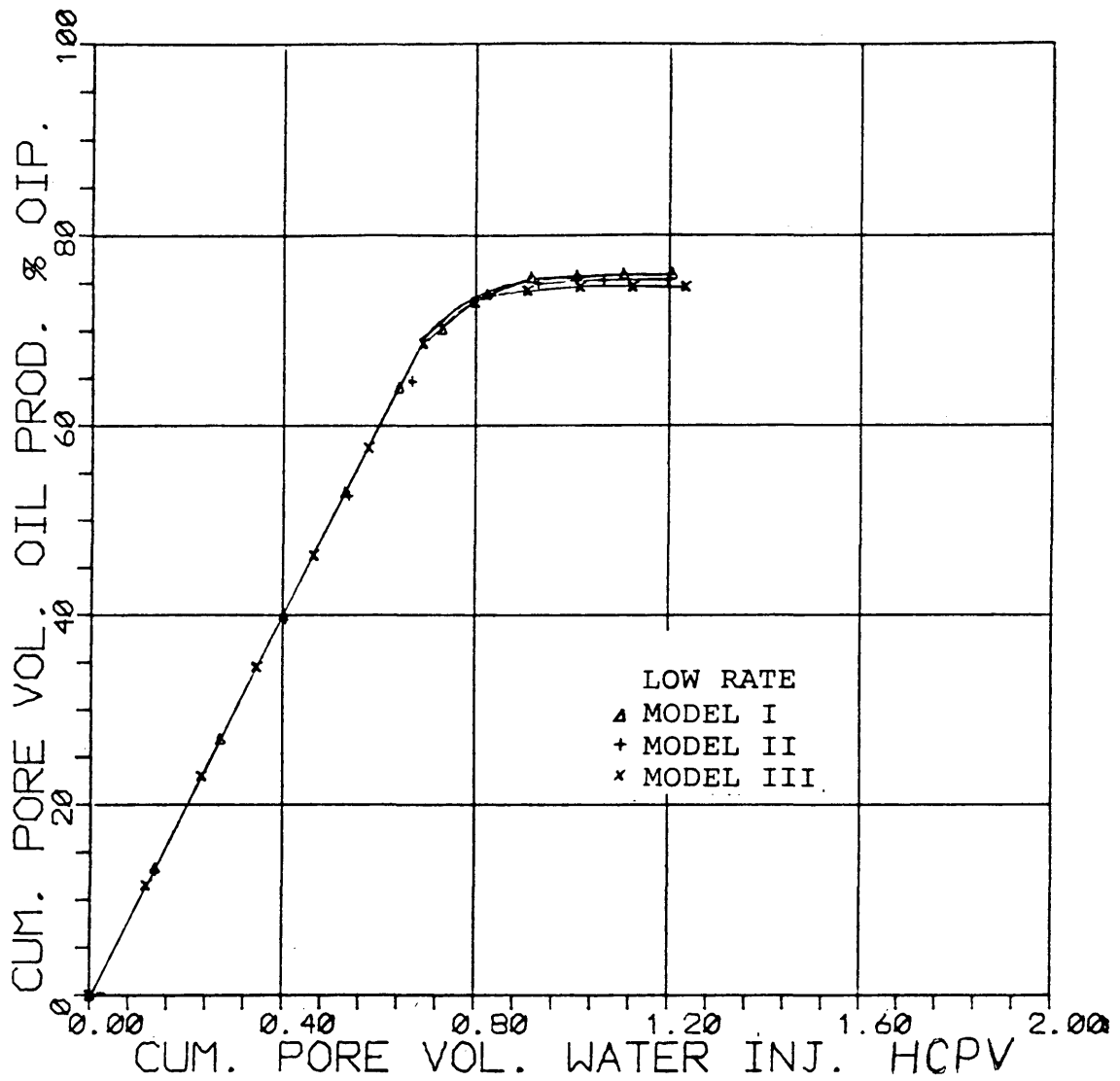


FIGURE 34 COMPARISON OF CUMULATIVE OIL RECOVERIES AT
LOW RATE (HEXANE, VISCOSITY RATIO = 0.34)

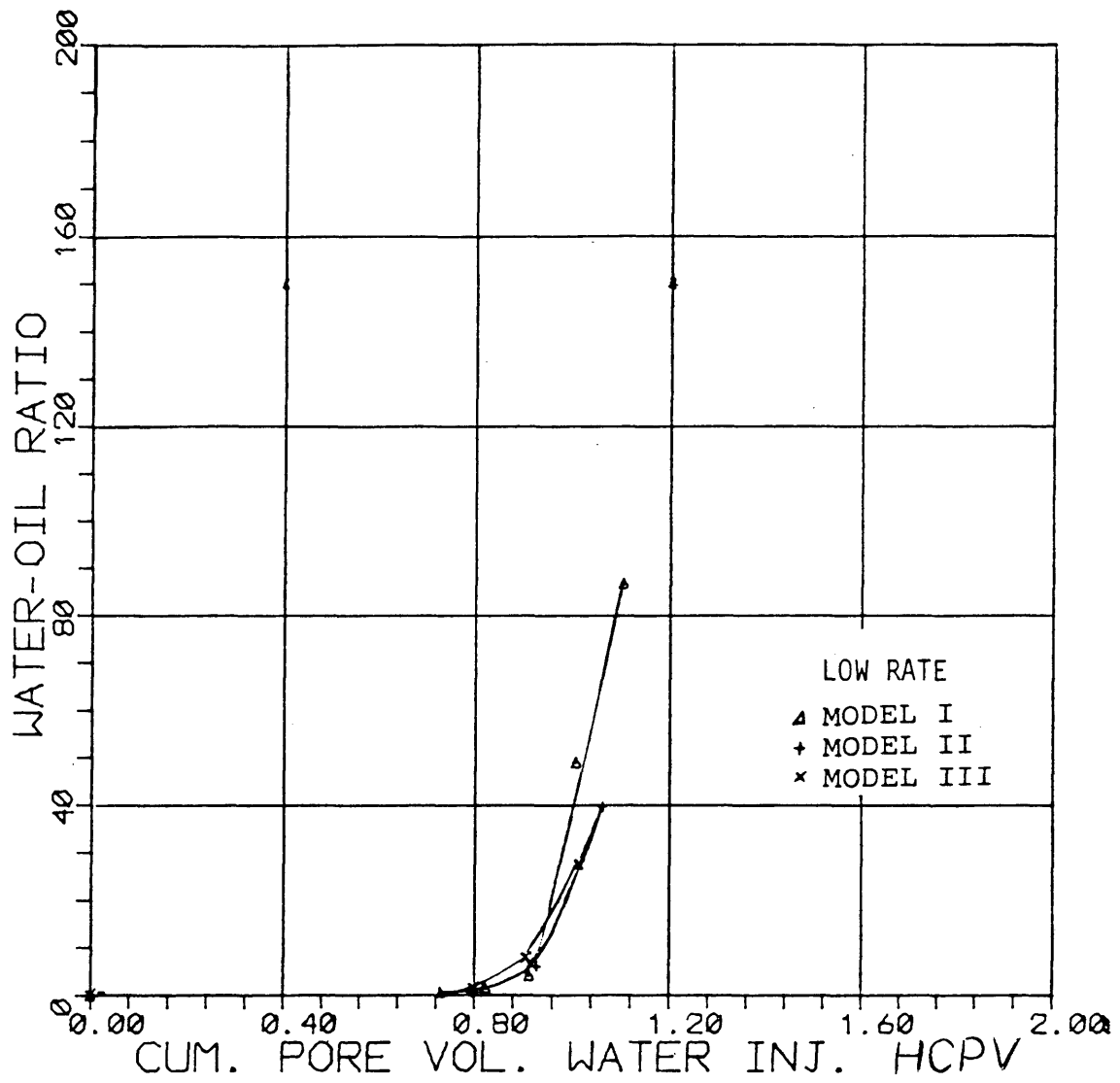


FIGURE 35 COMPARISON OF WATER-OIL RATIO CURVES AT
LOW RATE (HEXANE, VISCOSITY RATIO = 0.34)

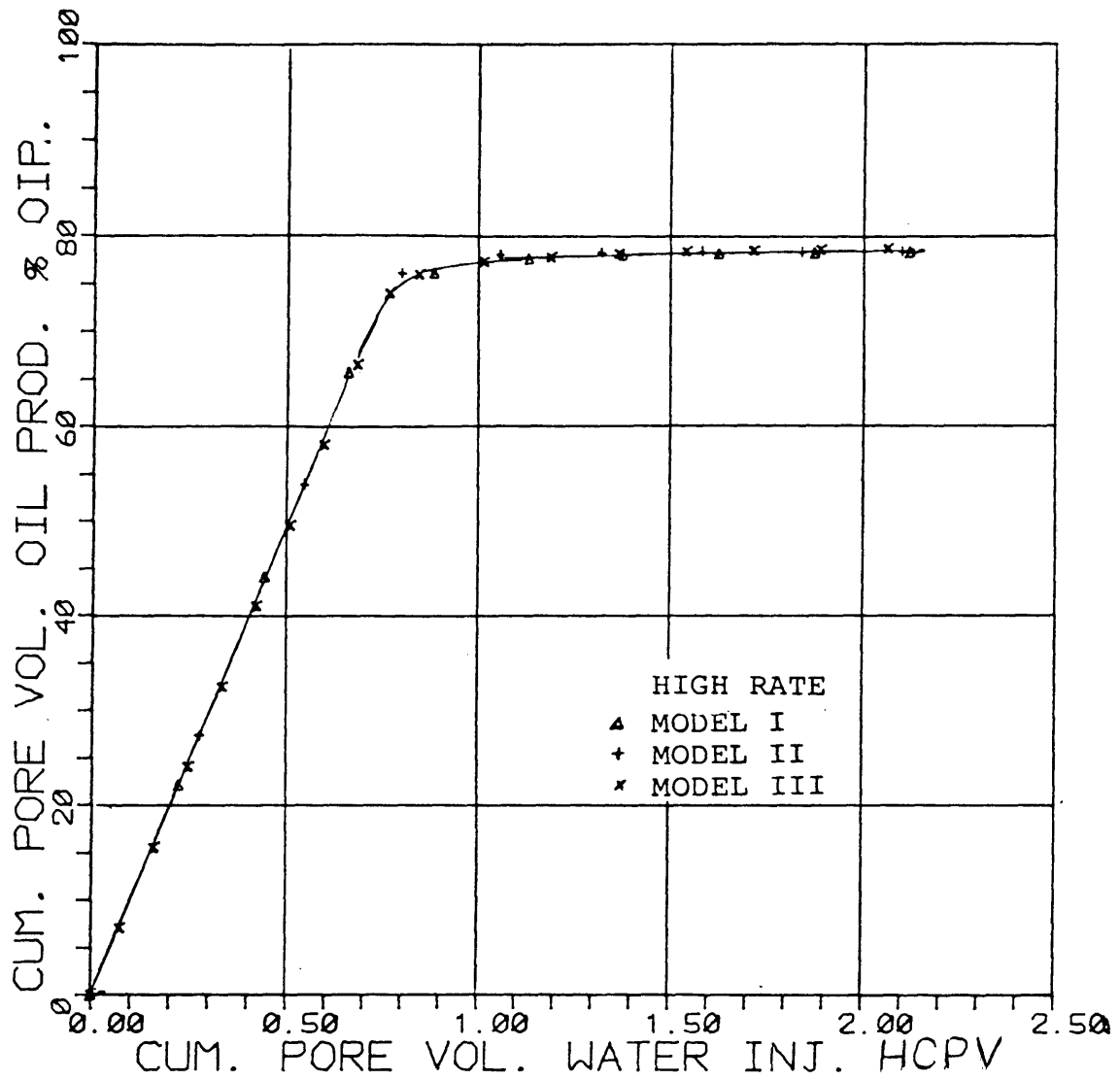


FIGURE 36 COMPARISON OF CUMULATIVE OIL RECOVERIES AT HIGH RATE (KEROSENE, VISCOSITY RATIO = 1.76)

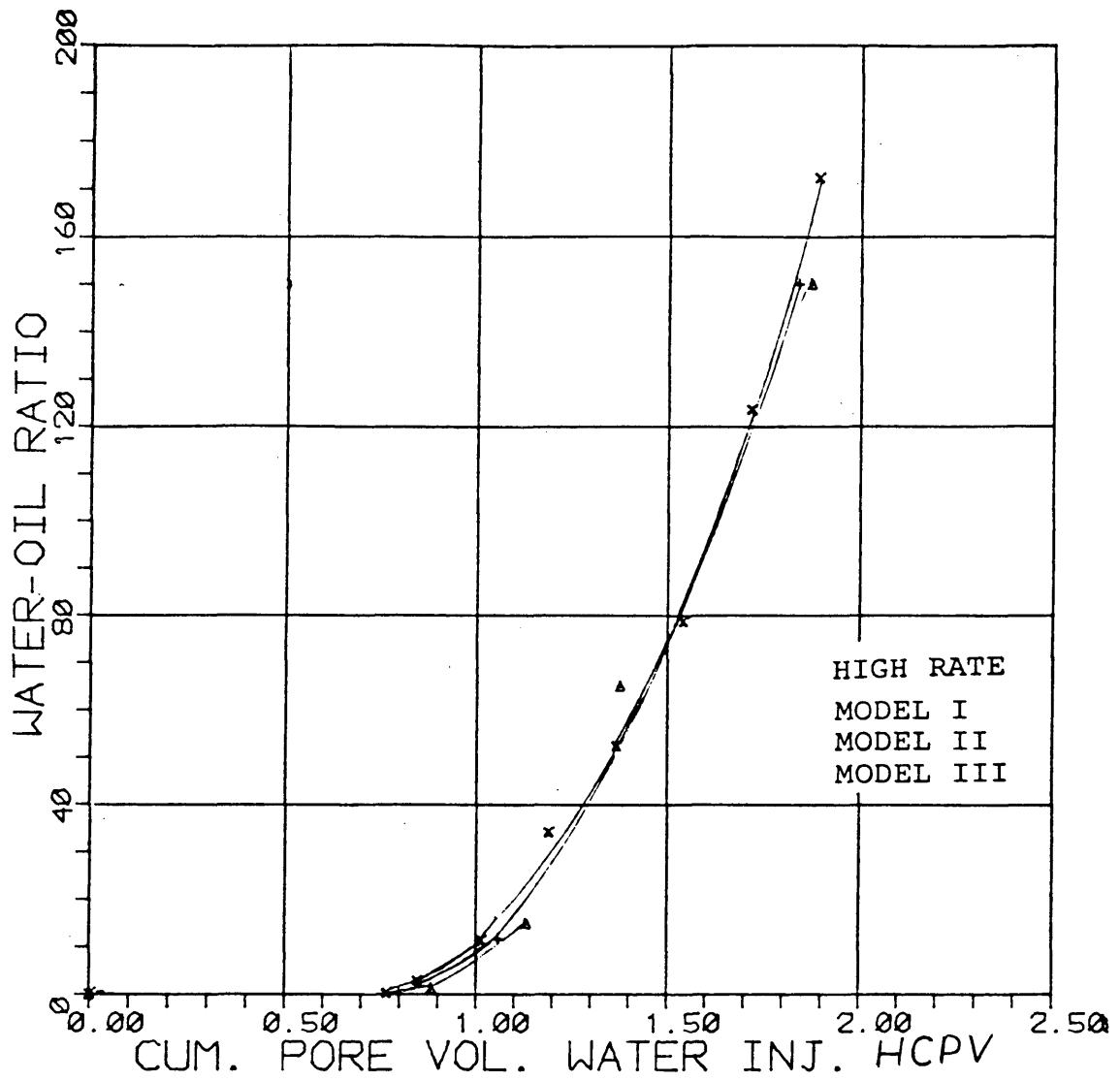


FIGURE 37 COMPARISON OF WATER-OIL RATIO CURVES AT
HIGH RATE (KEROSENE, VISCOSITY RATIO =
1.76)

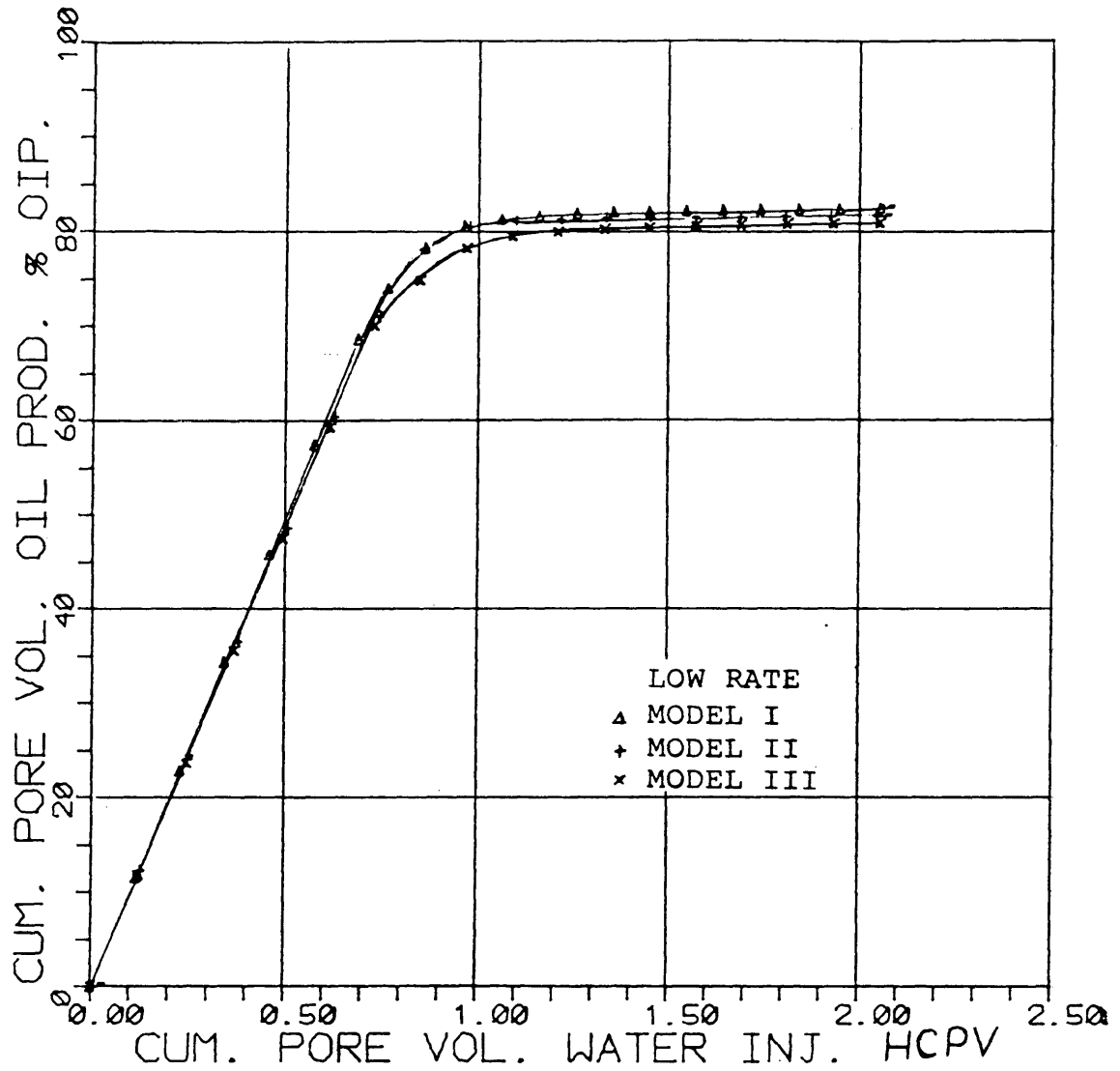


FIGURE 38 COMPARISON OF CUMULATIVE OIL RECOVERIES AT
LOW RATE (KEROSENE, VISCOSITY RATIO =
1.76)

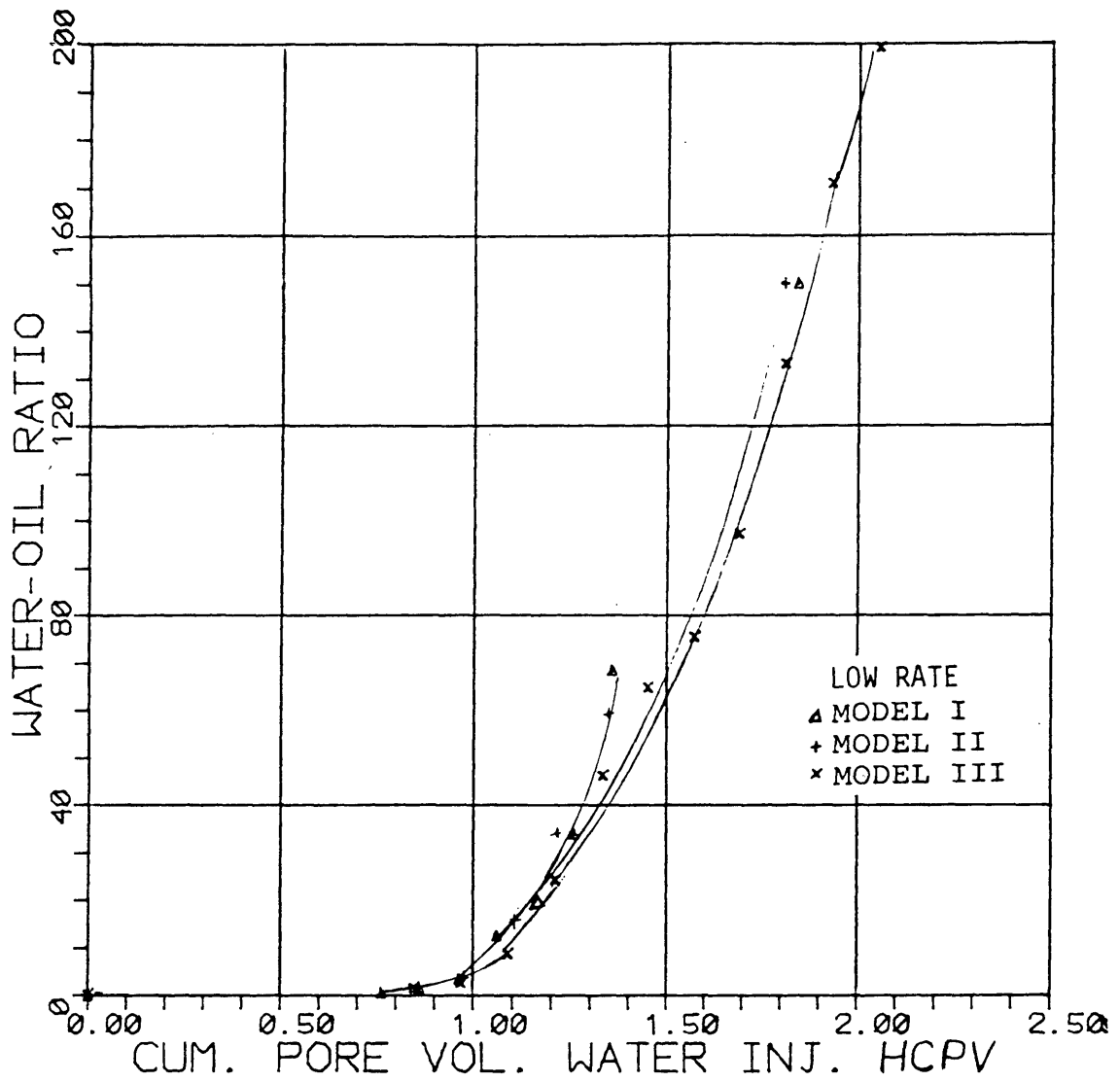


FIGURE 39 COMPARISON OF WATER-OIL RATIO CURVES AT
LOW RATE (KEROSENE, VISCOSITY RATIO =
1.76)

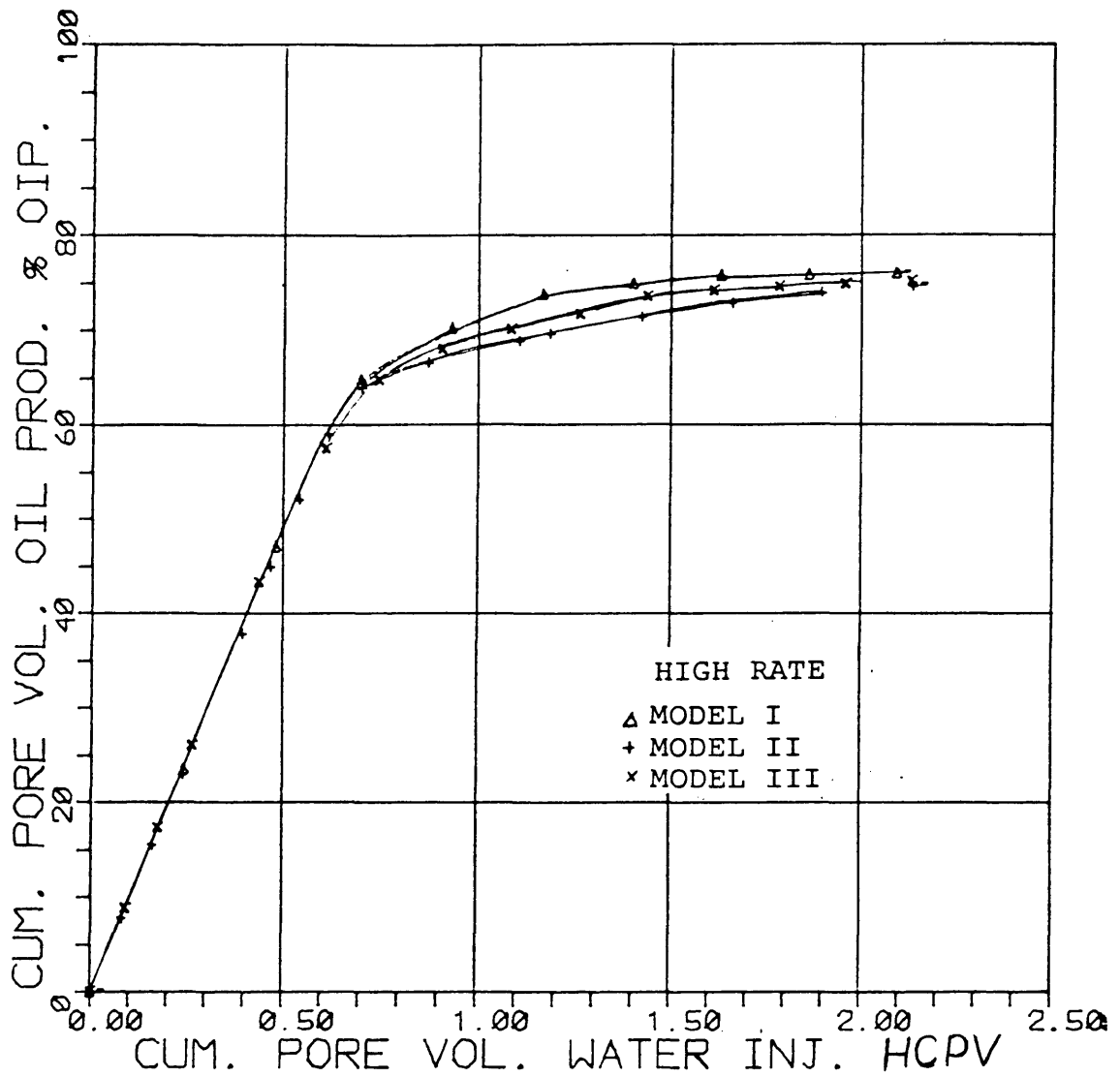


FIGURE 40 COMPARISON OF CUMULATIVE OIL RECOVERIES AT HIGH RATE (SOLTROL, VISCOSITY RATIO = 4.43)

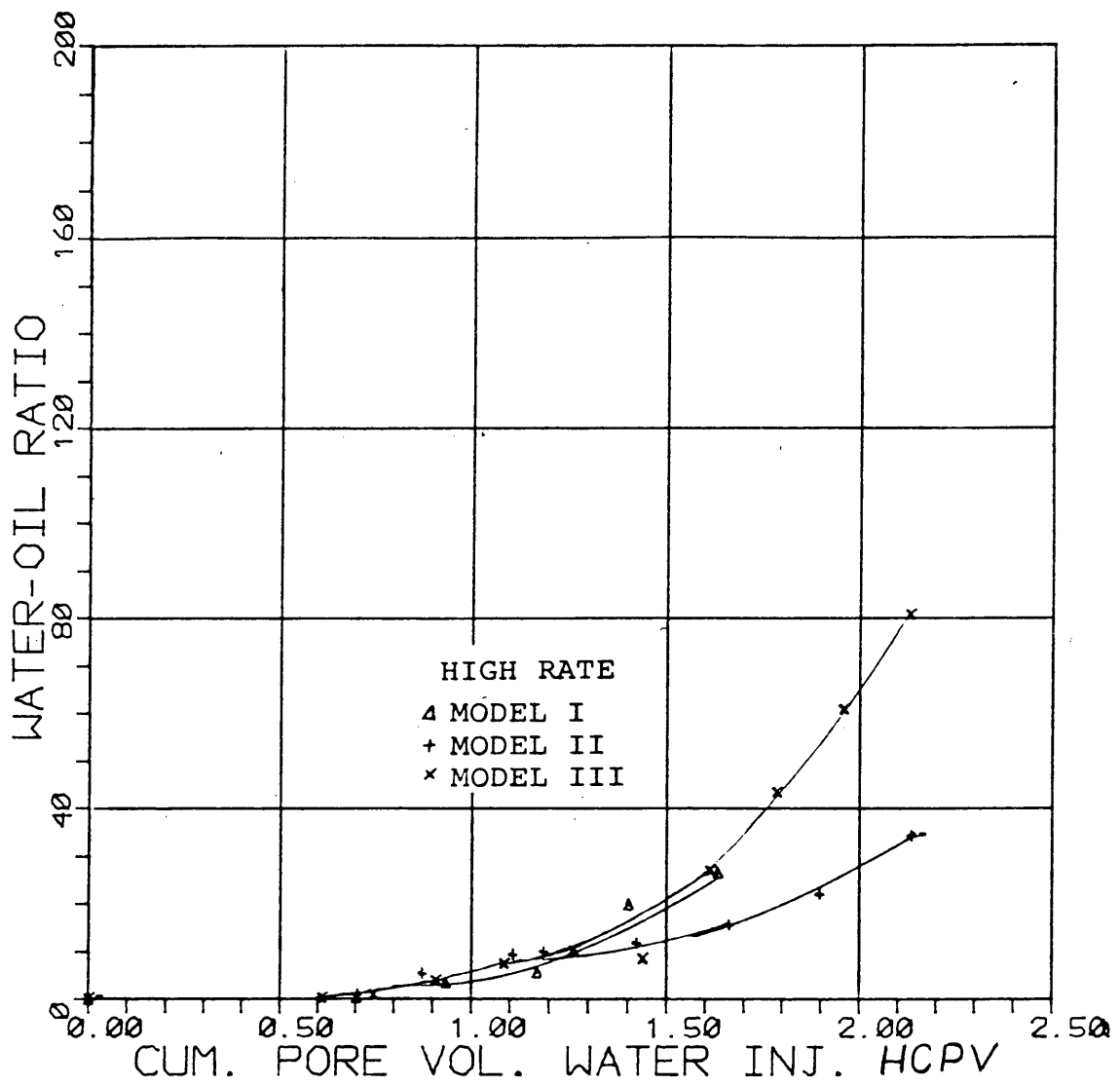


FIGURE 41 COMPARISON OF WATER-OIL RATIO CURVES AT
HIGH RATE (SOLTROL, VISCOSITY RATIO =
4.43)

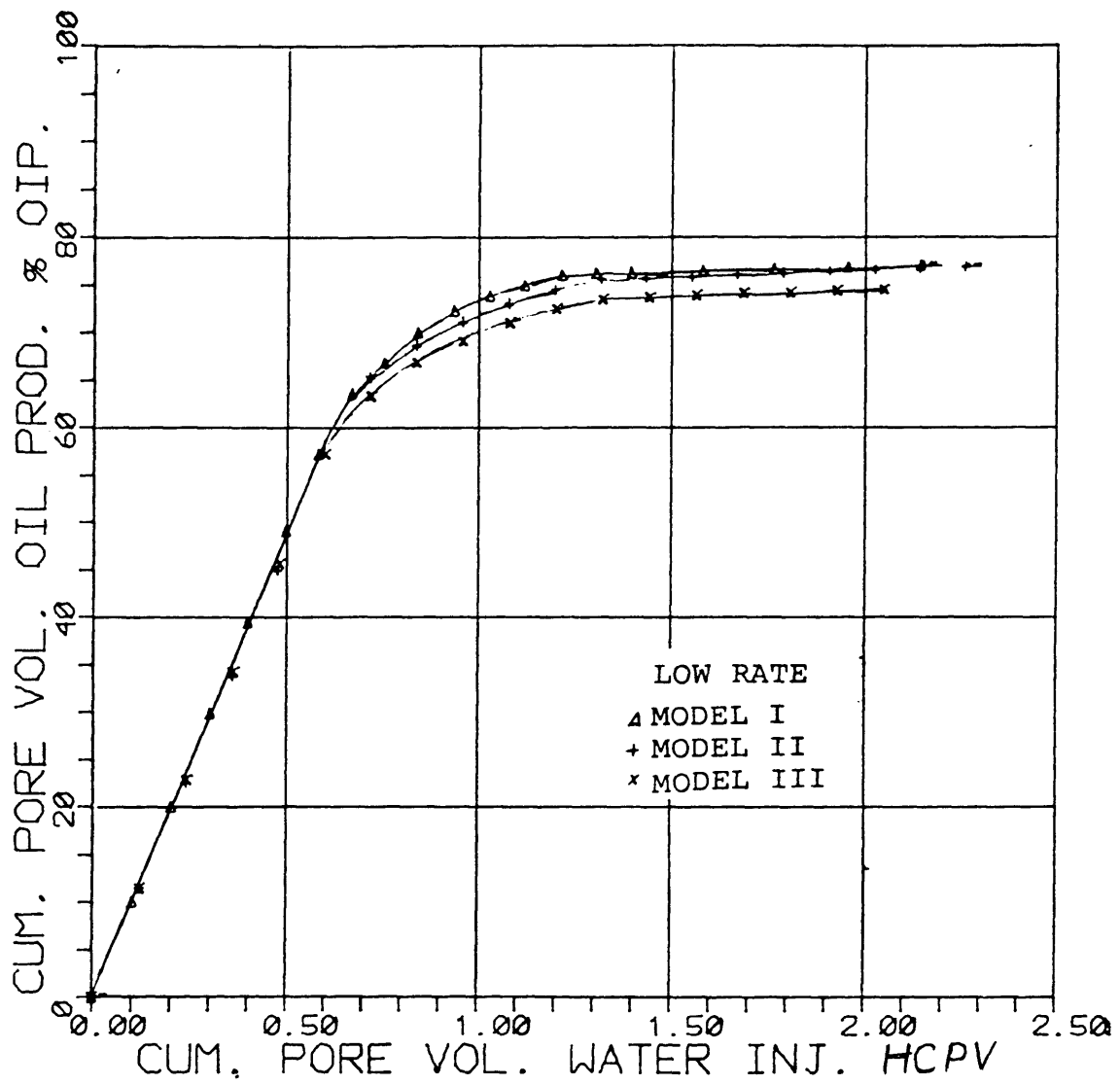


FIGURE 42 COMPARISON OF CUMULATIVE OIL RECOVERIES AT
LOW RATE (SOLTROL, VISCOSITY RATIO =
4.43)

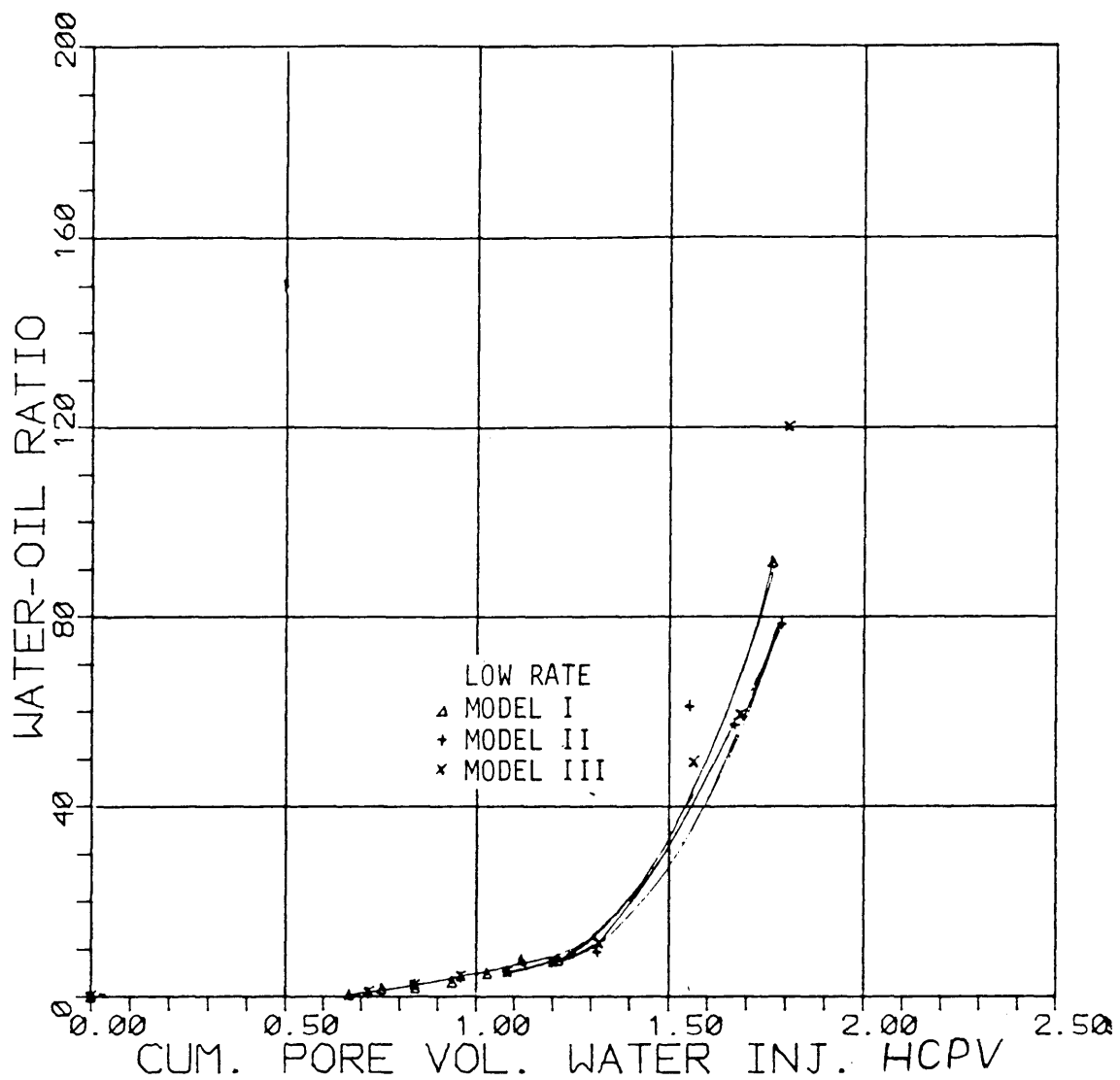


FIGURE 43 COMPARISON OF WATER-OIL RATIO CURVES AT
LOW RATE (SOLTROL, VISCOSITY RATIO =
4.43)

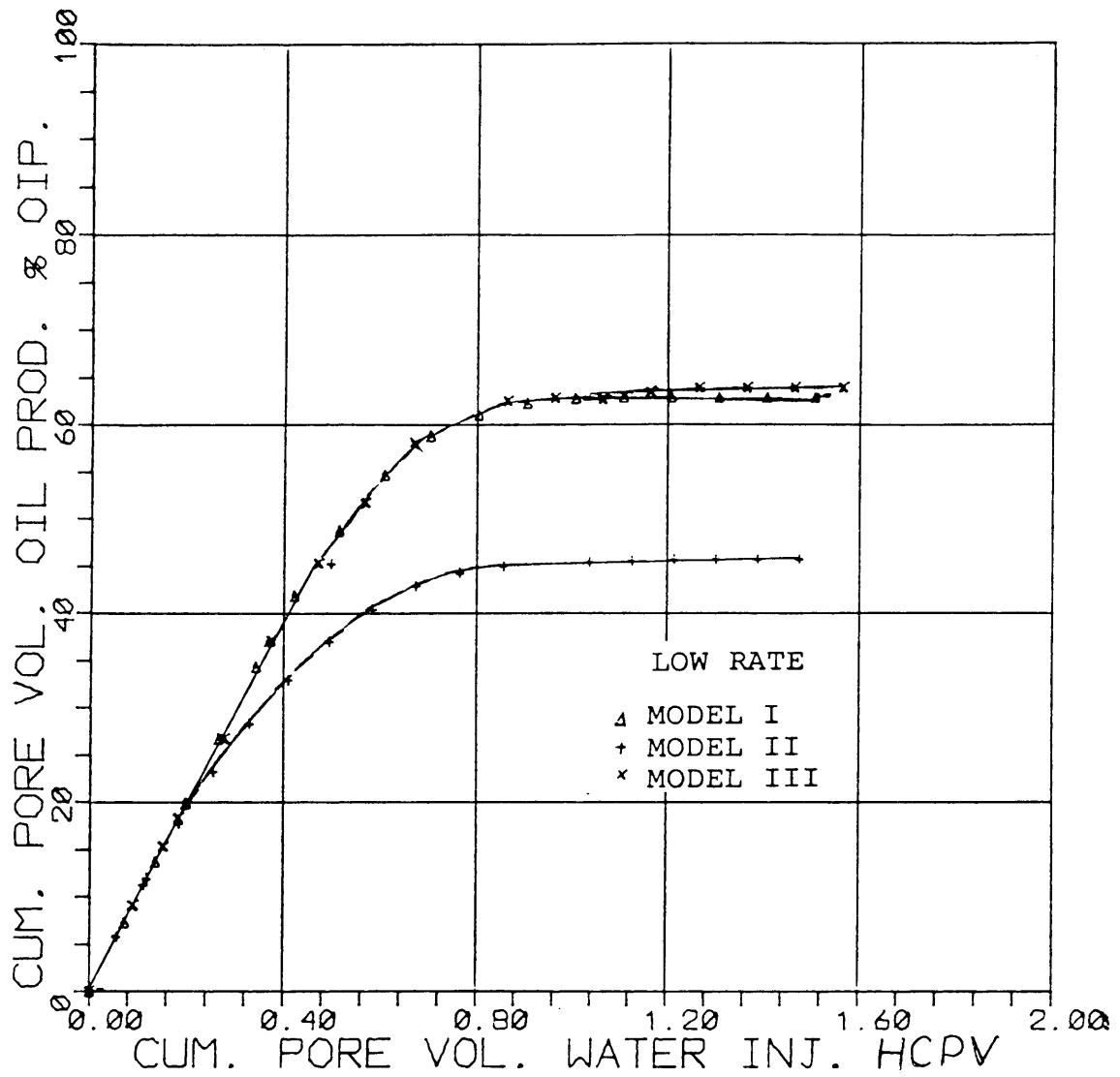


FIGURE 44 COMPARISON OF CUMULATIVE OIL RECOVERIES AT
LOW RATE (GLYCERINE-WATER, VISCOSITY
RATIO = 7.93)

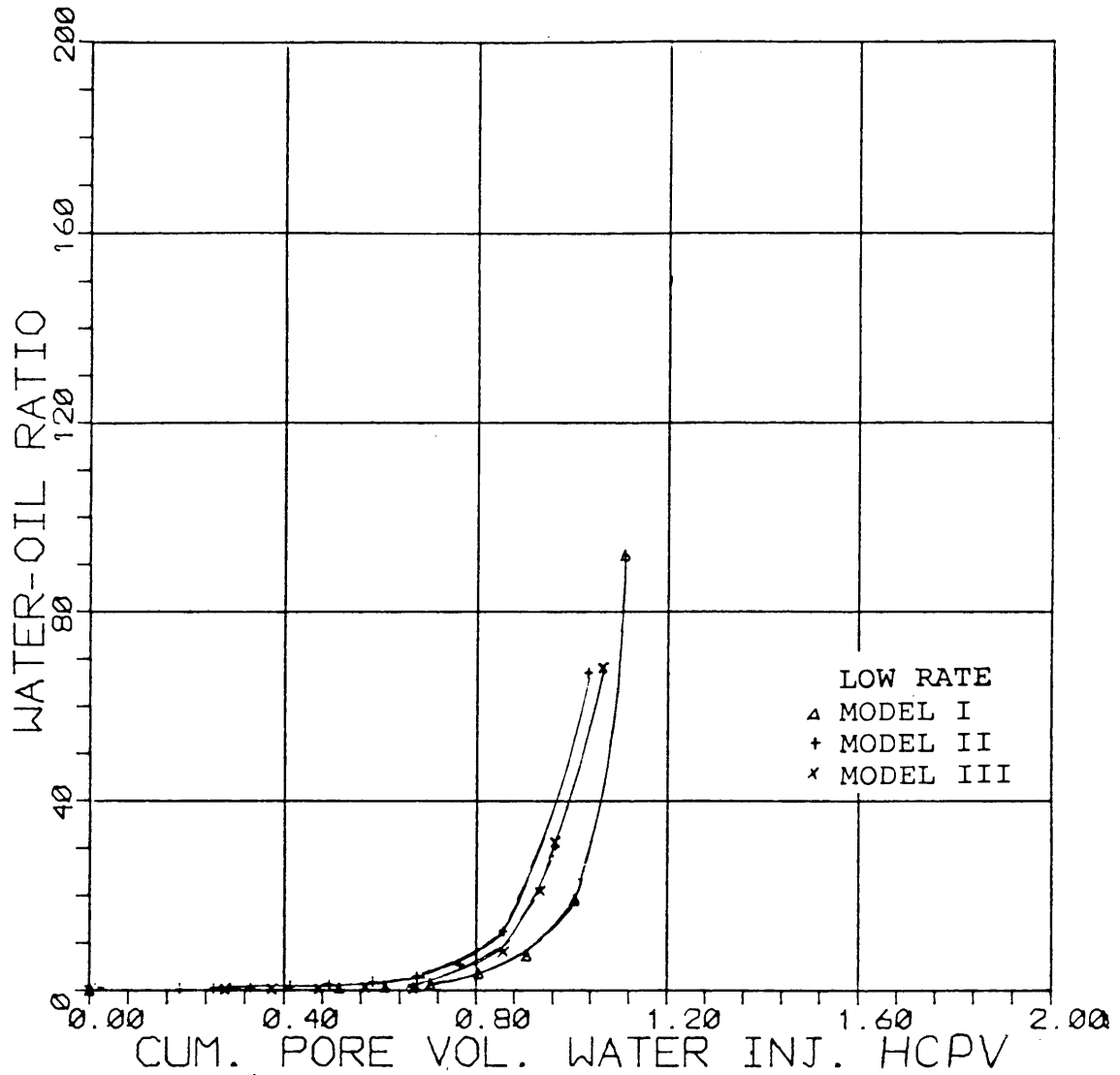


FIGURE 45 COMPARISON OF WATER-OIL RATIO CURVES AT
LOW RATE (GLYCERINE-WATER, VISCOSITY
RATIO = 7.93)

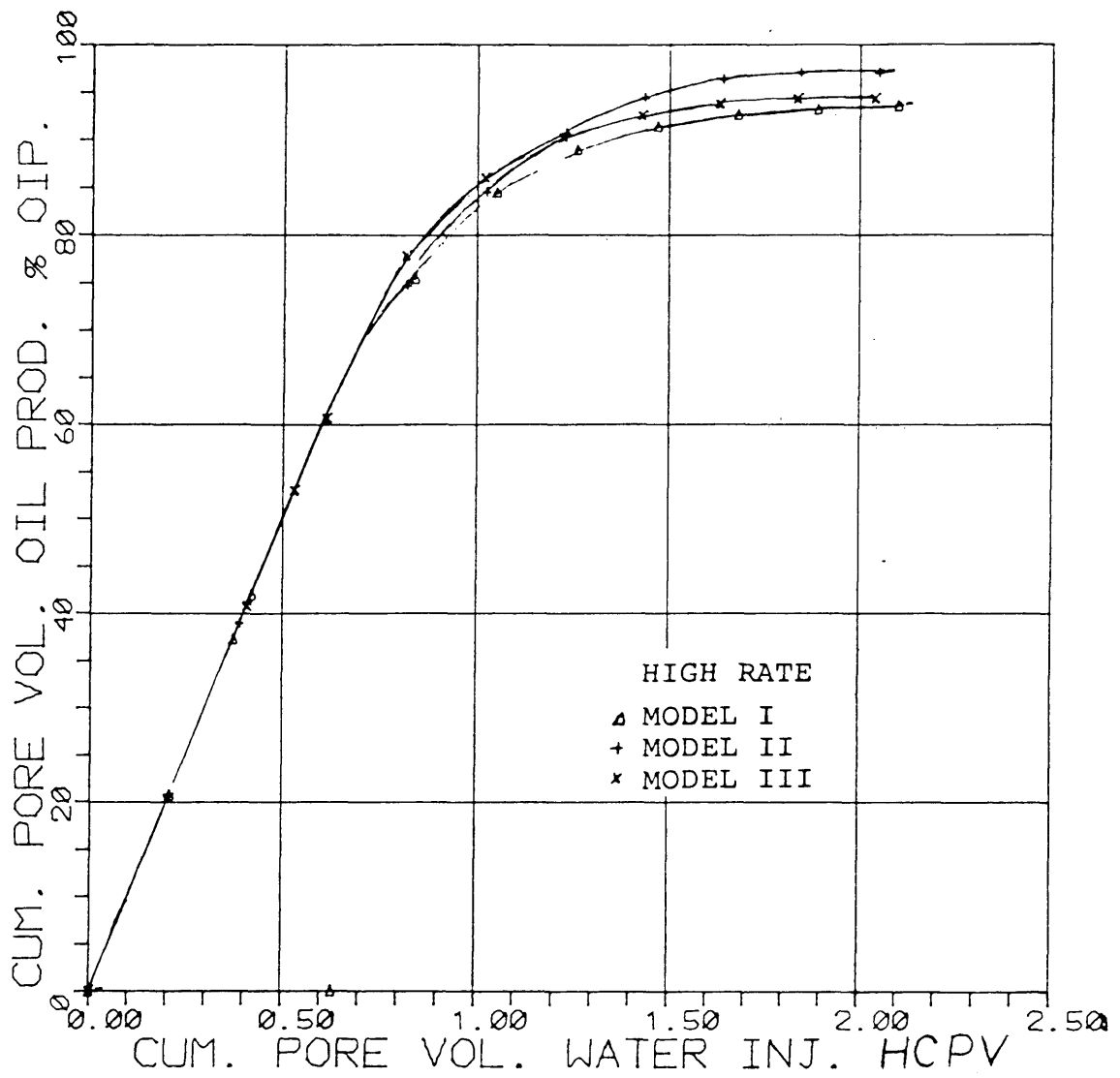


FIGURE 46 COMPARISON OF CUMULATIVE OIL RECOVERIES AT
HIGH RATE (FRESH WATER, VISCOSITY RATIO =
1.0)

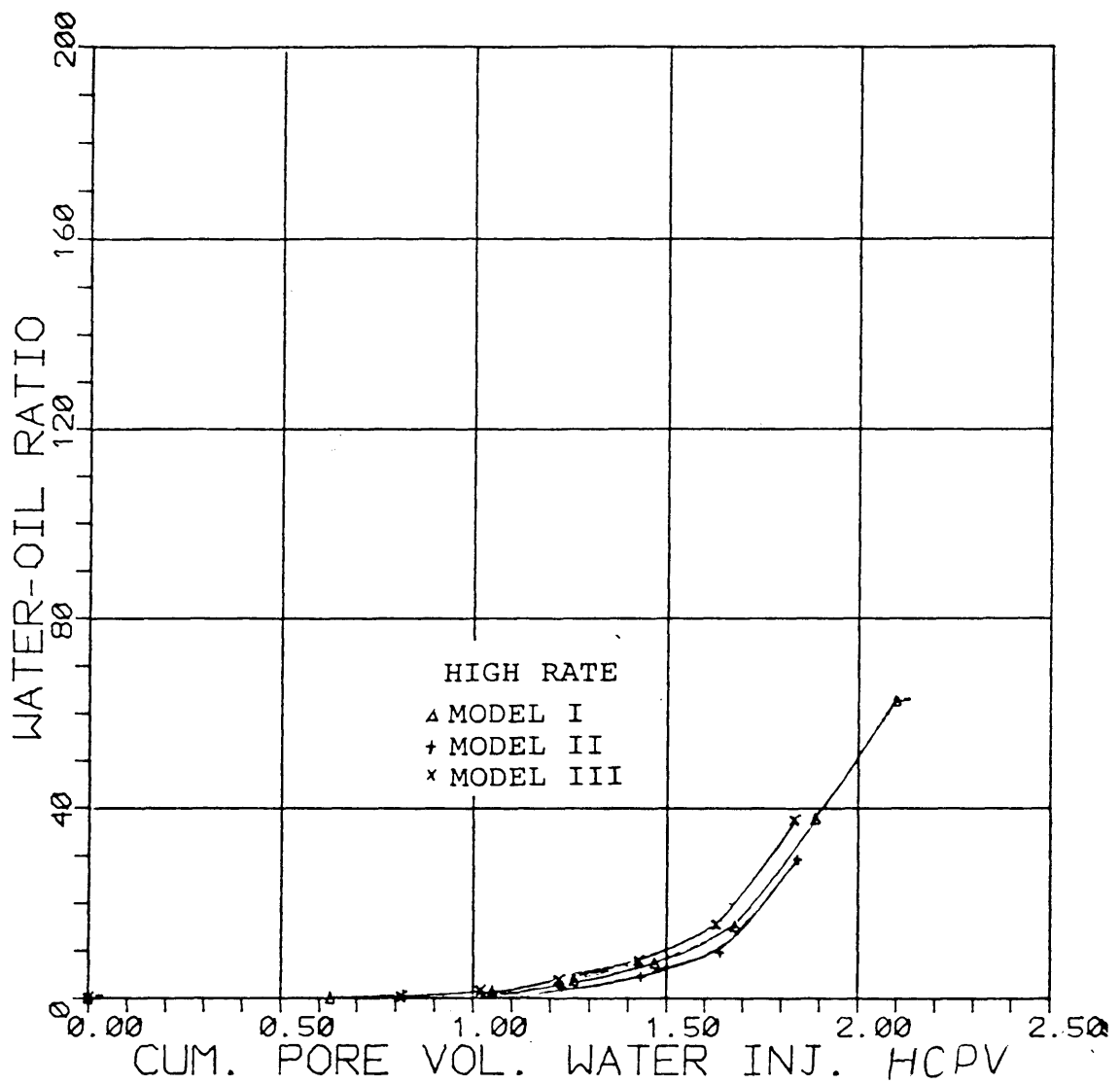


FIGURE 47 COMPARISON OF WATER-OIL RATIO CURVES AT
HIGH RATE (FRESH WATER, VISCOSITY RATIO =
1.0)

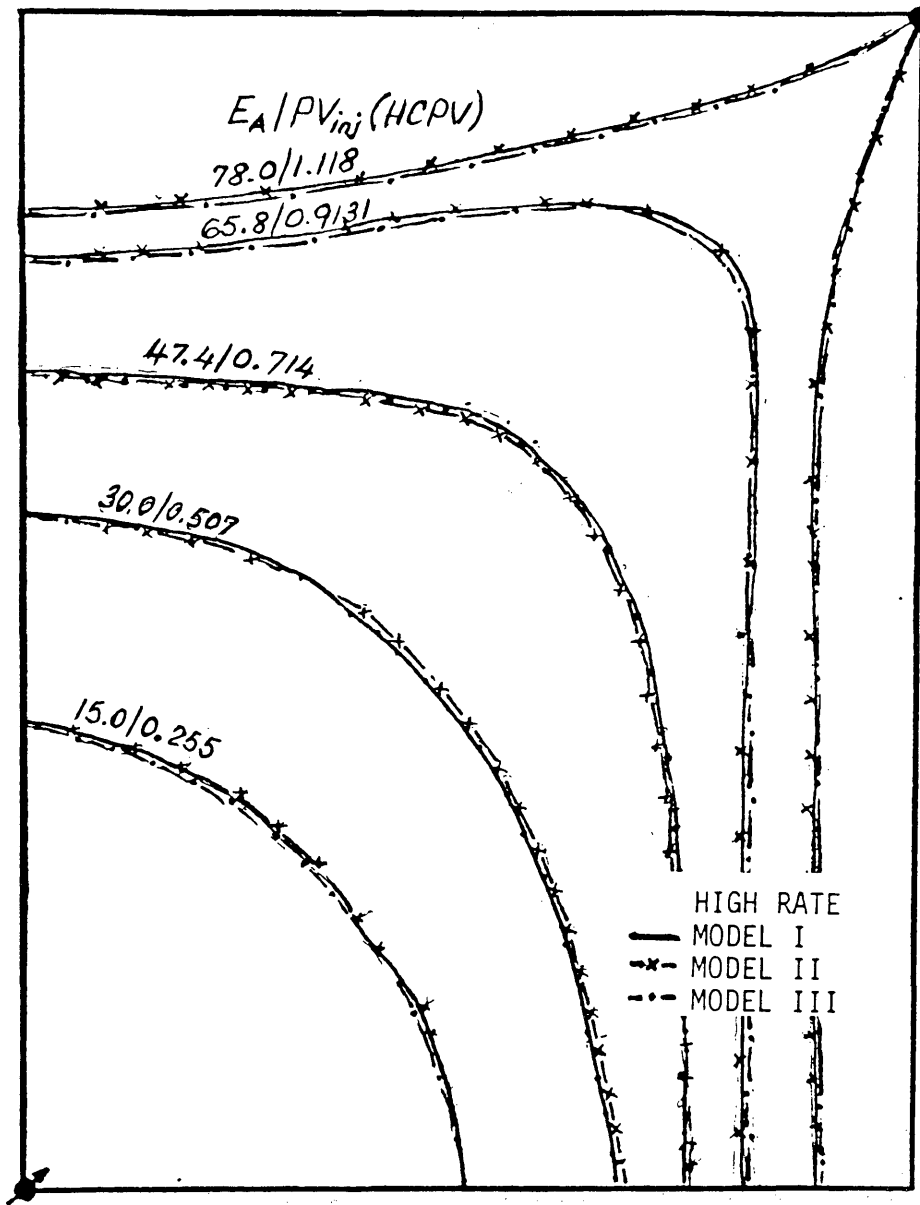


FIGURE 48 COMPARISON OF AREAL SWEEP EFFICIENCY AT HIGH RATE (HEXANE, VISCOSITY RATIO = 0.34)

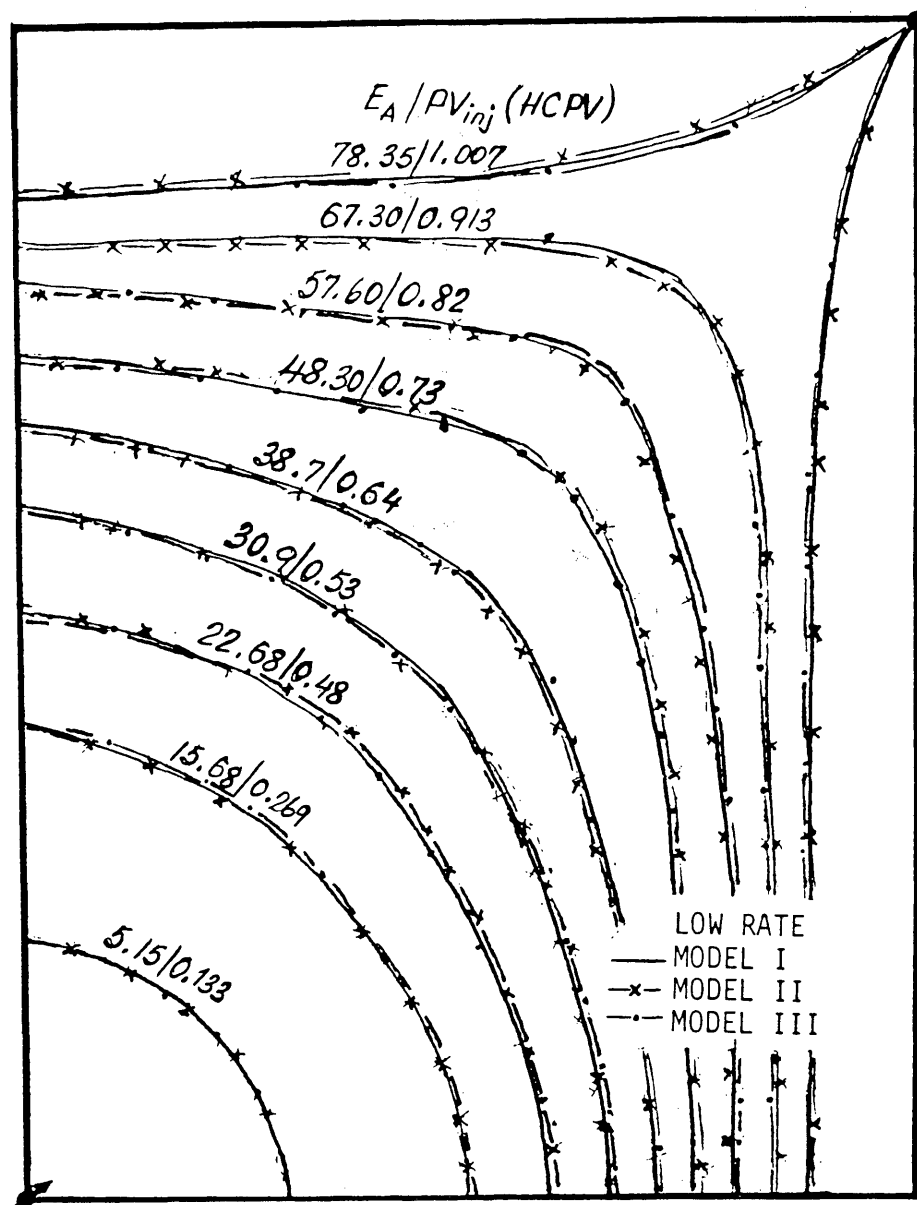


FIGURE 49 COMPARISON OF AREAL SWEEP EFFICIENCY AT
LOW RATE (HEXANE, VISCOSITY RATIO = 0.34)

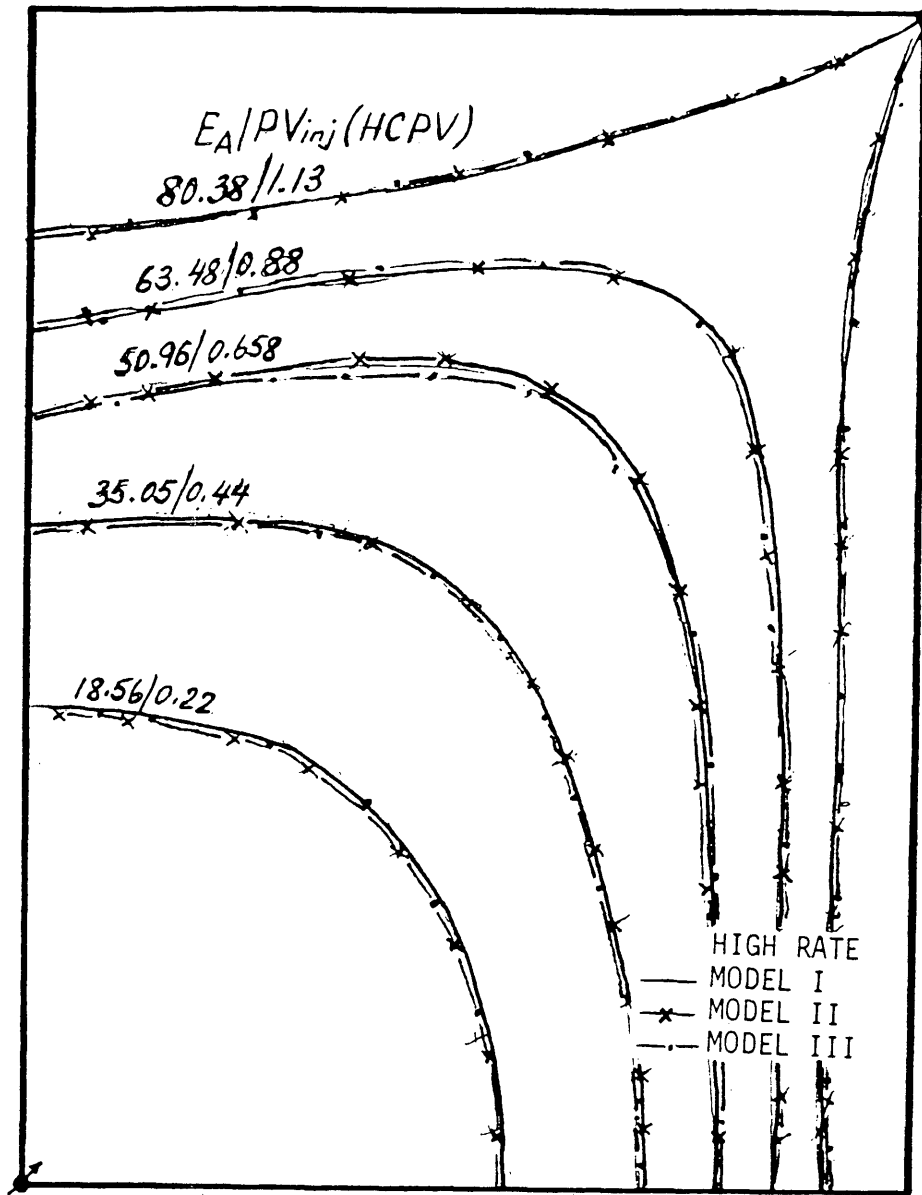


FIGURE 50 COMPARISON OF AREAL SWEEP EFFICIENCY AT
HIGH RATE (KEROSENE, VISCOSITY RATIO =
1.76)

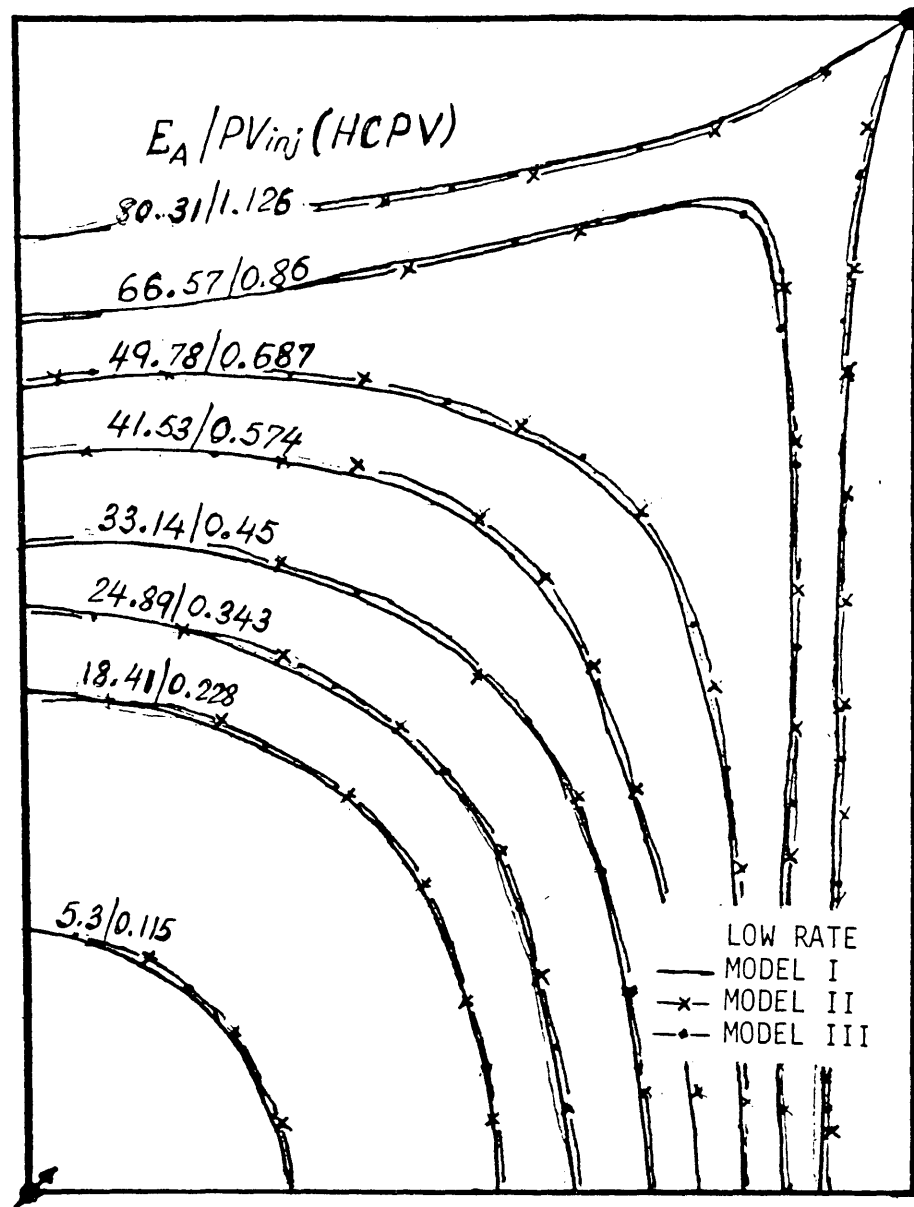


FIGURE 51 COMPARISON OF AREAL SWEEP EFFICIENCY AT
LOW RATE (KEROSENE, VISCOSITY RATIO =
1.76)

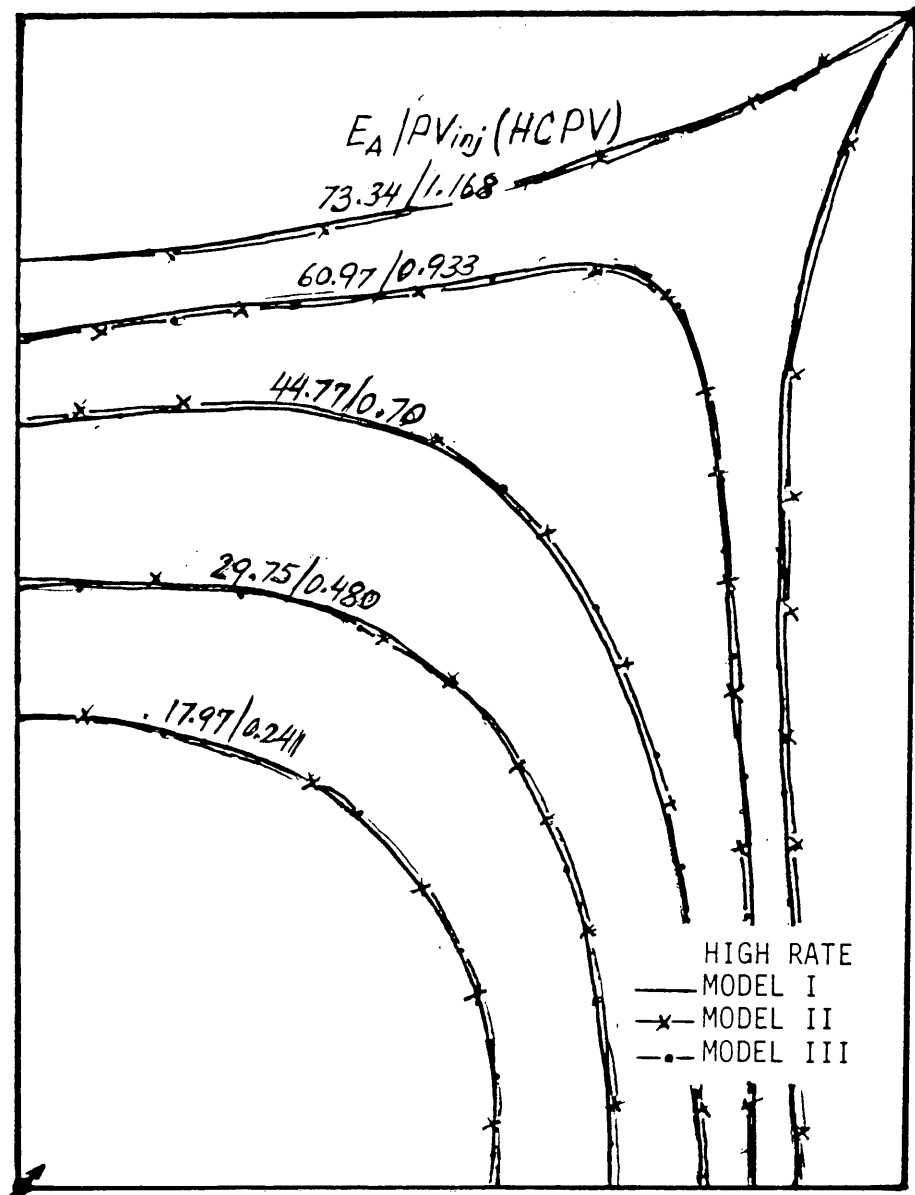


FIGURE 52 COMPARISON OF AREAL SWEEP EFFICIENCY AT
HIGH RATE (SOLTROL, VISCOSITY RATIO =
4.43)

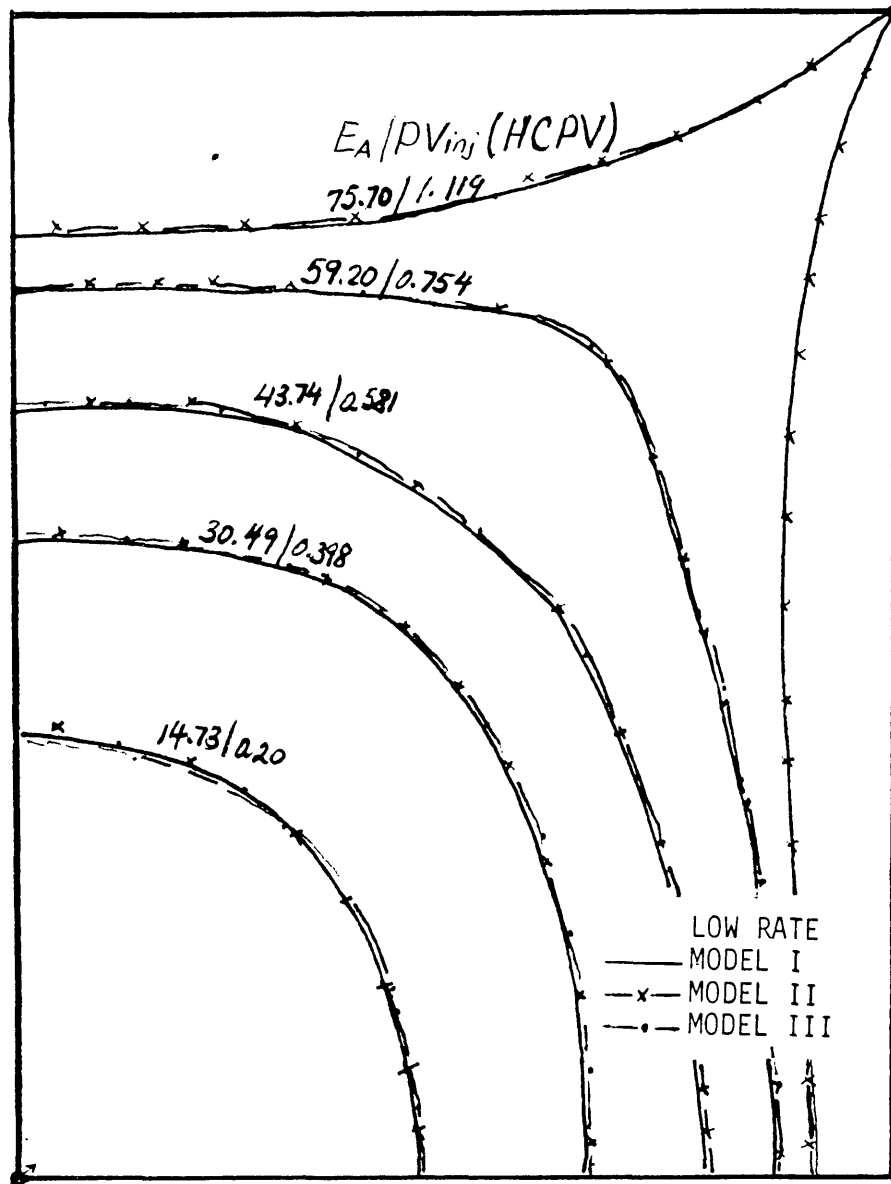


FIGURE 53 COMPARISON OF AREAL SWEEP EFFICIENCY AT
LOW RATE (SOLTROL, VISCOSITY RATIO =
4.43)

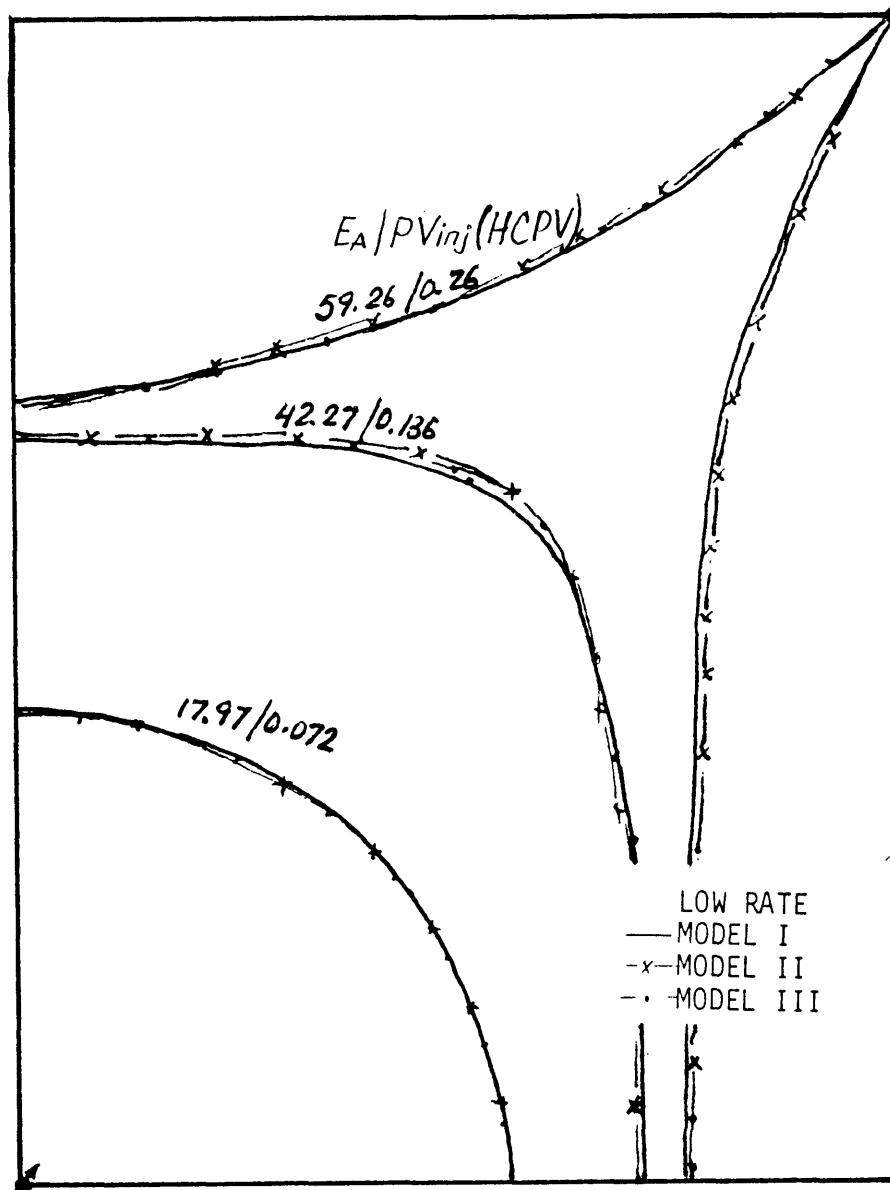


FIGURE 54 COMPARISON OF AREAL SWEEP EFFICIENCY AT
LOW RATE (GLYCERINE-WATER, VISCOSITY
RATIO = 7.93)

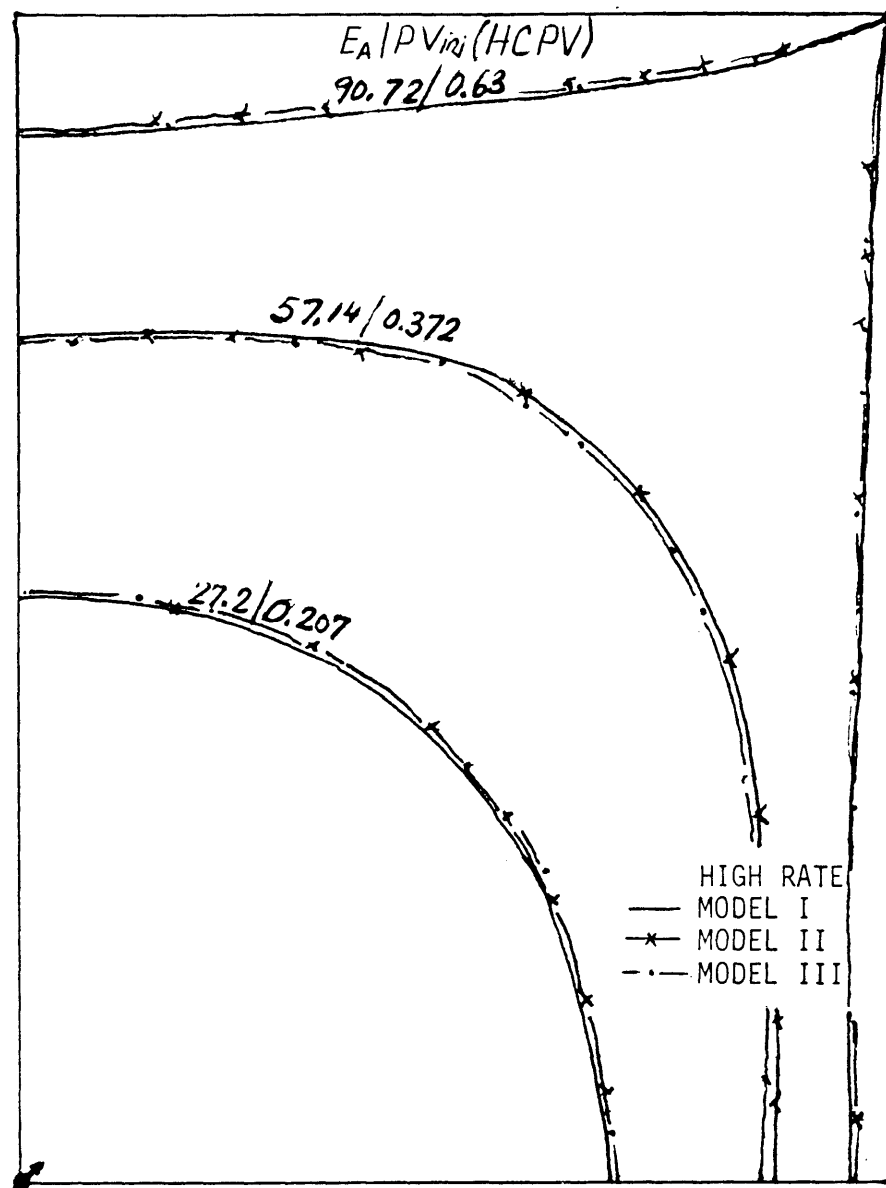


FIGURE 55 COMPARISON OF AREAL SWEEP EFFICIENCY AT
HIGH RATE (FRESH WATER, VISCOSITY RATIO =
1.0)

APPENDIX

EXPERIMENTAL RESULTS

TABLE A-2
 IMMISCIBLE DISPLACEMENT RUN
 MODEL I

Displaced Fluid HEXANE Injection Rate 21.5 cc/min
 Initial Water Saturation 0.30 Time to Breakthrough 218 mins.
 Test Date 12/1/78

Cum. Flow Time (min)	ΔP (psid)	Oil Prod. (cc)	Cum. Oil Prod. (%HCPV)	Cum. Water Inj. (HCPV)	WOR
30	1.21	610	0.1337	13.37	-
60	1.21	618	0.2692	26.92	-
90	1.21	600	0.4007	40.07	-
120	1.28	590	0.5300	53.00	-
150	2.62	502	0.6412	64.01	-
180	3.33	281	0.7302	70.17	0.45
210	3.33	168	0.8220	73.85	1.49
240	3.33	82	0.9130	75.65	4.06
270	3.33	9	1.1043	75.95	48.95
300	3.33	5	1.2052	75.95	86.63

TABLE A-3
 IMMISCIBLE DISPLACEMENT RUN
 MODEL II

Displaced Fluid HEXANE Injection Rate 180 cc/min
 Initial Water Saturation 0.27 Time to Breakthrough 98 mins
 Test Date 7/30/78

Cum. Flow Time (min)	ΔP (psid)	Oil Prod. (cc)	Cum. Oil Prod. (%HCPV)	Cum. Water Inj. (HCPV)	WOR
10	2.40	1666	8.69	0.0929	-
20	2.40	1670	17.41	0.1858	-
30	2.40	1673	26.14	0.2786	-
40	3.20	1676	34.88	0.3715	-
50	3.00	1682	43.66	0.4644	-
60	3.00	1632	52.17	0.5547	-
70	3.00	1608	60.56	0.6444	-
80	3.00	1534	68.57	0.7342	0.12
90	3.00	330	70.29	0.8114	3.49
100	3.00	50	70.55	0.8969	31.88
110	3.00	17	70.64	0.9866	98.67
120	3.00	12	70.70	1.0783	151.83
130	3.00	1	70.70	1.6398	too high

TABLE A-5
 IMMISCIBLE DISPLACEMENT RUN
 MODEL III

Displaced Fluid HEXANE Injection Rate 360 cc/min
 Initial Water Saturation 0.26 Time to Breakthrough 105 mins
 Test Date 10/5/78

Cum. Flow Time (min)	ΔP (psid)	Oil Prod. (cc)	Cum. Oil Prod. (%HCPV)	Cum. Water Inj. (HCPV)	WOR
10	1.99	3505	8.94	0.0923	-
20	1.99	3530	17.95	0.1850	-
30	3.30	3556	27.02	0.2783	-
40	3.89	3549	36.08	0.3713	-
50	3.89	3547	45.13	0.4641	-
60	3.89	3530	54.14	0.5565	-
70	3.89	3503	63.08	0.6488	-
80	3.89	2500	69.45	0.7409	0.45
90	3.89	598	70.98	0.8237	4.41
100	3.89	29	71.05	0.9105	123.0
110	3.89	5	71.08	1.0014	302.0
120	3.89	1	71.10	1.0921	452.0

TABLE A-6
 IMMISCIBLE DISPLACEMENT RUN
 MODEL III

Displaced Fluid HEXANE Injection Rate 172 cc/min
 Initial Water Saturation 0.20 Time to Breakthrough 216 mins
 Test Date 10/10/78

Cum. Flow Time (min)	ΔP (psid)	Oil Prod. (cc)	Cum. Oil Prod. (%HCPV)	Cum. Water Inj. (HCPV)	WOR
30	1.22	4891	11.55	0.1157	-
60	1.22	4862	23.03	0.2309	-
90	1.22	4854	34.49	0.3459	-
120	2.00	5001	46.30	0.4644	-
150	2.38	4807	57.65	0.5785	-
180	3.64	4646	68.62	0.6912	-
210	3.64	1833	72.95	0.7980	1.46
240	3.64	576	74.17	0.9061	7.86
270	3.64	162	74.55	1.0142	27.44
300	3.64	5	74.56	1.1230	too high

TABLE A-7
 IMMISCIBLE DISPLACEMENT RUN
 MODEL I

Displaced Fluid KEROSENE Injection Rate 45 cc/min
 Initial Water Saturation 0.17 Time to Breakthrough 89 mins
 Test Date 12/3/78

Cum. Flow Time (min)	ΔP (psid)	Oil Prod. (cc)	Cum. Oil Prod. (%HCPV)	Cum. Water Inj. (HCPV)	WOR
30	4.25	1205	22.14	0.2214	-
60	4.25	1195	44.13	0.4413	-
90	4.25	1174	65.70	0.6581	-
120	5.67	565	76.08	0.8813	1.15
150	5.67	85	77.64	1.1303	14.96
180	5.67	20	78.01	1.3746	65.02
210	5.67	8	78.16	1.6223	164.13
240	5.67	6	78.27	1.8703	224.45
270	5.67	3	78.32	2.1183	495.01

TABLE A-8
 IMMISCIBLE DISPLACEMENT RUN
 MODEL I

Displaced Fluid KEROSENE Injection Rate 21.5 cc/min
 Initial Water Saturation 0.25 Time to Breakthrough 203 mins
 Test Date 12/9/78

Cum. Flow Time (min)	ΔP (psid)	Oil Prod. (cc)	Cum. Oil Prod. (%HCPV)	Cum. Water Inj. (HCPV)	WOR
30	1.99	570	11.52	0.1152	-
60	2.34	560	22.83	0.2283	-
90	2.55	570	34.35	0.3435	-
120	2.55	565	45.77	0.4577	-
150	2.55	580	57.49	0.5749	-
180	2.55	555	68.70	0.6870	-
210	3.26	265	74.06	0.7638	0.43
240	5.25	210	78.30	0.8618	1.31
270	5.25	115	80.62	0.9638	3.40
300	5.25	35	81.33	1.0598	12.52
330	5.25	15	81.63	1.1588	31.93
360	5.25	15	81.94	1.2578	42.56
390	5.25	7	82.08	1.3550	68.43
420	5.25	5	82.12	1.4520	237.00

TABLE A-9
 IMMISCIBLE DISPLACEMENT RUN
 MODEL II

Displaced Fluid KEROSENE Injection Rate 180 cc/min
 Initial Water Saturation 0.22 Time to Breakthrough 88.5 min
 Test Date 8/20/78

Cum. Flow Time (min)	ΔP (psid)	Oil Prod. (cc)	Cum. Oil Prod. (%HCPV)	Cum. Water Inj. (HCPV)	WOR
30	2.60	5620	27.34	0.2773	-
60	2.60	5464	53.92	0.5468	-
90	3.00	4535	75.99	0.7986	0.14
120	3.20	420	78.03	1.0584	11.73
150	3.20	44	78.24	1.3214	124.23
180	3.20	16	78.32	1.5807	323.12
210	3.20	5	78.35	1.8403	864.29
240	3.20	6	78.38	2.1001	865.01
270	3.20	3	78.39	2.3611	2608.94

TABLE A-10
IMMISCIBLE DISPLACEMENT RUN

MODEL II

Displaced Fluid KEROSENE Injection Rate 86 cc/min

Initial Water Saturation 0.25 Time to Breakthrough 205 min

Test Date 8/27/78

Cum. Flow Time (min)	ΔP (psid)	Oil Prod. (cc)	Cum. Oil Prod. (%HCPV)	Cum. Water Inj. (HCPV)	WOR
30	2.60	2424	12.26	0.1279	-
60	2.60	2405	24.41	0.2546	-
90	2.60	2405	36.57	0.3810	-
120	2.60	2382	48.62	0.5061	-
150	2.60	2329	60.39	0.6284	-
180	2.60	2100	71.10	0.7447	-
210	3.00	1410	78.14	0.8605	0.64
240	3.00	480	80.57	0.9778	3.82
270	3.00	100	81.07	1.0991	23.26
300	3.00	38	81.26	1.2182	61.68
330	3.00	28	81.40	1.3363	83.35
360	3.00	14	81.48	1.4548	147.12
390	3.00	10	81.53	1.5734	236.00
420	3.00	6	81.56	1.6911	391

TABLE A-II
 IMMISCIBLE DISPLACEMENT RUN
 MODEL III

Displaced Fluid KEROSENE Injection Rate 360 cc/min
 Initial Water Saturation 0.20 Time to Breakthrough 9/ min
 Test Date 10/14/78

Cum. Flow Time (min)	ΔP (psid)	Oil Prod. (cc)	Cum. Oil Prod. (%HCPV)	Cum. Water Inj. (HCPV)	WOR
30	3.40	2994	7.09	0.0733	-
60	3.40	3558	15.52	0.1602	-
90	4.19	3588	24.02	0.2475	-
120	4.49	3554	32.44	0.3337	-
150	4.49	3620	41.02	0.4213	-
180	4.00	3598	49.54	0.5083	-
210	4.00	3596	58.06	0.5953	-
240	4.00	3563	66.50	0.6815	-
270	4.00	3126	73.91	0.7649	0.13
300	4.00	859	75.94	0.8428	2.84
330	4.00	590	77.34	1.0136	11.20
360	4.00	213	77.84	1.1894	34.16
390	4.00	140	78.17	1.3655	52.36
420	4.00	90	78.39	1.5406	78.59

TABLE A-12
 IMMISCIBLE DISPLACEMENT RUN
 MODEL III

Displaced Fluid KEROSENE Injection Rate 172 cc/min
 Initial Water Saturation 0.20 Time to Breakthrough 202 min
 Test Date 10/26/78

Cum. Flow Time (min)	ΔP (psid)	Oil Prod. (cc)	Cum. Oil Prod. (%HCPV)	Cum. Water Inj. (HCPV)	WOR
30	2.90	5004	11.81	0.1234	-
60	2.90	5010	23.63	0.2463	-
90	2.90	5050	35.55	0.3700	-
120	2.90	5033	47.43	0.4929	-
150	2.90	5012	59.26	0.6150	-
180	3.79	4613	70.14	0.7303	-
210	3.89	2000	74.86	0.8475	1.48
240	3.89	1445	78.27	0.9688	2.56
270	3.89	525	79.51	1.0890	8.69
300	3.89	205	79.99	1.2103	24.27
330	3.89	110	80.25	1.3332	46.27
360	3.89	75	80.43	1.4515	64.72
390	3.89	66	80.59	1.5739	75.70
420	3.89	50	80.71	1.6918	97.25

TABLE A-13
 IMMISCIBLE DISPLACEMENT RUN
 MODEL I

Displaced Fluid SOLTROL Injection Rate 45 cc/min
 Initial Water Saturation 0.20 Time to Breakthrough 82 min
 Test Date 12/14/78

Cum. Flow Time (min)	ΔP (psid)	Oil Prod. (cc)	Cum. Oil Prod. (%HCPV)	Cum. Water Inj. (HCPV)	WOR
30	7.94	1238	23.57	0.2414	-
60	7.94	1239	47.15	0.4809	-
90	8.51	1094	67.98	0.7011	0.24
120	8.37	323	74.13	0.9330	3.32
150	8.15	60	75.27	1.1681	5.55
180	8.15	21	75.67	1.4009	19.79
210	8.15	7	75.80	1.6314	26.44
240	8.15	5	75.90	1.8624	230.00
270	8.15	3	75.96	2.0899	378.16

TABLE A-14
 IMMISCIBLE DISPLACEMENT RUN
 MODEL I

Displaced Fluid SOLTROL Injection Rate 21.5 cc/min
 Initial Water Saturation 0.22 Time to Breakthrough 178 min
 Test Date 12/20/78

Cum. Flow Time (min)	ΔP (psid)	Oil Prod. (cc)	Cum. Oil Prod. (%HCPV)	Cum. Water Inj. (HCPV)	WOR
30	5.25	514	10.02	0.1014	-
60	5.25	514	20.04	0.2027	-
90	5.25	505	29.88	0.3021	-
120	5.25	490	39.43	0.3988	-
150	5.25	495	49.08	0.4967	-
180	6.66	417	57.21	0.5825	-
210	7.37	330	63.65	0.6682	0.33
240	7.37	165	68.42	0.7540	1.67
270	7.37	163	71.44	0.8427	1.78
300	7.37	116	73.55	0.9363	3.10
330	7.37	79	74.76	1.0279	4.91
360	7.37	58	75.40	1.1191	7.69
390	7.37	53	76.04	1.2156	7.70
420	7.37	10	76.24	1.3033	42.85

TABLE A-15
IMMISCIBLE DISPLACEMENT RUN

MODEL I (REPEATED RUN)

Displaced Fluid SOLTRDL Injection Rate 21.5 cc/min

Initial Water Saturation 0.20 Time to Breakthrough 171 min

Test Date 3/15/79

Cum. Flow Time (min)	ΔP (psid)	Oil Prod. (cc)	Cum. Oil Prod. (%HCPV)	Cum. Water Inj. (HCPV)	WOR
30	5.81	700	13.29	0.1329	-
60	5.81	710	26.77	0.2687	-
90	5.81	712	40.29	0.4053	-
120	5.81	695	53.49	0.5387	
150	7.30	472	62.45	0.6637	
180	7.09	195	66.15	0.7871	
210	7.09	125	68.52	0.9152	
240	7.09	73	69.91	1.0440	
270	7.09	45	70.77	1.1759	
300	7.09	30	71.33	1.3050	
330	7.09	15	71.62	1.4351	
360	7.09	13	71.87	1.5628	
390	7.09	10	72.06	1.6910	
420	7.09	10	72.25	1.8201	

TABLE A-16
 IMMISCIBLE DISPLACEMENT RUN
 MODEL II

Displaced Fluid SOLTROL Injection Rate 180 cc/min
 Initial Water Saturation 0.18 Time to Breakthrough 85 min
 Test Date 7/18/78

Cum. Flow Time (min)	ΔP (psid)	Oil Prod. (cc)	Cum. Oil Prod. (%HCPV)	Cum. Water Inj. (HCPV)	WOR
10	5.89	1724	7.78	0.0815	-
20	5.89	1704	15.48	0.1617	-
30	6.49	1666	23.00	0.2401	-
50	5.00	3286	37.84	0.3948	-
60	5.00	1575	44.95	0.4691	-
70	5.00	1577	52.07	0.5434	-
80	5.00	1548	59.06	0.6186	-
90	5.00	1070	63.89	0.7039	0.77
110	5.00	593	66.57	0.8728	5.30
140	5.00	504	68.85	1.1078	9.31
150	5.00	163	69.58	1.1868	9.82
180	5.00	410	71.44	1.4225	11.67
210	5.00	320	72.88	1.6607	15.54
240	5.00	229	73.91	1.8977	22.00

TABLE A-17
 IMMISCIBLE DISPLACEMENT RUN
 MODEL II

Displaced Fluid SOLTRON Injection Rate 86 cc/min

Initial Water Saturation 0.20 Time to Breakthrough 170 min

Test Date 7/27/78

Cum. Flow Time (min)	ΔP (psid)	Oil Prod. (cc)	Cum. Oil Prod. (%HCPV)	Cum. Water Inj. (HCPV)	WOR
30	3.59	2435	11.50	0.1226	-
60	3.59	2340	22.55	0.2404	-
90	3.59	2385	33.82	0.3594	-
120	3.59	2631	44.92	0.4767	-
150	3.59	711	55.90	0.5941	-
180	3.59	520	65.30	0.7181	0.56
210	3.00	400	68.66	0.8395	2.61
240	3.00	304	71.12	0.9600	3.90
270	3.00	243	73.01	1.0797	5.33
300	3.00	127	74.45	1.1980	7.22
330	3.00	40	75.60	1.3175	9.39
360	3.00	42	76.57	1.4354	20.14
390	3.00	31	77.39	1.5534	61.10
420	3.00	33	78.07	1.6700	57.30

TABLE A-18
 IMMISCIBLE DISPLACEMENT RUN
 MODEL III

Displaced Fluid SOLTRON Injection Rate 360 cc/min
 Initial Water Saturation 0.20 Time to Breakthrough 84 min
 Test Date 11/1/78

Cum. Flow Time (min)	ΔP (psid)	Oil Prod. (cc)	Cum. Oil Prod. (%HCPV)	Cum. Water Inj. (HCPV)	WOR
10	6.69	3748	8.85	0.0898	-
20	6.69	3607	17.36	0.1760	-
30	7.38	3687	26.06	0.2639	-
50	7.59	7334	43.37	0.4385	-
70	6.89	5995	57.52	0.6107	0.22
90	6.49	3063	64.75	0.7470	0.88
110	6.19	1398	68.05	0.9080	3.88
130	6.19	890	70.15	1.0843	7.39
150	6.19	678	71.75	1.2622	10.12
170	6.19	792	73.62	1.4381	15.41
190	6.19	262	74.24	1.6114	26.95
210	6.19	165	74.63	1.7846	43.41
230	6.19	118	74.91	1.9576	60.79
250	6.19	89	75.12	2.1292	80.71

TABLE A-19
 IMMISCIBLE DISPLACEMENT RUN
 MODEL III

Displaced Fluid SOLTROL Injection Rate 172 cc/min
 Initial Water Saturation 0.20 Time to Breakthrough 160 min
 Test Date 11/10/78

Cum. Flow Time (min)	ΔP (psid)	Oil Prod. (cc)	Cum. Oil Prod. (%HCPV)	Cum. Water Inj. (HCPV)	WOR
30	3.00	4884	11.45	0.1219	-
60	3.00	4855	22.83	0.2423	-
90	3.00	4860	34.22	0.3623	-
120	3.00	4863	45.62	0.4819	-
150	3.00	4932	55.18	0.6006	-
180	2.60	2632	60.49	0.7201	0.94
210	2.60	1498	64.13	0.8405	2.43
240	2.60	964	66.81	0.9609	4.32
270	2.60	823	68.89	1.0812	5.23
300	2.60	618	70.60	1.2016	7.30
330	2.60	418	71.99	1.3218	11.26
360	2.60	264	73.14	1.4423	25.94
390	2.60	102	74.11	1.6842	49.37
420	2.60	85	74.93	1.8053	59.50

TABLE A-20
MISCIBLE DISPLACEMENT RUN
MODEL I

Displaced Fluid FRESH WATER Injection Rate 45 cc/min
Time to Breakthrough 76 min Test Date 11/23/78

Cum. Flow Time (min)	ΔP (psid)	Salinity (ppm)	Cum. Oil Prod. (%HCPV)	Cum. Water Inj. (PV)	WOR
30	1.06	-	20.73	0.2073	-
60	1.06	-	37.21	0.3721	-
	1.06	204	42.00	0.4210	-
90	1.06	595	61.22	0.6306	-
120	1.06	3262	75.45	0.8402	-
150	1.06	5701	84.46	1.0498	1.33
180	1.06	7877	88.91	1.2594	3.71
210	1.06	8807	91.41	1.4690	7.38
240	1.06	9379	92.92	1.6786	15.12
270	1.06	9742	93.25	1.8882	37.81
300	1.06	9842	93.58	2.0978	62.52

TABLE A-21
 MISCIBLE DISPLACEMENT RUN
 MODEL II

Displaced Fluid FRESH WATER Injection Rate 180 cc/min
 Time to Breakthrough 78 min Test Date 7/10/78

Cum. Flow Time (min)	ΔP (psid)	Salinity (ppm)	Cum. Oil Prod. (%HCPV)	Cum. Water Inj. (PV)	WOR
30	2.40	-	20.50	0.2050	-
60	2.40	-	38.96	0.3896	-
90	2.40	97	40.99	0.4101	-
	2.40	556	60.35	0.6151	-
120	2.40	3003	74.70	0.8202	0.43
150	2.40	5219	84.50	1.0252	1.09
180	2.40	7001	90.65	1.2303	2.33
210	2.40	8165	94.41	1.4353	4.45
240	2.40	9053	96.35	1.6403	9.57
270	2.40	9668	97.03	1.8454	29.16
300	2.40	10,000	97.03	2.0504	salt water

TABLE A-22
 MISCIBLE DISPLACEMENT RUN
 MODEL III

Displaced Fluid FRESH WATER Injection Rate 360 cc/min
 Time to Breakthrough 78 min Test Date 10/2/78

Cum. Flow Time (min)	ΔP (psid)	Salinity (ppm)	Cum. Oil Prod. (%HCPV)	Cum. Water Inj. (PV)	WOR
30	2.00	-	20.39	0.2039	-
60	2.00	-	40.78	0.4078	-
90	2.00	-	53.01	0.5301	-
	2.00	601	60.67	0.6116	-
120	2.00	1569	77.86	0.8115	0.18
150	2.00	5998	86.02	1.0194	1.49
180	2.00	7915	90.27	1.2233	3.79
210	2.00	8867	92.58	1.4272	7.83
240	2.00	9391	93.82	1.6310	15.44
270	2.00	9740	94.35	1.8349	37.47
300	2.00	10,000	94.35	2.0388	salt water

TABLE A-23
 MISCIBLE DISPLACEMENT RUN
 MODEL I

Displaced Fluid GLY-WATER Injection Rate 21.5 cc/min
 Time to Breakthrough 56 min Test Date 12/24/78

Cum. Flow Time (min)	ΔP (psid)	Salinity (ppm)	Cum. Oil Prod. (%HCPV)	Cum. Water Inj. (PV)	WOR
30	10.49	-	7.29	0.0729	-
60	10.49	-	13.67	0.1367	-
90	10.49	-	19.90	0.1990	-
120	10.49	-	26.73	0.2673	-
150	10.49	-	34.34	0.3434	-
180	10.20	-	37.07	0.3707	-
	9.92	715	41.87	0.4224	-
210	8.08	2415	48.78	0.5135	0.32
240	8.08	3746	54.69	0.6080	0.59
270	7.23	5655	58.80	0.7026	1.30
300	6.38	7773	61.04	0.8032	3.49
330	6.23	8788	62.26	0.9039	7.25
360	5.67	9500	62.77	1.0059	19.00
390	5.67	9842	62.88	1.1081	91.91

TABLE A-24
 MISCIBLE DISPLACEMENT RUN
 MODEL II

Displaced Fluid GLY-WATER Injection Rate 86 cc/min
 Time to Breakthrough 43 min Test Date 8/10/78

Cum. Flow Time (min)	ΔP (psid)	Salinity (ppm)	Cum. Oil Prod. (%HCPV)	Cum. Water Inj. (PV)	WOR
30	2.59	-	5.77	0.0577	-
60	2.99	-	11.21	0.1121	-
90	2.99	-	11.91	0.1192	-
	2.99	1210	17.72	0.1853	0.14
120	1.99	2252	23.19	0.2559	0.29
150	1.99	3231	28.28	0.3311	0.48
180	1.99	4203	32.90	0.4108	0.72
210	1.99	5195	36.95	0.4951	1.08
240	1.99	6170	40.37	0.5844	1.61
270	1.99	7287	42.83	0.6751	2.68
300	1.99	8425	44.26	0.7659	5.35
330	1.99	9251	44.94	0.8567	12.35
360	1.99	9425	45.21	0.9475	260.10
390	1.99	9674	45.35	1.0383	385.35

TABLE A-25
 MISCIBLE DISPLACEMENT RUN
 MODEL III

Displaced Fluid GLY-WATER Injection Rate 172 cc/min
 Time to Breakthrough 56 min Test Date 11/13/78

Cum. Flow Time (min)	ΔP (psid)	Salinity (ppm)	Cum. Oil Prod. (%HCPV)	Cum. Water Inj. (PV)	WOR
30	6.39	-	9.10	0.0910	-
60	4.19	-	15.33	0.1533	-
	3.99	-	18.32	0.1841	-
90	3.59	1050	26.71	0.2786	0.12
120	3.29	1914	37.12	0.3744	0.14
150	3.19	2778	45.33	0.4713	0.18
180	2.79	3643	51.74	0.5689	0.52
210	2.79	4693	59.92	0.6667	0.86
240	2.59	5496	61.65	0.6746	1.88
270	2.59	6360	62.52	0.8634	20.70
300	2.59	7163	62.83	0.9632	31.19
330	2.59	8028	63.14	1.0634	128.32
360	2.59	9633	63.54	1.1637	237.10
390	2.59	9942	63.92	1.2639	salt water.